UNIVERSITÁ DEGLI STUDI

DI NAPOLI FEDERICO II

Dottorato di Ricerca in

Ingegneria Elettrica e delle Telecomunicazioni

XXII Ciclo

SYNCHRONIZATION ALGORITHMS FOR FBMC SYSTEMS

Angelo Petrella

Il Coordinatore — **Ch.mo Prof. N.Rinaldi**

Il Tutore — **Ch.mo Prof. M.Tanda**

A.A. 2008/2009

To my family

To Vale, rara avis in terris

Veritas autem non a felicitate temporis alicujus,
quae res varia est; sed a lumine naturae et
experientiae, quod aeternum est, petenda est.
Francis Bacon

Acknowledgements

Thanks to my colleagues, but above all friends, of the Department of Biomedical, Electronic and Telecommunications Engineering of University of Napoli Federico II for making my working days much less stressful.
Thanks to my family for helping me to reach this aim.
Thanks to Valentina for always believing in me.

Index

List of Figures

Notations

j	Imaginary unit
a	Scalar
a^*	Complex conjugate of scalar a
$\lvert a \rvert$	Absolute value of a
$\Re\{a\}$	Real part of a complex scalar a
$\Im\{a\}$	Imaginary part of a complex scalar a
$\angle a$ or $\arg\{a\}$	Argument of a complex number in $[0, 2\pi)$
$\hat{a}$	Estimate of the parameter a
$\tilde{a}$	Trial value for a
$\mathbf{a}$	Vector
$\mathbf{a}^*$	Complex conjugate of vector $\mathbf{a}$
$\mathbf{a}^T$	Transpose of vector $\mathbf{a}$
$\mathbf{a}^H$	Hermitian of vector $\mathbf{a}$
$\mathbf{A}$	Matrix
$[\mathbf{A}]_{(m,l)}$	(m,l)th enty of matrix $\mathbf{A}$
$\mathbf{A}^T$	Transpose of matrix $\mathbf{A}$
$\mathbf{A}^H$	Hermitian of matrix $\mathbf{A}$
$\mathbf{A}^{-1}$	Inverse of matrix $\mathbf{A}$
$\det\{\mathbf{A}\}$	Determinant of matrix $\mathbf{A}$

$\mathbf{I}_n$	$n \times n$ identity matrix
$E[\cdot]$	Statistical expectation
$\text{diag}\{\cdot\}$	Diagonal matrix
$\otimes$	Discrete time convolution operator
$\lceil \cdot \rceil$	Rounds its argument to the nearest integer towards infinity
$\lfloor \cdot \rfloor$	Rounds its argument to the nearest integer towards minus infinity
$\langle \cdot \rangle$	Time average
$\delta(m)$	Kronecker delta
$\text{sinc}(t) \triangleq \frac{\sin(\pi t)}{\pi t}$	Sinc function
$\text{sgn}(\cdot)$	Signum function
$lcm\{a,b\}$	Least common multiple between a and b
$\mathcal{O}$	Landau symbol
$\dot{g}(\cdot)$	First derivative of $g(\cdot)$
N	Number of subcarriers
N_m	Delay spread
N_u	Number of used subcarriers
N_v	Number of virtual subcarriers
K	Oversampling factor
α	Roll – off factor

T	Symbol interval
T_s	Sampling interval
f_s	Sampling frequency
τ	Symbol timing
ϕ	Carrier phase
Δf	Carrier frequency offset
ε	Carrier frequency offset normalized to the intercarrier spacing
$P = lcm\{N, K\}$	for FMT system
$P = N$	for OFDM/OQAM system

Acronyms

3GPP	Third Generation Partnership Project
AML	Approximated Maximum Likelihood
AWGN	Additive White Gaussian Noise
BER	Bit Error Rate
BLU	Best Linear Unbiased
BPSK	Binary Phase Shift Keying
BS	Base Station
CFO	Carrier Frequency Offset
CMLLS	Conjugate Maximum Likelihood for Low Signal to noise ratio
CP	Cyclic Prefix
CRVB	Cramér – Rao Vector Bound
CS	Ciblat Serpedin
DAC	Digital to Analog Converter
DFT	Discrete Fourier Transform
DTFT	Discrete Time Fourier Transform
FBMC	Filter Bank Multi Carrier
FFT	Fast Fourier Transform
FIM	Fisher Information Matrix
FMT	Filtered Multi Tone

ICI	Inter Carrier Interference
IDFT	Inverse Discrete Fourier Transform
IFFT	Inverse Fast Fourier Transform
ISI	Inter Symbol Interference
LLSS	Lottici Luise Saccomando Spalla
LS	Least Squares
MA	Multiple Access
MAT	Modified Assalini Tonello
MCRB	Modified Cramér – Rao Bound
MFIM	Modified Fisher Information Matrix
ML	Maximum Likelihood
MLLS	Maximum Likelihood for Low Signal to noise ratio
MSE	Mean Square Error
OFDM	Orthogonal Frequency Division Multiplexing
OFDM/OQAM	Orthogonal Frequency Division Multiplexing based on Offset Quadrature Amplitude Modulation
OFDMA	Orthogonal Frequency Division Multiple Access
PAM	Pulse Amplitude Modulation
QAM	Quadrature Amplitude Modulation
QPSK	Quadrature Phase Shift Keying

RCFO	Residual Carrier Frequency Offset
RHS	Right Hand Side
RMSE	Root Mean Square Error
RTO	Residual Timing Offset
SNR	Signal to Noise Ratio
SRRC	Square Root Raised Cosine
TR1	Tonello Rossi 1
TR2	Tonello Rossi 2
UTRAN	UMTS Terrestrial Radio Access Network
UMLLS	Unconjugate Maximum Likelihood for Low Signal to noise ratio
VDSL	Very high Digital Subscriber Line

Introduction

Recently, filter bank multicarrier (FBMC) systems have received considerable attention for wired and wireless high-data-rate transmissions in frequency selective channels. Conventional multicarrier systems, know as orthogonal frequency division multiplexing (OFDM) systems, provide robustness to multipath channels, thanks to the introduction of a cyclic prefix (CP) that efficiently combats the intersymbol interference (ISI) in dispersive channels. However, the insertion of CP is pure redundancy, that decreases the spectral efficiency. Moreover, in OFDM systems the adopted pulse-shaping filter is a rectangular function, which exhibits poor frequency-decay. On the contrary, FBMC systems employ band limited pulse-shaping filters that overlap in time. This involves several advantages such as reduced sensitivity to narrowband interference, high flexibility to allocate group of subchannels to different users and a high spectral containment. The computational complexity of FBMC systems is higher than that of CP-OFDM systems. However, since the subchannel filters are obtained by complex modulation of a single filter, efficient polyphase implementations are possible [1]. FMBC systems referred to as Filtered Multitone (FMT) systems have been proposed for high-speed digital subscriber line (VDSL) standards [2] and are under investigation also for broadband wireless applications [3], [4]. FBMC systems based on offset quadrature amplitude modulation (OQAM), known

as OFDM/OQAM systems, have been considered by the 3GPP standardization forum for improved downlink UTRAN interfaces [5].

As all the multicarrier modulation schemes, one of the major disadvantages of FBMC systems is their sensitivity to carrier frequency and symbol timing errors. Specifically, as investigated in [6] and in [7], phase noise and misalignments in time and frequency can considerably degrade the performance of FMT and OFDM/OQAM systems, giving rise to interference between successive symbols and adjacent subcarriers. Therefore, reliable and accurate symbol timing and carrier-frequency offset (CFO) synchronization schemes must be implemented for these systems. Several studies have been focused on parameter estimation for FBMC systems based on data-aided or blind techniques. In the first case it is in demand the transmission of known sequences or the use of a training symbol with a known structure while blind estimation algorithms use exclusively the statistic properties of the transmitted signal. For example, in [8] and [9], blind CFO and symbol timing estimators based on the maximum likelihood (ML) principle and obtained under the hypothesis of low signal-to-noise ratio (SNR), have been considered. Moreover in [10], it has been derived a blind joint symbol timing and frequency offset synchronization scheme for FMT systems. In [11], a blind joint CFO and symbol timing estimator based on the unconjugate cyclostationarity property of the OFDM signal with pulse shaping filters has been also proposed. In [12], it is claimed that accurate CFO estimation algorithms robust to dispersive

channels can be obtained by using the conjugate cyclostationarity property of the received signal. However, the derived estimator assures a satisfactory performance only when a large number of OFDM/OQAM symbols is considered. The conjugate correlation function of the received signal has been also used in [13] to derive a CFO estimator for multipath channels exploiting the insertion of weighted subcarriers. Moreover, in [14] the authors derived data-aided joint symbol timing and frequency offset synchronization schemes in the time-domain for FMT systems, while in [15] the problem of data-aided synchronization and channel estimation in the frequency domain for OFDM/OQAM systems has been considered.

In this thesis the problem of CFO and symbol timing synchronization is examined and new data-aided and blind estimation techniques are proposed (see [16], [17], [18], [19], [20], [21]). Specifically, it is presented a new joint symbol timing and CFO synchronization algorithm based on the least squares (LS) approach, which exploits the known structure of a training sequence made up of identical parts. This method, as illustrated by numerical simulations, can assure in a multipath channel sufficiently accurate symbol timing and CFO estimates [16]. Moreover, the joint ML phase offset, CFO and symbol timing estimator for a multiple access (MA) OFDM/OQAM system is considered. The derived estimator exploits a short known preamble embedded in the burst of each of U users. Under the assumption that the CFO of each user is sufficiently small, the considered approach leads to U different

approximate ML (AML) joint phase offset, CFO and symbol timing estimators. In particular, the phase and CFO estimators are in closed form, while the AML symbol timing estimator requires a one-dimensional maximization procedure [17].

As regards blind synchronization techniques, it is proposed a closed-form CFO estimator based on the best linear unbiased (BLU) estimation principle for FMT systems [18]. Although the BLU estimator is derived under the hypothesis of additive white Gaussian noise (AWGN) channel, it demonstrates a remarkable robustness against multipath fading. Moreover, it does not require the knowledge of the symbol timing. Numerical results show that the BLU estimator outperforms the ones proposed in [10], [11] and [22] and can outperform the ML algorithm for weak signal proposed in [8] in the presence of large values of the timing offset. Blind CFO estimators based on the ML principle and obtained under the hypothesis of low SNR are also considered. Specifically, the proposed CFO estimators can exploit both the conjugate and the unconjugate properties of the received OFDM/OQAM signal. Moreover, due to the significant computational complexity of the derived ML estimators, a closed-form CFO synchronization algorithm based on the LS method is considered [19]. It is also derived, under the assumption of low SNR, the joint ML symbol timing and phase offset estimator for AWGN channel. Since the phase estimate is in closed form, by substituting its expression in the likelihood function, a blind symbol timing estimator that requires only a one-

dimensional maximization procedure is obtained. The ML symbol timing estimator exploits both the conjugate and the unconjugate cyclostationarity properties of the OFM/OQAM signal that are related to the bandwidth of the adopted pulse-shaping filter [20].

The thesis is organized as follows. In Chapter I, an introduction to FBMC systems is provided. The transmitter and receiver for both FMT and OFDMOQAM systems are presented and it is put in evidence the central role of prototype filters very well localized in time and frequency. In Chapter II, the sensitivity of FBMC systems to the presence of synchronization errors is analyzed. Chapter III deals with data-aided synchronization techniques for FBMC systems both in downlink and up-link scenarios. The joint LS CFO and symbol timing estimator for FMT and OFDM/OQAM systems is derived. The joint CFO and symbol timing estimator in multi-user OFDM/OQAM systems is also proposed. In Chapter IV, it is looked at blind synchronization algorithms for FBMC systems. Blind CFO estimator for noncritically sampled FMT systems is proposed. Moreover, non data-aided CFO estimators for low SNR conditions for OFDM/QAM systems are presented. The ML symbol timing estimator for low SNR conditions for OFDM/OQAM systems is also derived. Finally, conclusions are drawn in Chapter V.

Chapter 1

FBMC Systems

In this chapter, two kinds of FBMC systems, FMT and OFDM/OQAM, are presented. In the first part FMT system is introduced and the description of its transmitter and receiver is considered. In the second part, OFDM/OQAM system is analyzed, by describing the structure of both transmitter and receiver. Finally, it is put in evidence the important role of the prototype filter.

1.1 FMT Systems

FMT is a filter-bank modulation technique where the N-branch filters are frequency-shifted versions of a baseband filter, referred to as prototype filter, that achieves a high level of spectral containment, such as the ICI is negligible compared to other noise signals [2].

The FMT time-continuous transmitted signal is given by

$$x(t)=\sum_{i=0}^{N-1}\sum_{k=-\infty}^{+\infty} A_i(kT)\,h(t-kT)\,e^{j2\pi f_i t} \qquad (1.1)$$

where, $h(t)$ indicates the prototype filter, N is the number of subcarriers, $A_i(k)$ denotes the data symbol transmitted on the lth subcarrier of the kth

FMT symbol and $T = KN$ represents the symbol period, being K the oversampling factor.

Two different implementations of FMT systems are possible:

- critical sampling filter bank, when $K = N$;
- noncritical sampling filter bank, when $K > N$.

Commonly, filter characteristics are chosen to satisfy the perfect reconstruction constraint in order to ensure that transmission is free of ISI within a subchannel as well as free of ICI. The perfect reconstruction conditions are expressed in the time-domain as [1]

$$\sum_k h_i(k) h_{i'}^*(k - lN) = \delta(i - i')\delta(l) \qquad (1.2)$$
$$0 \le i, i' \le N - 1, \qquad l = \ldots, -1, 0, 1, \ldots$$

where $h_i(k) = h(k)e^{j2\pi ki/N}$. It is generally not practical to include the characteristics of the nonideal transmission channel in the perfect reconstruction conditions. Therefore, at the receiver the orthogonality between subchannels is destroyed with the consequence of unacceptable performance degradation. The FMT modulation technique follows another approach, whereby spectral overlap between the subchannels is avoided by resorting to noncritically sampled filter-bank systems and employing per-branch filter characteristics that achieve tight subchannel spectral containment. Since the transmission medium does not destroy the orthogonality realized in the described mode, the insertion of cyclic extension is not necessary.

The length of the prototype filter, under the hypothesis of critical sampling, is an integer multiple of the number of subcarriers. This parameter is called overlap parameter and it is indicated by γ. Typical values of γ are between 8 and 20.

In Figure 1 and Figure 2, spectral characteristics of the first five subcarriers of FMT system with $N = 128$ are reported. Note that the spectral energy outside of a subchannel is suppressed by more than 70 dB, and this suppression increases as the length of the prototype filter becomes higher.

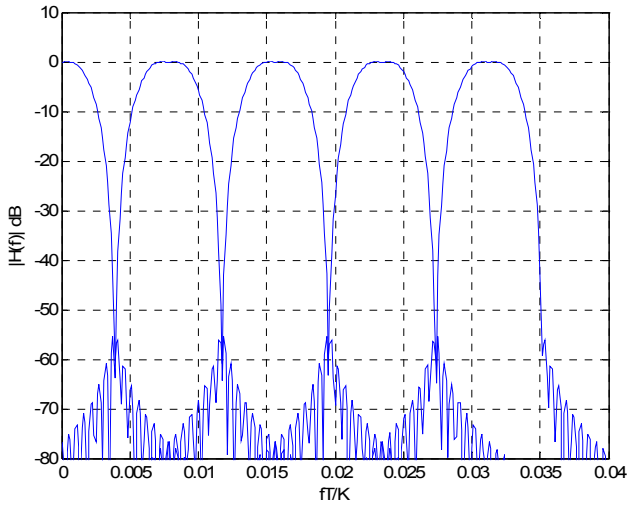

Figure 1: Spectral characteristics of the FMT signal for $\gamma = 8$.

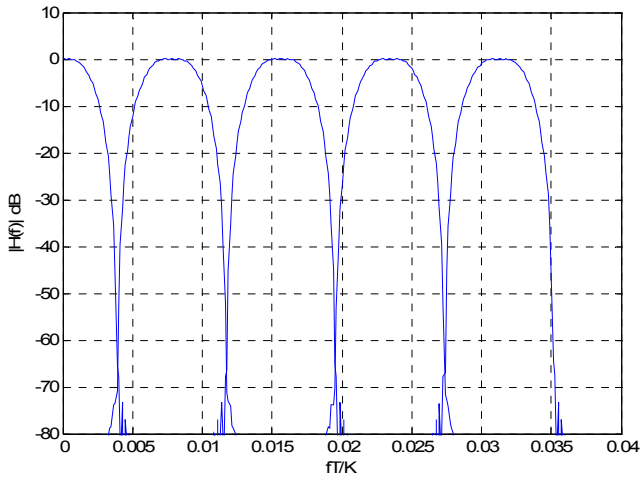

Figure 2: Spectral characteristics of the FMT signal for $\gamma = 16$ **.**

1.2 FMT Transmitter Model

In this section it is analyzed the realization of the FMT transmitter in the case of both critical sampled and noncritical sampled system. It is first presented the direct implementation and then due to its computational complexity it is derived the efficient implementation.

1.2.1 Critical Sampled FMT System

The direct implementation of a critical sampled FMT system is illustrated in Figure 3 [22].

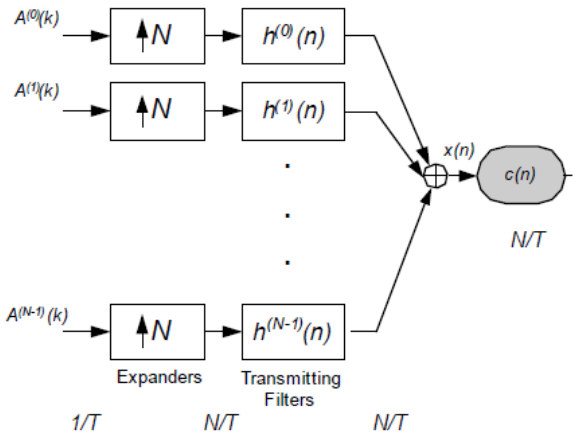

Figure 3: Direct implementation of FMT transmitter

After upsampling by a factor of N, each modulation symbol $A_i(k)$ is filtered at a rate N/T, where T is the FMT symbol period, by the subchannel filter

$$H^{(i)} = H^{(0)}\left(f - \frac{i}{T}\right) \underset{DTFT}{\Leftrightarrow}$$

$$\underset{DTFT}{\Leftrightarrow} h^{(i)}(n) = h^{(0)}(n) e^{j2\pi n \frac{i}{N}}, \qquad (1.3)$$

$$i = 0,\ldots,N-1,\ n = 0,\ldots,N\gamma - 1$$

centered at the frequency $f_i = i/T$. The transmitted signal (1.1) is obtained at the transmission rate N/T by adding together the N filter output signals that have been appropriately frequency shifted. Due to the impossibility of a physical implementation of a sharp filter, a spectral overlapping is present, as shown in Figure 4.

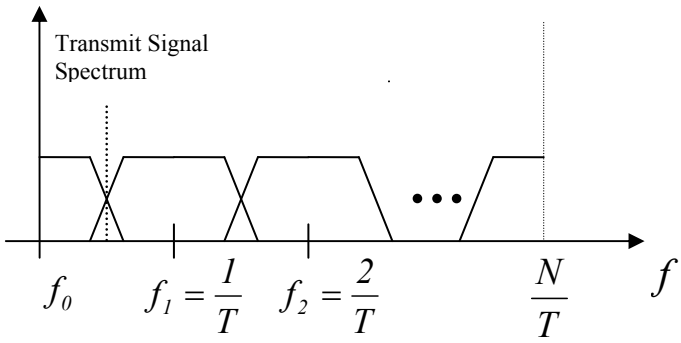

Figure 4: Subdivision in contiguous bands with overlapping

An efficient implementation of the system reported in
Figure 3 can be obtained by exploiting the polyphase representation of the filter responses [1].
Let us introduce the Z-transform of the prototype filter

$$H(z) = \sum_{n=-\infty}^{+\infty} h(n) z^{-n} \tag{1.4}$$

For any integer N, $H(z)$ can be decomposed in

$$\begin{aligned} H(z) &= \sum_{n=-\infty}^{+\infty} h(nM) z^{-nM} \\ &= z^{-1} \sum_{n=-\infty}^{+\infty} h(nM+1) z^{-nM} + \ldots \\ & z^{-(M-1)} \sum_{n=-\infty}^{+\infty} h(nM+M-1) z^{-nM} \end{aligned} \tag{1.5}$$

Therefore, the kth phase of $h(n)$ is defined as

$$h_{(k)}(m) = h(mN+k) \tag{1.6}$$

By sampling the transmitted signal (1.1) at a rate $T_c = \frac{1}{f_c} = \frac{1}{2W} = \frac{T}{N}$, we get

$$x[n] = x(nT_c)$$
$$= \sum_{i=0}^{N-1} \sum_{k=-\infty}^{+\infty} A_i(kT)\, h[n-kN]\, e^{j2\pi n \frac{i}{N}}. \quad (1.7)$$

By considering a change of variables $n = lN + m,\ 0 \le m \le N-1$, it is possible to introduce the polyphase components of the prototype filter

$$x[\,lN+m\,]$$
$$= \sum_{k=-\infty}^{+\infty} h[\,(l-k)N+m\,] \sum_{i=0}^{N-1} A_i(kT)\, e^{j2\pi i \frac{m}{N}} \quad (1.8)$$

or a in more synthetic form

$$x_{(m)}[l]$$
$$= \sum_{k=-\infty}^{+\infty} h_{(m)}[l-k] \left\{ \sum_{i=0}^{N-1} A_i(kT)\, e^{j2\pi i \frac{m}{N}} \right\} \quad (1.9)$$

The quantity $\sum_{i=0}^{N-1} A_i(kT)\, e^{j2\pi i \frac{m}{N}}$ represents the IDFT of the symbol sequence $A^{(i)}(kT)$, for $i = 0,...,N-1$ and evaluated for $m = 0,...,N-1$. Hence, we obtain

$$x_{(m)}[l] = \sum_{k=-\infty}^{+\infty} h_{(m)}[l-k]\ a_m(kT) \quad (1.10)$$

The mth output of the IFFT is filtered by the mth polyphase component of $h(n)$ and this filtering operation is performed at rate $1/T$ and not N/T. From (1.10), we can derive the efficient implementation of a critical sampled FMT system, shown in Figure 5.

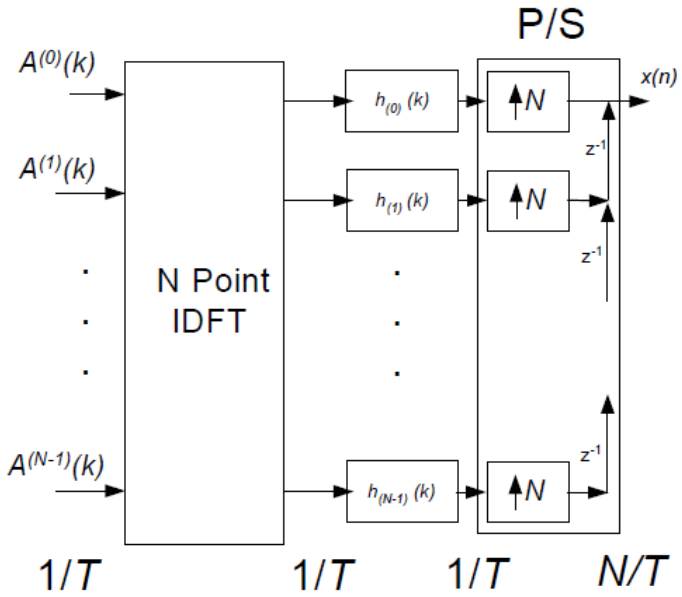

Figure 5: Efficient implementation of a critical sampled FMT transmitter

1.2.2 Noncritical Sampled FMT System

For a noncritical sampled filter bank, the bandwidth for each subcarrier is equal to K / NT, that is larger of that used in the case of critical sampling, since $K > N$. The number of subcarriers is N, therefore the subdivision of the transmit signal into contiguous bands is obtained without overlapping, as shown in Figure 6

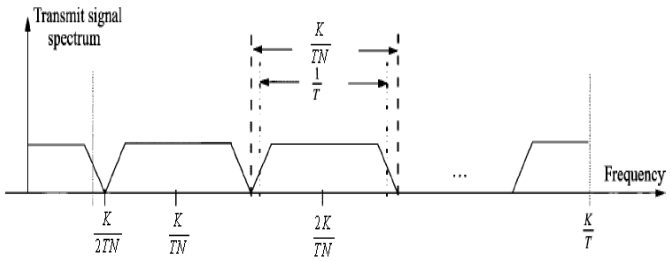

Figure 6: Subdivision in contiguous bands without overlapping

In the case of noncritical sampled filter banks, modulation with an excess bandwidth of $\frac{1+\alpha}{2T} = \frac{K}{2NT} \Rightarrow \alpha = \frac{K}{N} - 1$ within each subcarrier is feasible and ensures total spectral containment within a subcarrier. As K tends to N, the loss in bandwidth efficiency becomes vanishingly small at the price of an increase in implementation complexity because filters with increasingly sharper spectral roll-off must the be realized.

Figure 7 shows the direct implementation of a non critical sampled FMT system with N subcarriers.

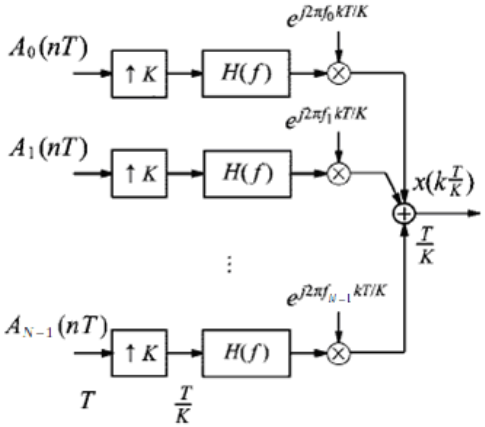

Figure 7: Direct implementation of a non critical sampled FMT transmitter

The complex-valued modulation symbols $A_m(nT),\ m=0,...,N-1$ are provided at the symbol rate of $\frac{1}{T}$. After upsampling by a factor K, each symbol stream is filtered by a proper shifted frequency version of the same prototype filter. The transmitted signal $x\left(k\frac{T}{K}\right)$ is obtained at the transmission rate of K/T by adding the N filter-output signals. By exploiting the polyphase decomposition, it is possible to derive an efficient implementation for the scheme in Figure 7. At time $k\frac{T}{K}$, the signal $x\left(k\frac{T}{K}\right)$ input to the channel is given by

$$\begin{aligned} x\left(k\frac{T}{K}\right) &= \sum_{m=0}^{N-1}\sum_{n=-\infty}^{+\infty} A_m(nT)h\left[\left(k-nK\right)\frac{T}{K}\right] \\ &\times e^{j2\pi m\left(K/NT\right)k\left(T/K\right)} \\ &= \sum_{n=-\infty}^{+\infty}\sum_{m=0}^{N-1} A_m(nT)\ h\left[k\frac{T}{K}-nT\right] \\ &\times e^{j2\pi m\left(K/NT\right)k\left(T/K\right)} \end{aligned} \tag{1.11}$$

By considering the change of variables $k\frac{T}{K}=\left(lN+i\right)\frac{T}{K},\ i=0,...,N-1$, we get

$$\begin{aligned} &x\left(lN\frac{T}{K}+i\frac{T}{K}\right) \\ &= \sum_{n=-\infty}^{+\infty} a_i\left(nT\right)h\left[lN\frac{T}{K}+i\frac{T}{K}-nT\right] \end{aligned} \tag{1.12}$$

where

$$a_i(nT) \triangleq \sum_{m=0}^{N-1} A_m(nT) e^{j2\pi m(K/NT)i(T/K)}, \quad i = 0,...,N-1$$

are the IDFT of $A_m(nT)$. Moreover, by adopting the general expression for signal interpolation where three indices are introduced

"filter index" $q = \left\lfloor \frac{lN+i}{K} \right\rfloor - n$

"basepoint index" $\eta_{l,i} = \left\lfloor \frac{lN+i}{K} \right\rfloor$

"fractional index" $\nu_{l,i} = \frac{lN+i}{K} - \eta_{l,i}$

we obtain

$$\begin{aligned} & x\left(lN\frac{T}{K} + i\frac{T}{K} \right) \\ & = \sum_{q=-\infty}^{+\infty} a_i\left[(\eta_{l,i} - q)T \right] h\left[(\nu_{l,i} + q)T \right] \\ & = \sum_{q=-\infty}^{+\infty} a_i\left[(\eta_{l,i} - q)T \right] h^{\nu_{l,i}K}(qT), \end{aligned} \tag{1.13}$$

$i = 0,...,N-1$

where $0 \le \nu_{l,i} < 1$ and $\nu_{l,i}K = (lN+i)_{\mathrm{mod}\,K}$. Therefore, the transmit signal at time $k\frac{T}{K}$ is computed by convolving the signal samples stored in the $(k \bmod K)$ th polyphase component with respect to K of the prototype filter. The integer number $\nu_{l,i}K$ provides the address of the polyphase component that needs to be applied at the $(k \bmod N)$ th output of the IDFT to generate the transmitted signal

$x\left(k\frac{T}{K}\right)$. Hence, each element of the IDFT output frame is filtered by a periodically time-varying filter with period equal to $\left[lcm\left(N,K\right)\right]T/K$, where $\left[lcm\left(N,K\right)\right]$ stands for least common multiple of N and K [2].

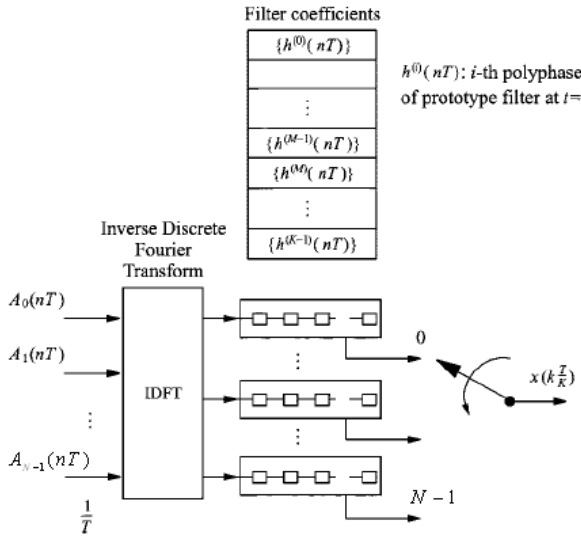

Figure 8: Efficient implementation of a noncritical sampled FMT transmitter

1.3 FMT Receiver Model

In the presence of AWGN $w(t)$, the time-continuous received signal is given by

$$y(t) = x(t) + w(t) \tag{1.14}$$

In the receiver filter bank architecture (shown in Figure 9) the receiving filters $\left\{g^{(i)}(n)\right\}$ are designed to be matched to the corresponding ones in the transmitter i.e., $G_{(i)}(f)=\left(H_{(i)}(f)\right)^{*}$, $i=0,...,N-1$.

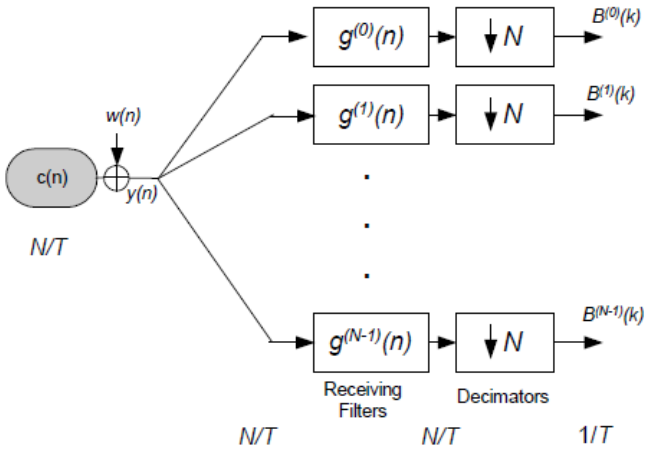

Figure 9: Direct implementation of a FMT receiver (critical sampling)

By using the fact that the inverse Fourier Transform of $\left(H_{(i)}(f)\right)^{*}$ is $h^{*}_{(i)}(-n)$, we get

$$g_{(i)}'(n)=\left(h_{(i)}(-n)\right)^{*}, \quad i=0,...,N-1,\ n=-N\gamma+1,...,-1,0 \tag{1.15}$$

However, this filter is not causal. Since $g'(n)$ is defined for $n=-N\gamma+1,...,-1,0$, we need to apply a minimum delay of $N\gamma-1$ samples to make it causal. Specifically, we delay it of $N\gamma$ samples and we call this response $g_{(i)}(n)$. This delay is what will allow us to define the efficient implementation. We should

note that since we are using multirate blocks, this difference of one sample makes a change to the overall response of the filter. In the efficient implementation, it will also allow us to take blocks of N samples in a different way, otherwise, there will be an offset in the way we take the blocks of samples in the transmitter and in the receiver. Applying the delay to the receiver filters in (1.15) we obtain

$$g_{(i)}(n) = g'_{(i)}(n - N\gamma) \tag{1.16}$$

1.3.1 Critical Sampled FMT System

The time-continuous received signal is given by

$$y(t) = \sum_{i=0}^{N-1} \sum_{k=-\infty}^{+\infty} A_i(kT) h(t - kT) \times e^{j2\pi f_i t} + w(t) \tag{1.17}$$

By sampling at a rate $T_c = \frac{T}{N}$ and taking into account that $f_i = \frac{i}{T}$, we get

$$y[n] = \sum_{i=0}^{N-1} \sum_{k=-\infty}^{+\infty} A_i(kT) h[n - kN] \times e^{j2\pi n \frac{i}{N}} + w[n] \tag{1.18}$$

From (1.15) and (1.16), we can derive the expression of the filter on the receiver side

$$
\begin{aligned}
g_{(i)}[n] &= \left(h_{(i)}\left[-(n-N\gamma)\right]\right)^* \\
&= h\left[-(n-N\gamma)\right]\, e^{j\frac{2\pi}{N}(n-N\gamma)i} \\
&= h\left[N\gamma-n\right]e^{j\frac{2\pi}{N}ni}, \\
&i=0,...,N-1 \quad n=1,...,N\gamma
\end{aligned}
\tag{1.19}
$$

Since $h(n)$ is symmetric, then the receiver filter at the ith subcarrier is

$$
g_{(i)}[n] = h[\,n-1\,]e^{j2\pi\frac{ni}{N}},\ n=1,...,N\gamma \tag{1.20}
$$

By applying (1.19), at the output of the ith subcarrier in Figure 9, we obtain

$$
\begin{aligned}
B_{(i)}(kT) &= \sum_{n=1}^{N\gamma} y[kN-n]\, g_{(i)}(n) \\
&= \sum_{n=1}^{N\gamma} y[kN-n]\, h[\,n-1\,]e^{j2\pi\frac{ni}{N}}
\end{aligned}
\tag{1.21}
$$

To introduce the polyphase components of $h(n)$ defined in (1.6), we decompose n as $n=lN+t$, $l=0,1,...,\gamma-1$ and $t=1,2,...,N$ to yield

$$
\begin{aligned}
B_{(i)}(kT) &= \sum_{t=1}^{N}\sum_{l=0}^{\gamma-1} y[kN-lN-t] \\
&\times h[\,lN+t-1\,]e^{j2\pi\frac{(lN+t)\,i}{N}} \\
&= \sum_{t=1}^{N}\sum_{l=0}^{\gamma-1} y[(k-l)N-t]\; h[\,lN+t-1\,] \\
&\times e^{j2\pi\frac{ti}{N}}
\end{aligned}
\tag{1.22}
$$

If we make a change of variable $m=t-1$, the equation (1.22) becomes

$$B_{(i)}(kT)=\sum_{m=0}^{N-1}\sum_{l=0}^{\gamma-1}y\left[(k-l)N-(m+1)\right] \times h\left[\,lN+m\,\right]e^{j2\pi\frac{(m+1)i}{N}} \tag{1.23}$$

By applying

$$e^{j\frac{2\pi}{N}(m+1)i}=e^{-j\frac{2\pi}{N}(N-m-1)i} \tag{1.24}$$

we get

$$B_{(i)}(kT)=\sum_{m=0}^{N-1}\sum_{l=0}^{\gamma-1}y\left[(k-l)N-m-1\right] \times h_{(m)}[l]e^{-j2\pi\frac{(N-m-1)i}{N}} \tag{1.25}$$

From (1.25), we are able to derive the efficient implementation shown in Figure 10 where we apply the DFT operation (efficiently implemented with the FFT) to the N outputs of the N polyphase filters.

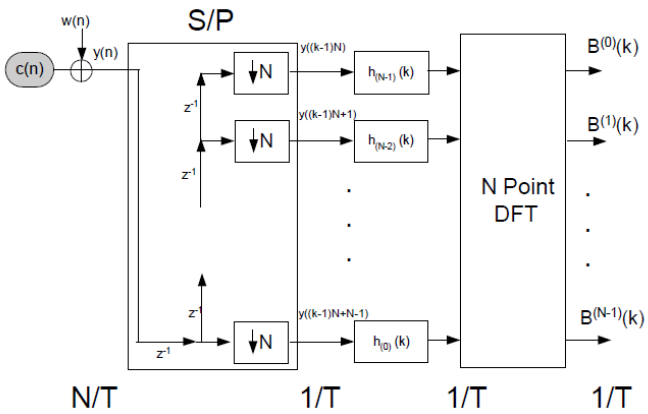

Figure 10: Efficient implementation of a critical sampled FMT receiver

We can make some comments about (1.25) to see how the efficient implementation is derived.

- Since the receiving filters are defined as in (1.20), and due to the downsampler in Figure

10, the first output in the receiver filter bank will be at $k=1$ (N samples at rate N/T) and not at $k=0$.

- If we analyze (1.25), we will see that for $k=1$, we need the inputs $[y(0),...,y(N-1)]$. This is consistent with what we do in the efficient implementation shown in Figure 10.
- The polyphase components of $h(n)$ are in reverse order with respect the DFT. That is why the first polyphase component in Figure 10 is in the last branch of the filter bank.

We can also see from (1.25) that the implementation in Figure 10 is mirrored (matched) to the implementation in Figure 5. Since the prototype is symmetric and has $N\gamma$ samples, for each of the polyphase components $h_{(i)}(n)=h(nN+i)$, the matched filter is actually

$h(nM+M-1-i)=h_{(M-1-i)}(n),\ i=0,1,...M-1$.

That is why they are in reverse order to the ones in Figure 5, since the whole implementation is matched to that of Figure 5 [22].

1.3.2 Noncritical Sampled FMT System

In figure, it is reported the direct implementation of a noncritical sampled FMT receiver. The main difference with respect to the case of critical sampling is the fact that the downsampling factor is $K>N$.

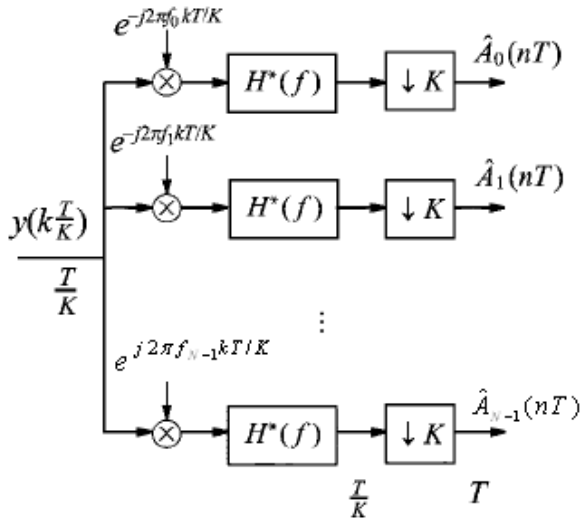

Figure 11: Direct implementation of a noncritical sampled FMT receiver

In the following it will be derived the efficient implementation of a noncritical sampled FMT receiver. We assume for the received signal the same sampling rate as for the transmitted signal and consider in general a downsampling factor $L \le K$ (i.e. in Figure 11 replace $\downarrow K$ with $\downarrow L$). The received signal $y\left(k\frac{T}{K}\right)$ and the filtering elements on the N branches are given by the polyphase components with respect to N of a prototype filter $\{g(kT/K)\}$ with T/K -spaced coefficients, defined as

$$g_{(m)}(l) = g\left[(lN+m)\left(\frac{T}{K}\right)\right], \qquad (1.26)$$

$$m = 0,\ldots,N-1$$

The *i*th output signal of the FMT demodulator at time $n'(L/K)T$ is given by

$$B_{(i)}\left(n'\frac{L}{K}T\right)=\sum_{k=-\infty}^{+\infty}y\left(k\frac{T}{K}\right)\times e^{-j2\pi i\left(\frac{K}{NT}\right)k\frac{T}{K}}g\left[\left(Ln'-k\right)\frac{T}{K}\right] \tag{1.27}$$

By letting $k\frac{T}{K}=\left(lN+m\right)\frac{T}{K}$, $m=0,1,...N-1$, (1.27) becomes

$$B_{(i)}\left(n'L\frac{T}{K}\right)=\sum_{m=0}^{N-1}\sum_{l=-\infty}^{+\infty}y\left(\left(lN+m\right)\frac{T}{K}\right)\times\ g\left[\left(Ln'-lN-m\right)\frac{T}{K}\right]e^{-j2\pi\frac{im}{N}} \tag{1.28}$$

(1.28) can be simplified as

$$B_{(i)}\left(n'L\frac{T}{K}\right)=\sum_{m=0}^{M-1}u_m\left(n'L\frac{T}{K}\right)e^{-j2\pi\frac{im}{N}} \tag{1.29}$$

where

$$u_m\left(n'L\frac{T}{K}\right)\triangleq\sum_{l=-\infty}^{+\infty}y\left(\left(lN+m\right)\frac{T}{K}\right)\times g\left[\left(Ln'-lN-m\right)\frac{T}{K}\right],\quad m=0,...,N-1 \tag{1.30}$$

It is evident that $B_{(i)}\left(n'L\left(T/K\right)\right)$, $i=0,...,N-1$ are obtained from $u_m\left(n'L\left(T/K\right)\right)$, $m=0,...,N-1$, via discrete Fourier transform. Moreover, if we define the polyphase components with respect to N of the received signal as

$$y_{(m)}\left(l\frac{NT}{K}\right)=y\left[\left(lN+m\right)\frac{T}{K}\right],\quad m=0,...,N-1 \tag{1.31}$$

and introduce

- "filter index" $q' = \left\lfloor \frac{Ln' - m}{N} \right\rfloor - l$
- "basepoint index" $\eta'_{n',m} = \left\lfloor \frac{Ln' - m}{N} \right\rfloor$
- "fractional index" $\nu'_{n',m} = \frac{Ln' - m}{N} - \eta'_{n',m}$

we obtain

$$u_m\left(n'L\frac{T}{K}\right) \triangleq \sum_{l=-\infty}^{+\infty} y_{(m)}\left(\eta'_{n',m} - q'\right) \times g_{\left(\nu'_{n',m}N\right)}\left(q'\right) \tag{1.32}$$

Note that if the receive prototype filter is causal and matched to the transmit prototype filter, i.e.

$$g\left(n'\frac{T}{K}\right) = h^*\left(\gamma N - n'\frac{T}{K}\right) \tag{1.33}$$

where $N\gamma$ denotes the length of the filter $h(n)$, (1.32) becomes

$$u_m\left(n'L\frac{T}{K}\right) \triangleq \sum_{l=-\infty}^{+\infty} y_{(m)}\left(\eta'_{n',m} - q'\right) \times h^*\left[\left(l + \gamma + \frac{m - Ln'}{N}\right)\frac{NT}{K}\right], \tag{1.34}$$

$m = 0,\ldots,N-1$

In general, a new DFT output frame at time $kT/K = n'LT/K$ is obtained by the following method (see Figure 12): the commutator is circularly rotated L steps from its position at time $\left(n'-1\right)/T$, allowing a set of L consecutive received signals $y\left(kT/K\right)$ to be input into the N delay lines. The content of each delay line is then convolved with a

polyphase component (with respect to N) of the receive prototype filter. The integer number $\nu'_{n',m} N$ provides the address of the polyphase component that needs to be applied at the mth branch. The resulting signals are then input to the DFT to finally yield the signals $B_{(i)}\left(n' L\left(T/K\right)\right)$, $i = 0,1,...,N-1$. Note that the DFT output frames are obtained at the rate of $\left(K/L\right)/T$. Clearly, it is possible to consider in general a FMT system where the sampling rate of the analog-to-digital (A/D) converter is given by K'/T, with $K' > K$. In this case a digital interpolation filter is first employed to convert the rate of the received signal samples from K'/T to K/T. The obtained signal is then input to the FMT demodulator [2].

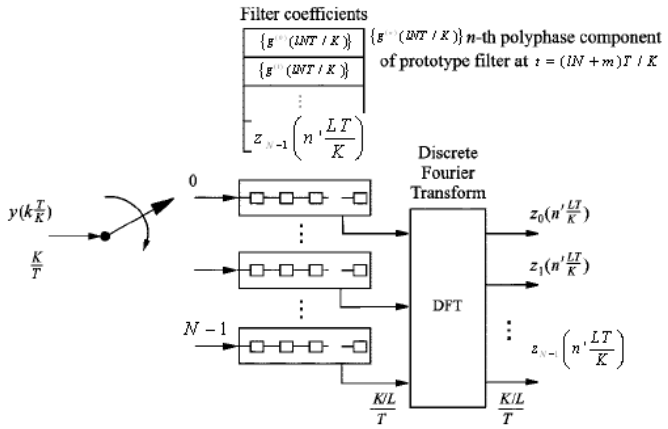

Figure 12: Efficient implementation of a noncritical sampled FMT receiver

1.4 OFDM/OQAM Systems

The main idea of OFDM/OQAM systems is to transmit the real and imaginary part of QAM symbol shifted of half a symbol period by exploiting filters that guarantee the orthogonality between subcarriers. In Figure 13 it is shown an OFDM/OQAM system with N subcarriers frequency-separated of $1/T$, where T is the symbol period. The time-continuous transmitted signal is given by

$$s(t)=\sum_{k=0}^{N-1}\sum_{n=-\infty}^{+\infty} e^{j\left(\frac{2\pi}{T}t+\frac{\pi}{2}\right)k}\left[a_k^R(n)g\left(t-nT\right)\right. \\ \left.+ja_k^I(n)g\left(t-nT-\frac{T}{2}\right)\right] \tag{1.35}$$

where $g(t)$ is the prototype filter, $a_k^R(n)$ and $a_k^I(n)$ denote the real and imaginary part of the complex data symbol transmitted on the kth subcarrier of the nth OFDM/OQAM symbol.

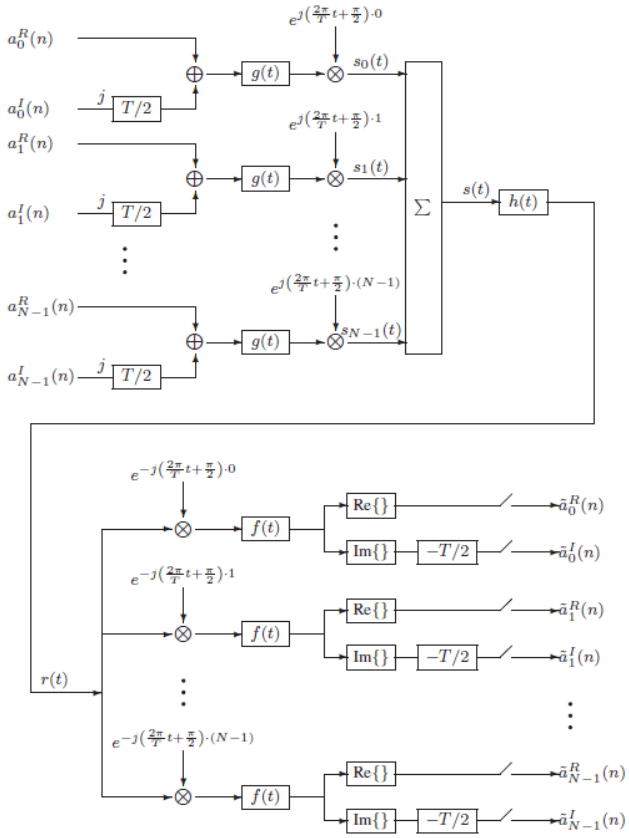

Figure 13: OFDM/OQAM system model

1.5 OFDM/OQAM Transmitter Model

By sampling the transmitted signal (1.35) at a rate of $T_c = T / N$, we get

$$s(l)=\sum_{k=0}^{N-1}\sum_{n=-\infty}^{+\infty}e^{j\left(\frac{2\pi}{N}l+\frac{\pi}{2}\right)k}\left[a_k^R(n)g\left(l-nN\right)+ja_k^I(n)g\left(l-nN-\frac{N}{2}\right)\right] \tag{1.36}$$

where $s(l)=s\left(lT/N\right)$.

Note that (1.36) can be written as

$$s(l)=s_R(l)+js_I(l) \tag{1.37}$$

where

$$s_R(l)=\sum_{k=0}^{N-1}\sum_{n=-\infty}^{+\infty}e^{j\left(\frac{2\pi}{N}l+\frac{\pi}{2}\right)k}a_k^R(n)g\left(l-nN\right) \tag{1.38}$$

and

$$s_I(l)=\sum_{k=0}^{N-1}\sum_{n=-\infty}^{+\infty}e^{j\left(\frac{2\pi}{N}l+\frac{\pi}{2}\right)k}a_k^I(n)\times g\left(l-nN-N/2\right) \tag{1.39}$$

By exploiting the same procedure as seen in the case of FMT transmitter, it is possible to derive an efficient implementation of the OFDM/OQAM transmitter. Let us take into account first the contribute (1.38). By considering a change of variables $l=qN+m,\ 0\le m\le N-1$, it is possible to introduce the polyphase components of the prototype filter

$$s_{(m)}^R[q]=\sum_{k=-\infty}^{+\infty}g_{(m)}[q-n]\sum_{k=0}^{N-1}j^k a_k^R\left(n\right)e^{j\frac{2\pi}{N}km} \tag{1.40}$$

and consequently

$$s_{(m)}^I[q]=\sum_{k=-\infty}^{+\infty}g_{(m)}[q-n-1/2]\sum_{k=0}^{N-1}j^k a_k^I\left(n\right)e^{j\frac{2\pi}{N}km}. \tag{1.41}$$

Therefore, the efficient implementation of the OFDM/OQAM system can be obtained as follows [23]

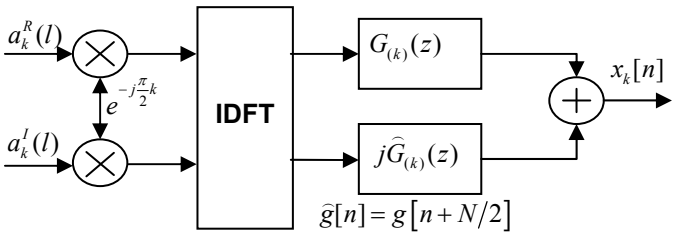

Figure 14: Efficient implementation of the *k*th subcarrier of the OFDM/OQAM transmitter

In Figure 15 it is shown the filter bank implementation of the OFDM/OQAM transmitter. We can note that the oversampling factor is equal to $N/2$.

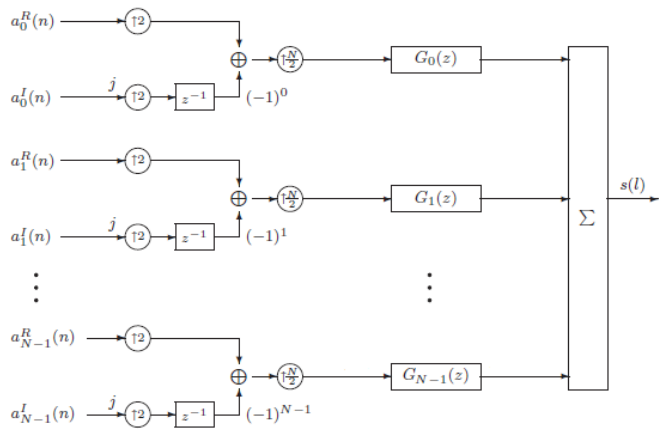

Figure 15: Filter bank implementation of the OFDM OQAM transmitter

1.6 OFDM/OQAM Receiver Model

In order to derive an efficient implementation of the OFDM/OQAM receiver, we consider the received signal after a LTI channel with impulse response $h(l)$. The impulse response of the equivalent channel made up of the mth transmitted subcarrier and the kth received subcarrier is given by

$$p_{m,l}(k) = j^{m-k}\left[g(l)e^{j\frac{2\pi}{N}(m-k)l} \right] \otimes \left[h(l)e^{-j\frac{2\pi}{N}kl} \right] \otimes f(l). \tag{1.42}$$

The received sequence on the kth subcarrier is

$$\begin{aligned} r_k(l) &= r(l)e^{j\left(\frac{2\pi}{N}l+\frac{\pi}{2}\right)k} \otimes f(l) \\ &= \sum_{m=0}^{N-1}\sum_{n=-\infty}^{+\infty}\left[a_m^R(n)p_{m,k}(l-nN) \right. \\ &\left. + ja_m^I(n)p_{m,k}(l-nN-N/2) \right] \end{aligned} \tag{1.43}$$

where $f(l)$ is the matched filter to $g(l)$.

In order to derive a filter bank implementation, it is useful to define the impulse response of the equivalent filter of the kth subcarrier as

$$f_k(l) = (-j)^k f(l)e^{-j\frac{2\pi}{N}kl} \tag{1.44}$$

Therefore, (1.43) becomes

$$
\begin{aligned}
r_k(l) &= r(l)e^{j\left(\frac{2\pi}{N}l+\frac{\pi}{2}\right)k} \otimes f(l) \\
&= (-j)^k \sum_{l'=-\infty}^{+\infty} r(l-l')f(l')e^{-j\frac{2\pi}{N}kl} \\
&= \left[r(l) \otimes f_k(l)\right]e^{j\frac{2\pi}{N}kl}
\end{aligned}
\tag{1.45}
$$

Down-sampling by $N/2$ times the received subchannel sequence $r_k(l)$ and taking the real and imaginary parts alternately, we get the received symbols

$$
\begin{aligned}
\hat{a}_k^R(n) &= \Re\left\{r_k(l)\right\}\Big|_{l=nN} \\
\hat{a}_k^I(n) &= \Im\left\{r_k(l)\right\}\Big|_{l=nN+N/2}
\end{aligned}
\tag{1.46}
$$

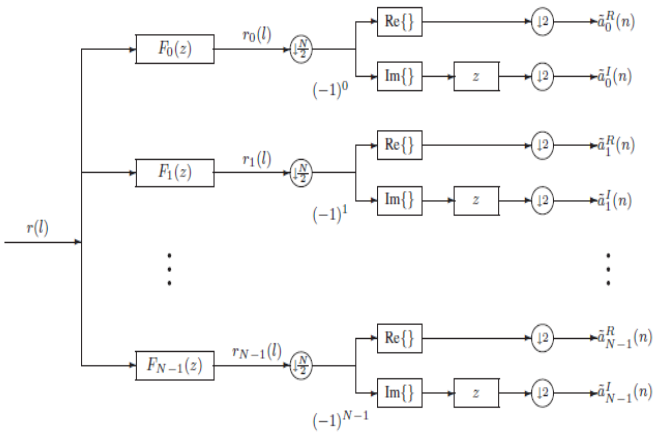

Figure 16: Efficient implementation of the OFDM/OQAM receiver

1.7 Prototype Filter Design

In the FBMC modulation, the prototype filter completely defines the system. The choice of the prototype filter for the realization of the polyphase filter bank allows various tradeoffs among the number of subcarriers, the level of spectral containment, the complexity of implementation and signal latency to be made. These tradeoffs are possible because the number of subcarriers can be reduced without incurring a transmission efficiency loss, whereas in OFDM the minimum number of subcarriers is constrained by efficiency requirements owing to the use of the cyclic prefix. The prototype filter has to demonstrate a good time-frequency localization to increase spectral efficiency and, moreover, it has to satisfy orthogonality conditions (see Appendix A for further details) to destroy, at least in the case of ideal channel, ISI and ICI.

The orthogonality conditions, in the case of ideal channel, can be written as

$$\Re\left\{ j^k \int_{-\infty}^{+\infty} g(\tau) f\left(nT-\tau\right) e^{j\frac{2\pi}{T}k\tau} d\tau \right\} = \delta(k)\delta(n) \tag{1.47}$$

$$\Im\left\{ j^k \int_{-\infty}^{+\infty} g(\tau) f\left(nT-\tau-T/2\right) e^{j\frac{2\pi}{T}k\tau} d\tau \right\} = 0 \tag{1.48}$$

It is possible to shown that the orthogonality conditions are both satisfied if

- $g(t)$ and $f(t)$ are bound limited in the range $\left[-1/T, 1/T\right]$.
- $g(t) \equiv f(t)$ are symmetric real-valued filters.
- $\rho(t) = g(t) \otimes f(t)$ satisfies Nyquist criterion.

A possible choice for the prototype filter is represented by the SRRC filter whose frequency response is given by

$$X(f) = \begin{cases} T \quad for \quad 0 \le |f| \le \dfrac{1-\alpha}{2T} \\ \dfrac{T}{2}\left[1 + \cos\dfrac{\pi T}{\alpha}\left(|f| - \dfrac{1-\alpha}{2T}\right)\right] \\ for \quad \dfrac{1-\alpha}{2T} \le |f| \le \dfrac{1+\alpha}{2T} \\ 0 \quad for \quad |f| \ge \dfrac{1+\alpha}{2T} \end{cases} \tag{1.49}$$

where $0 \le \alpha \le 1$ is the roll-off factor.

To design the prototype filter is also possible to exploit the so-called frequency sampling technique, which is presented with the following parameters $L = 2048,\ N = 512,\ K = 4$ [24].

The design starts with the determination of L desired values $H(k/L),\ 0 \le k \le L-1$ in the frequency domain by

$$\begin{aligned} &H(0) = 1 \\ &H(1/L) = 0.971960 \\ &H(2/L) = 1/\sqrt{2} \\ &H(3/L) = \sqrt{1 - H^2(1/L)} = 0.235147 \\ &H(k/L) = 0 \quad \text{for} \quad 4 \le k \le L-1 \end{aligned} \tag{1.50}$$

Then, the prototype filter coefficients are obtained by IDFT as

$$h(m) = 1 + 2\sum_{k=1}^{K-1}(-1)^k H(k/L)$$
$$\times \cos(2\pi km/L) \quad \text{for} \quad 1 \le m \le L-1 \qquad (1.51)$$
$$h(0) = 0$$

In fact, the condition $h(0) = 0$ determines the desired values $H(1/L)$ and $H(3/L)$. It is useful to make the number of coefficients an odd number, in which case the filter delay can be adjusted to be an integer number of sample periods. The frequency response obtained is shown in Figure 17. In this figure, the sub-channel spacing Δf is taken as unity (Δf =1). It is important to notice that the filter attenuation exceeds 60 dB for the frequency range above 2 sub-channel spacing.

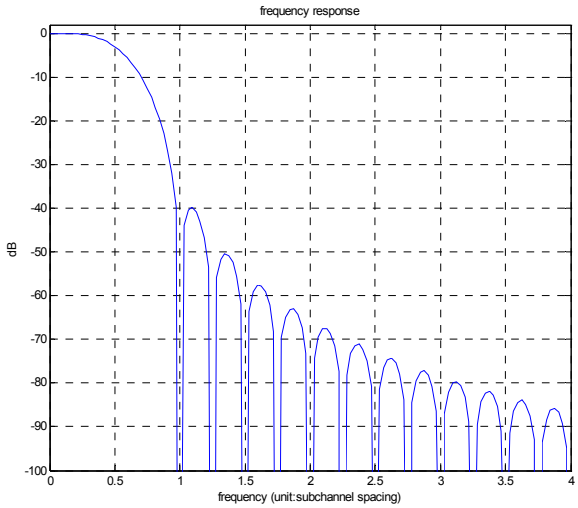

Figure 17: Frequency response of the prototype filter

Chapter 2

Sensitivity of FBMC Systems to Synchronization Errors

In this chapter the sensitivity of FBMC systems to synchronization errors in both the uplink and the downlink scenarios is investigated. In particular, the performance degradation caused by synchronization errors is evaluated analytically and with numerical simulations and compared with that of OFDM systems. It is shown that, as all multicarrier systems, FBMC systems are very sensitive to synchronization errors, since timing errors and carrier frequency offsets produce intercarrier interference and interference between successive symbols, which can lead to a severe performance degradation. However, in an asynchronous multi-user scenario FBMC systems are more robust than OFDM systems to time and frequency misalignments among the users.

2.1 Downlink Synchronization Tasks

In this section the effects of time and frequency synchronization errors in an FBMC-based downlink transmission are investigated. From a physical layer

perspective, the multiuser FBMC downlink is equivalent to a single user FBMC system. The only difference is that in a multiuser system the transmitted signal conveys the information for multiple users while in a single user scenario the transmitted block carries information data for only one subscriber.

2.1.1 OFDM/OQAM System Model with Synchronization Errors

Let us consider an OFDM/OQAM system with N subcarriers of which N_u are modulated by data symbols and $N_v = N - N_u$ remain unmodulated (virtual subcarriers). As indicated in Figure 18, the real and imaginary parts of the transmitted complex data symbol $a_l^R(p)$ and $a_l^R(p)$ are separated in time by $T/2$ and transmitted in parallel on the N subchannels. Each subchannel is then shaped by a prototype filter with impulse response $g(t)$ and successively the N contributes are summed up giving the $T_s = T/N$ sampled multicarrier signal

$$\begin{aligned} s(kT_s) = \sqrt{\frac{N}{2N_u}} \sum_{p=-\infty}^{+\infty} \sum_{l \in \mathcal{A}} e^{jl\left(\frac{2\pi}{T} kT_s + \frac{\pi}{2}\right)} \\ \times \Big[a_l^R(p) g\left(kT_s - pT\right) \\ + j a_l^I(p) g\left(kT_s - pT - T/2\right) \Big] \end{aligned} \tag{2.1}$$

In (2.1), $\mathcal{A}$ denotes the set of indices of data subcarriers, T is the signalling interval and $g(t)$ is the real pulse shaping filter with unit energy and assumed to be a SRRC Nyquist filter with roll-off factor α $(0 \le \alpha \le 1)$.

The transmitted sequence $s(kT_s)$ feeds a digital-to-analog converter (DAC) and propagates trough a physical channel characterized by AWGN noise $n(t)$ with a power spectral density $S_n(f) = \sigma_n^2$. The received signal $r(t)$ is filtered with an ideal low pass filter with a bandwidth of $1/T_s$ and sampled with frequency $f_s = 1/T_s$, yielding the sequence

$$r(kT_s) = e^{j(2\pi\Delta f T_s k + \phi)} s(kT_s - \tau) + n(kT_s) \qquad (2.2)$$

where τ is the timing offset, Δf the CFO and ϕ the carrier phase offset, moreover $n(kT_s)$ denotes the zero-mean circular complex white Gaussian noise with a variance σ_n^2 / T_s.

In subchannel m at the receiver side, the received sequence $r(kT_s)$ is first down-converted by multiplying with $e^{-j\left(\frac{2\pi}{T}kT_s + \frac{\pi}{2}\right)m}$, then filtered by the matched filter $\tilde{g}(kT_s)$ to generate the signal

$$y_m(kT_s) = r(kT_s) e^{-j\left(\frac{2\pi}{T}kT_s + \frac{\pi}{2}\right)m} \otimes \tilde{g}(kT_s) \qquad (2.3)$$

Down-sampling by $N/2$ times the received subchannel sequence $y_m(kT_s)$ and taking the real and imaginary parts alternately, we get the received symbols:

$$\tilde{a}_m^R(k) = \Re\left\{ y_m\left(qT_s\right)\Big|_{q=kN} \right\} \tag{2.4}$$

$$\tilde{a}_m^I(k) = \Re\left\{ y_m\left(qT_s\right)\Big|_{q=kN+N/2} \right\} \tag{2.5}$$

Substituting (2.3) in (2.4) and (2.5) and accounting for the expression of the received signal we obtain

$$\begin{aligned}
\tilde{a}_m^R(k) &= \Re\left\{ r\left(qT_s\right)e^{-j\left(\frac{2\pi}{T}qT_s+\frac{\pi}{2}\right)m} \otimes \tilde{g}\left(qT_s\right)\Big|_{q=kN} \right\} \\
&= a_m^R(k)\Re\left\{ p_{m,m}^{\Delta f}(-\tau)e^{j\left(\phi-\frac{2\pi}{T}\tau m\right)} \right\} \\
&+ \sum_{\substack{m'\in\mathcal{A}\\ m'\neq m}} a_{m'}^R(k)\Re\left\{ p_{m',m}^{\Delta f}(-\tau)e^{j\left(\phi-\frac{2\pi}{T}\tau m\right)} \right\} \\
&+ \sum_{m'\in\mathcal{A}} \sum_{\substack{k'=-\infty\\ k'\neq k}}^{+\infty} a_{m'}^R(k') \\
&\times\Re\left\{ p_{m',m}^{\Delta f}\left(\left(k'-k\right)NT_s-\tau\right)e^{j\left(\phi-\frac{2\pi}{T}\tau m\right)} \right\} \\
&- \sum_{m'\in\mathcal{A}} \sum_{k'=-\infty}^{+\infty} a_{m'}^I(k') \\
&\times\Im\left\{ p_{m',m}^{\Delta f}\left(\left(k'-k\right)NT_s-NT_s/2-\tau\right)e^{j\left(\phi-\frac{2\pi}{T}\tau m\right)} \right\} \\
&+\Re\left\{ n\left(qT_s\right)e^{-j\left(\frac{2\pi}{T}qT_s+\frac{\pi}{2}\right)m} \otimes \tilde{g}\left(qT_s\right)\Big|_{q=kN} \right\}
\end{aligned} \tag{2.6}$$

and

$$
\begin{aligned}
&\tilde{a}_m^I(k) \\
&= \Im\left\{ r\left(qT_s\right) e^{-j\left(\frac{2\pi}{T} qT_s + \frac{\pi}{2}\right)m} \otimes \tilde{g}\left(qT_s\right) \Big|_{q=kN+N/2} \right\} \\
&= a_m^I(k) \Im\left\{ \breve{p}_{m,m}^{\Delta f}(-\tau) e^{j\left(\phi - \frac{2\pi}{T}\tau m\right)} \right\} \\
&+ \sum_{\substack{m' \in \mathcal{A} \\ m' \neq m}} a_{m'}^I(k) \Im\left\{ \breve{p}_{m',m}^{\Delta f}(-\tau) e^{j\left(\phi - \frac{2\pi}{T}\tau m\right)} \right\} \\
&+ \sum_{m' \in \mathcal{A}} \sum_{\substack{k'=-\infty \\ k' \neq k}}^{+\infty} a_{m'}^I(k') \\
&\times \Im\left\{ \breve{p}_{m',m}^{\Delta f}\left(\left(k'-k\right)NT_s - \tau\right) e^{j\left(\phi - \frac{2\pi}{T}\tau m\right)} \right\} \\
&- \sum_{m' \in \mathcal{A}} \sum_{k'=-\infty}^{+\infty} a_{m'}^R(k') \\
&\times \Re\left\{ p_{m',m}^{\Delta f}\left(\left(k'-k\right)NT_s + NT_s/2 - \tau\right) e^{j\left(\phi - \frac{2\pi}{T}\tau m\right)} \right\} \qquad (2.7) \\
&+ \Im\left\{ n\left(qT_s\right) e^{-j\left(\frac{2\pi}{T} qT_s + \frac{\pi}{2}\right)m} \otimes \tilde{g}\left(qT_s\right) \Big|_{q=kN+N/2} \right\}
\end{aligned}
$$

where

$$
\begin{aligned}
&p_{m',m}^{\Delta f}\left(\left(k'-k\right)NT_s - \tau\right) \triangleq \sqrt{\frac{N}{2N_u}} j^{m'-m} \\
&\times \left\{ \tilde{g}\left(qT_s\right) \otimes \left[e^{j2\pi q\left(\Delta f T_s + \frac{m'-m}{N}\right)} \right.\right. \qquad (2.8) \\
&\left.\left. \times g\left(qT_s - k'NT_s - \tau\right) \right] \right\} \Big|_{q=kN}
\end{aligned}
$$

$$\breve{p}_{m',m}^{\Delta f}\left(\left(k'-k\right)NT_s-\tau\right)\triangleq\sqrt{\frac{N}{2N_u}}j^{m'-m}$$
$$\times\left\{\tilde{g}\left(qT_s\right)\otimes\left[e^{j2\pi q\left(\Delta fT_s+\frac{m'-m}{N}\right)}\right.\right. \tag{2.9}$$
$$\left.\left.\times g\left(qT_s-k'NT_s-\tau\right)\right]\right\}\Big|_{q=kN+N/2}$$

From (2.6) and (2.7) we can note that in the presence of frequency and timing synchronization errors, the useful term is subject to an attenuation and a phase rotation related to the subchannel index m, the timing offset τ, the phase offset ϕ, the CFO Δf and the index of the information symbol k. Furthermore, intercarrier interference, intersymbol interference and interference between real and imaginary part of data symbols are present.

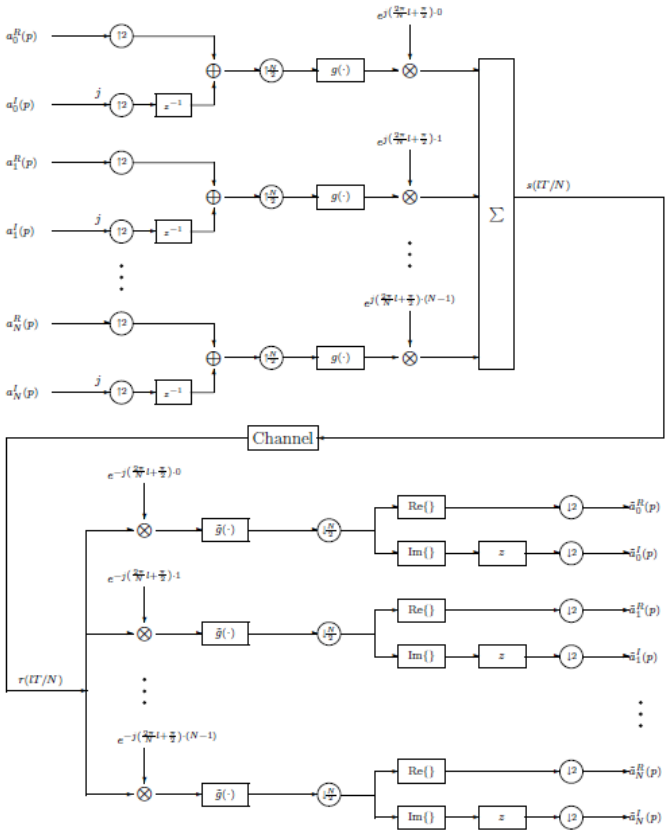

Figure 18: OFDM/OQAM System

2.1.2 FMT System Model with Synchronization Errors

Into the case of an FMT system, as shown in Figure 19, the baseband discrete-time transmitted signal obtained by sampling the continuous-time signal

with a sampling frequency $f_s = 1/T_s = K/T$ is given by

$$s(kT_s) = \sqrt{\frac{K}{N_u}} \sum_{p=-\infty}^{+\infty} \sum_{l \in \mathcal{A}} a_l(p) g(kT_s - pT) \times e^{j2\pi \frac{K}{NT} lkT_s} \tag{2.10}$$

where T is the signalling interval, $K \triangleq N(1+\alpha)$ is the oversampling factor, $a_l(p)$ is the data symbol transmitted on the lth subcarrier of the pth FMT symbol and $g(t)$ is the real prototype filter with unit energy and assumed to be an SRRC Nyquist filter with a roll-off factor $\alpha = (K-N)/N \quad (0 \le \alpha \le 1)$. We can note that, differently from OFDM/OQAM systems, for FMT systems the frequency spacing between adjacent subcarriers is given by $K/(NT) = (1+\alpha)/T$ and, thus, it depends on the oversampling factor. Precisely, if the oversampling factor is equal to the number of subcarriers $K = N$, the system is referred to as critically sampled FMT system and the frequency spacing is equal to $1/T$. Otherwise when $\alpha > 0$, the system is referred to as non-critically sampled FMT system and the frequency spacing increases minimizing the amount of ICI at the price of an increment in the implementation complexity and of a reduction of bandwidth efficiency.

Let us suppose now that the FMT signal is transmitted trough an AWGN channel. The received signal in the presence of a CFO Δf, a carrier phase offset ϕ and a timing offset τ, is given by

$$r\left(kT_s\right)=e^{j\left(2\pi\Delta fT_s k+\phi\right)}s\left(kT_s-\tau\right)+n\left(kT_s\right) \tag{2.11}$$

At the receiver side the FMT signal is filtered with a bank of matched filters and downsampled of the factor K, thus, we obtain

$$\begin{aligned}\tilde{a}_m(k)&=r\left(qT_s\right)e^{-j\frac{2\pi}{T}m(1+\alpha)qT_s}\otimes\tilde{g}\left(qT_s\right)\Big|_{q=kK}\\&=a_m(k)q_{m,m}^{\Delta f}(-\tau)e^{j\left[\phi-\frac{2\pi}{T}m(1+\alpha)\tau\right]}\\&+\sum_{\substack{m'\in\mathcal{A}\\m'\neq m}}a_{m'}(k)q_{m',m}^{\Delta f}(-\tau)e^{j\left[\phi-\frac{2\pi}{T}m(1+\alpha)\tau\right]}\\&+\sum_{m'\in\mathcal{A}}\sum_{\substack{k'=-\infty\\k\neq k'}}^{\infty}a_{m'}(k)\\&\times q_{m',m}^{\Delta f}\left(\left(k-k'\right)KT_s-\tau\right)e^{j\left[\phi-\frac{2\pi}{T}m(1+\alpha)\tau\right]}\\&+n\left(qT_s\right)e^{-j\frac{2\pi}{T}m(1+\alpha)qT_s}\otimes\tilde{g}\left(qT_s\right)\Big|_{q=kK}\end{aligned} \tag{2.12}$$

with

$$\begin{aligned}q_{m',m}^{\Delta f}\left(\left(k'-k\right)KT_s-\tau\right)\triangleq\sqrt{\frac{K}{N_u}}\Bigg[&e^{j2\pi q\left(\Delta fT_s+\frac{m'-m}{N}\right)}\\&\times g\left(qT_s-k'KT_s-\tau\right)\otimes\tilde{g}\left(qT_s\right)\Bigg]\Big|_{q=kK}\end{aligned} \tag{2.13}$$

Therefore, in the presence of synchronization errors and in the case of a non dispersive channel, the useful term is subject to the attenuation and the phase rotation due to the term

$$
\begin{aligned}
q_{m,m}^{\Delta f}(-\tau)e^{j\left[\phi-\frac{2\pi}{T}m(1+\alpha)\tau\right]} &= \sqrt{\frac{K}{N_u}}e^{j\left[\phi-\frac{2\pi}{T}m(1+\alpha)\tau\right]} \\
&\times\left[e^{j2\pi q\Delta fT_s}g\left(qT_s-kKT_s-\tau\right)\otimes\tilde{g}\left(qT_s\right)\right]\Big|_{q=kK} \\
&= \sqrt{\frac{K}{N_u}}e^{j\left[\phi-\frac{2\pi}{T}m(1+\alpha)\tau\right]} \\
&\times\sum_{p=-\infty}^{+\infty}e^{j2\pi\Delta f\left(kKT_s-pT_s\right)}g\left(pT_s-\tau\right)g\left(pT_s\right)
\end{aligned}
\tag{2.14}
$$

and moreover it is affected by ICI, ISI and additive noise.

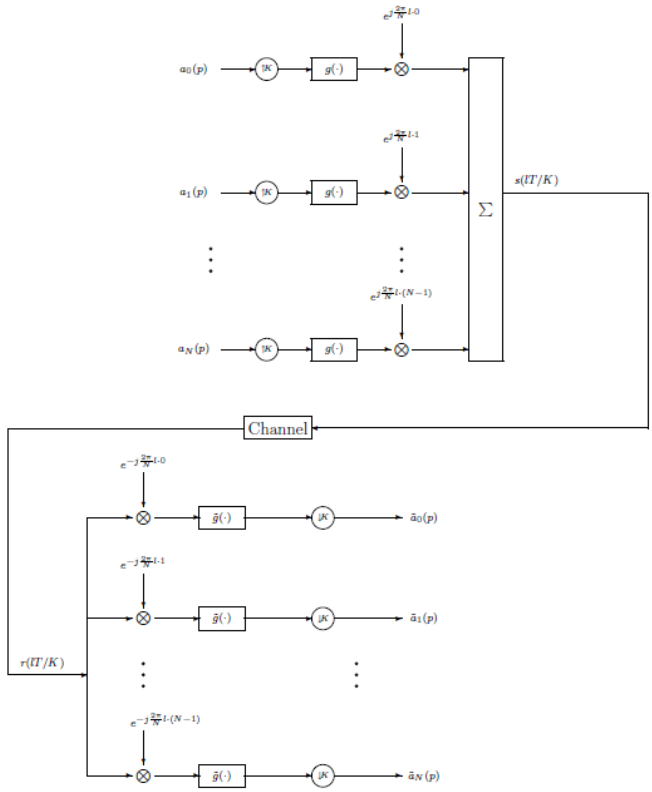

Figure 19: FMT System

2.1.3 Numerical Results

In this section the sensitivity of FBMC systems to synchronization errors is assessed via computer simulations. A number of 10^4 Monte Carlo trials has been performed under the following conditions:

- The prototype filter is obtained by truncating the sampled version of an SRRC Nyquist filter with a roll-off factor α. Specifically, it is a FIR filter of length $N_g = 8K$ for FMT systems and $N_g = 4N$ for OFDM/OQAM systems.
- The values of the number of subcarriers and of the roll-off factor parameter for the considered FMT system are $N = 64$ and $\alpha = 0.125$, respectively.
- The values of the number of subcarriers and of the roll-off factor parameter for the considered OFDM/OQAM system are $N = 64$ and $\alpha = 0.6$, respectively.
- The multipath channel has been modelled to consist of $N_m + 1 = 5$ independent Rayleigh-fading taps with an exponentially decaying power delay profile. Specifically, $E\left[\left|h(l)\right|^2\right] = Ce^{-l/4}$, $l \in \{0,\ldots,N_m\}$, where C is a constant such that $\sum_{l=0}^{N_m} E\left[\left|h(l)\right|^2\right] = 1$. Moreover, the channel is fixed in each run but independent from one run to another.

- The complex data symbols $a_p(l)$, when the FMT system is considered, belong to a QPSK constellation.
- The data symbols $a_p^R(l)$ and $a_p^I(l)$, when the OFDM/OQAM system is considered, belong to a BPSK constellation.

In Figure 20 the sensitivity of the FBMC signals in terms of bit error rate (BER) on the digital data is reported in the case of $N = 64$ subcarriers and $\mathrm{SNR} = 10\mathrm{dB}$ as a function of the timing offset normalized to the sampling interval. The BER of the same FBMC systems as a function of the normalized CFO is shown in Figure 21. Note that in the presence of frequency and timing synchronization errors at the output of each subchannel is observed an attenuation and a phase rotation of the useful data related to the subchannel index, the timing offset, the phase offset, the CFO and the index of information symbol. The phase rotation incorporated in the channel gain should be compensated by the subcarrier equalizer. It is assumed that on each subchannel it is exploited a one-tap equalizer with perfect channel knowledge and of the timing offset and of the CFO. The results reported in Figure 20 show that the sensitivity to a timing offset is lower in multipath channel and, moreover, in this case an accuracy of ± 6 samples ($\simeq \pm 10\%$ of FBMC symbol interval) is sufficient to assure a contained performance degradation with respect to the case of perfect synchronization. Moreover, as shown in Figure 21, in multipath channel the absolute value of

the CFO should be less than 5% to assure a reduced performance degradation.

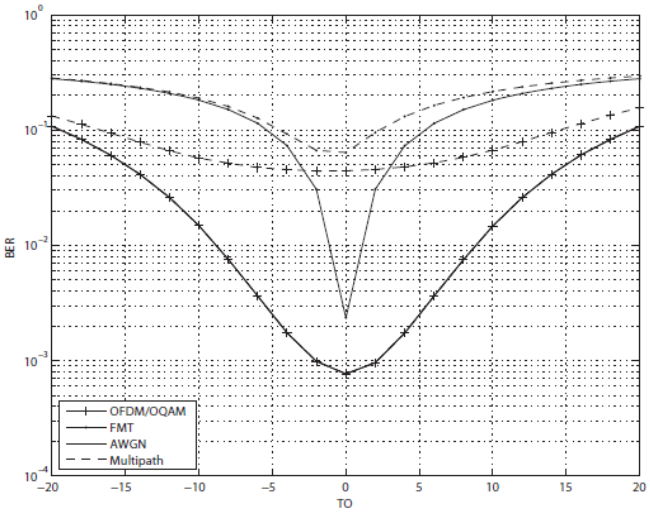

Figure 20: BER of the considered FBMC systems as a function of the timing offset in AWGN (solid lines) and multipath channel (dashed lines) for SNR=10dB

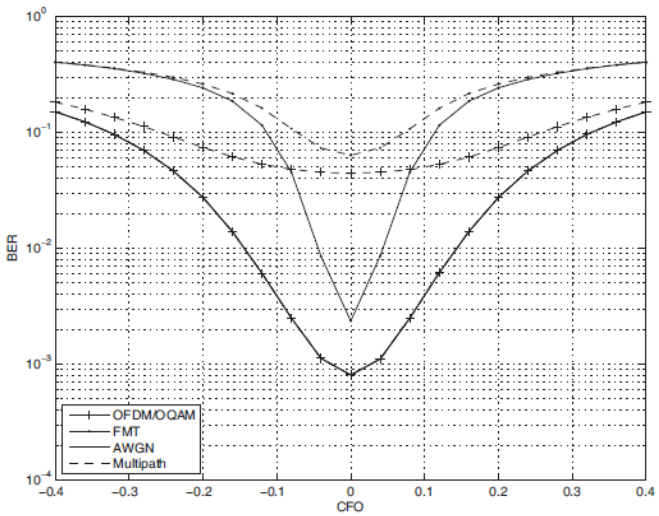

Figure 21: BER of the considered FBMC systems as a function of the CFO in AWGN (solid lines) and multipath channel (dashed lines) for SNR=10dB

2.2 Uplink Synchronization Tasks

In this section we analyze the effects of synchronization errors in the case of FBMC uplink transmission.

2.2.1 OFDM/OQAM Multiple Access System Model with Synchronization Errors

In the uplink of an OFDM/OQAM system each block conveys information of several subscribers. Let us consider a system with U users with equal power σ_s^2 and N subcarriers, the transmitted signal takes the form

$$s(t)=\sum_{m=1}^{U}s_m(t)=\sum_{m=1}^{U}\sigma_s\left[s_m^R(t)+js_m^I(t)\right] \tag{2.15}$$

with

$$s_m^R(t)=\sqrt{\frac{N}{2U_m}}\sum_{p=-\infty}^{\infty}\sum_{l\in\mathcal{A}_m}a_l^R(p)e^{jl\left(\frac{2\pi}{T}t+\frac{\pi}{2}\right)}g(t-pT) \tag{2.16}$$

$$s_m^I(t)$$

$$=\sqrt{\frac{N}{2U_m}}\sum_{p=-\infty}^{\infty}\sum_{l\in\mathcal{A}_m}a_l^I(p)e^{jl\left(\frac{2\pi}{T}t+\frac{\pi}{2}\right)}g\left(t-pT-\frac{T}{2}\right) \tag{2.17}$$

where $\mathcal{A}_m$ is the subcarrier set of the mth user of size U_m.

The received signal in the presence of synchronization errors Δf_m, ϕ_m and τ_m is given by

$$r(t) = \sum_{m=1}^{U} s_m\left(t-\tau_m\right) e^{j\left(2\pi\Delta f_m t+\phi_m\right)} + n(t) \tag{2.18}$$

Let the mth user be the user of interest, we will assume that the base station can perfectly estimate and compensate its time offset τ_m, its CFO Δf_m and its phase offset ϕ_m but the remaining $U-1$ users are completely asynchronous to each other. In this case the compensated mth signal

$$r_m(t) = r\left(t+\tau_m\right) e^{-j\left(2\pi\Delta f_m t+\phi_m\right)} \tag{2.19}$$

is filtered with a bank of matched filters and $N/2$ times downsampled to generate for $l \in \mathcal{A}_m$ the sequences

$$\begin{aligned}
\tilde{a}_l^R(k) &= \Re\left\{ r_m(t) e^{-j\left(\frac{2\pi}{T}t+\frac{\pi}{2}\right)l} \otimes \tilde{g}(t)\Big|_{t=kT} \right\} \\
&= \sigma_s \sqrt{\frac{N}{2U_m}} a_l^R(k) \\
&\quad + \sum_{\substack{m'=1 \\ m'\neq m}}^{U} \Re\left\{ \tilde{g}(t) \otimes \Gamma_{m',m}^{f}(t)\Big|_{t=kT} \right\} \\
&\quad + \Re\left\{ n(t) e^{-j\left(\frac{2\pi}{T}t+\frac{\pi}{2}\right)l} \otimes \tilde{g}(t)\Big|_{t=kT} \right\}
\end{aligned} \tag{2.20}$$

and

$$\begin{aligned}\tilde{a}_l^I(k) &= \Im\left\{ r_m(t) e^{-j\left(\frac{2\pi}{T}t+\frac{\pi}{2}\right)l} \otimes \tilde{g}(t)\Big|_{t=kT+T/2} \right\} \\ &= \sigma_s \sqrt{\frac{N}{2U_m}} a_l^I(k) \\ &+ \sum_{\substack{m'=1 \\ m'\neq m}}^{U} \Re\left\{ \tilde{g}(t) \otimes \Gamma_{m',m}^f(t)\Big|_{t=kT+T/2} \right\} \\ &+ \Im\left\{ n(t) e^{-j\left(\frac{2\pi}{T}t+\frac{\pi}{2}\right)l} \otimes \tilde{g}(t)\Big|_{t=kT+T/2} \right\}\end{aligned} \tag{2.21}$$

where

$$\begin{aligned}&\Gamma_{m',m}^f(t) \triangleq s_{m'}\left(t+\tau_m-\tau_{m'}\right) \\ &\times e^{j\left[2\pi\left(\Delta f_{m'}-\Delta f_m\right)t+\phi_{m'}-\phi_m\right]} e^{-j\left(\frac{2\pi}{T}t+\frac{\pi}{2}\right)l}\end{aligned} \tag{2.22}$$

From (2.21) and (2.22) we can note that in the considered scenario, under the assumption of a pulse filter satisfying the orthogonality conditions [25], the received signal does not present ISI, ICI and interference between imaginary and real part but presents multiple access interference.

2.2.2 FMT Multiple Access System Model with Synchronization Errors

Let us consider a multiuser FMT system with U users, the expression of the received signal in the presence of synchronization errors is that reported in (2.18) where

$$s_m(t) = \sigma_s \sqrt{\frac{N(1+\alpha)}{U_m}} \sum_{n=-\infty}^{+\infty} \sum_{k \in \mathcal{A}_m} a_k(n) g(t-nT) e^{j\frac{2\pi}{T} kt(1+\alpha)} \quad (2.23)$$

Let the mth user be the use of interest, with a perfect time and frequency synchronization, the received signal $r_m(t) = r\left(t+\tau_m\right) e^{-j\left(2\pi \Delta f_m t + \phi_m\right)}$ is filtered with a bank of matched filters satisfying the condition of perfect reconstruction and K times downsampled to generate for $l \in \mathcal{A}_m$ the sequence

$$\begin{aligned} \tilde{a}_l(k) &= r_m(t) e^{-j\frac{2\pi}{T} lt(1+\alpha)} \otimes \tilde{g}(t) \Big|_{t=kT} \\ &= \sigma_s \sqrt{\frac{N(1+\alpha)}{U_m}} a_l(k) \\ &\quad + \sum_{\substack{m'=1 \\ m' \neq m}}^{U} \tilde{g}(T) \otimes \Lambda_{m',m}^{f}(t) \Big|_{t=kT} \\ &\quad + n(t) e^{-j\frac{2\pi}{T} lt(1+\alpha)} \otimes \tilde{g}(t) \Big|_{t=kT} \end{aligned} \quad (2.24)$$

with

$$\begin{aligned} \Lambda_{m',m}^{f}(t) &\triangleq s_{m'}\left(t+\tau_m-\tau_{m'}\right) \\ &\times e^{j\left[2\pi\left(\Delta f_{m'}-\Delta f_m\right)t+\phi_{m'}-\phi_m\right]} e^{-j\frac{2\pi}{T} lt(1+\alpha)} \end{aligned} \quad (2.25)$$

From (2.24) we can note that in the considered asynchronous scenarios the received signal is affected uniquely by multiple access interference.

2.2.3 Numerical Results

In this section the sensitivity of FBMC-MA systems to synchronization errors is assessed via computer simulations and compared with that of OFDMA systems. A number of 10^4 Monte Carlo trials has been performed under the following conditions (unless otherwise stated)

- The length of the prototype filter is $L = \gamma N$, where the overlap parameter γ is fixed at $\gamma = 4$. Specifically, the so-called frequency sampled technique is used to design the prototype filter [24]. The desired values of the filter in the frequency domain are $G(0) = 1$, $G(1/L) = 0.971960$, $G(2/L) = 1/\sqrt{2}$, $G(3/L) = \sqrt{1 - G^2(1/L)}$, $G(k/L) = 0$ for $4 \le k \le L-1$.
- The number of subcarriers is fixed at $N = 1024$.
- The number of users is equal to $U = 4$.
- The modulation format on all subcarriers is QPSK.
- The considered multipath channel model is the ITU Vehicular A, which has six independent Rayleigh fading taps with delays 0, 0.31, 071, 1.09, 1.73 and 2.51 μs and relative power 0, -1, -9, -10, -15 and -20dB [26]. Moreover, the channel is fixed in each run but it is independent from one run to another.

In our simulation analysis, we have considered three different allocations schemes: blockwise, interleaved and interleaved b assignment schemes. In particular, as illustrated in Figure 22, in the blockwise and interleaved b allocation schemes group of adjacent subcarriers are allocated to the same user or different users, respectively, while in the interleaved allocation scheme one subcarrier is dropped between two adjacent users.

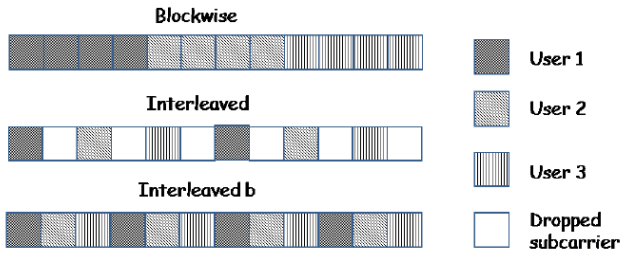

Figure 22: Allocation scheme

In Figure 23 it is shown that, in the case of a multi-user system in which the user of interest is perfectly synchronized to the base station (BS), the FBMC-MA systems are much more robust with respect to misalignments between different users than CP-OFDMA systems, assuring in the case of the blockwise assignment a performance practically coincident with that obtained in the case of perfect synchronization. We have considered the case of an asynchronous scenario with $U = 4$ users, where three of them have normalized frequency offsets uniformly distributed in the range ± 0.125 and timing offsets uniformly distributed within $\{-T/2, \ldots, T/2-1\}$. The BER depicted in Figure 23 corresponds to the perfect synchronized user, who is

suffering from the multiple access interference of the three asynchronous users. Figure 23(a), (b) and (c) show always the same performance for the FBMC system while comparing it with CP-OFDM with different CP-length. It is obvious, that FBMC with blockwise allocation of subcarriers per user is always the best choice and the performance advantage over CP-OFDM is higher as longer is the CP.

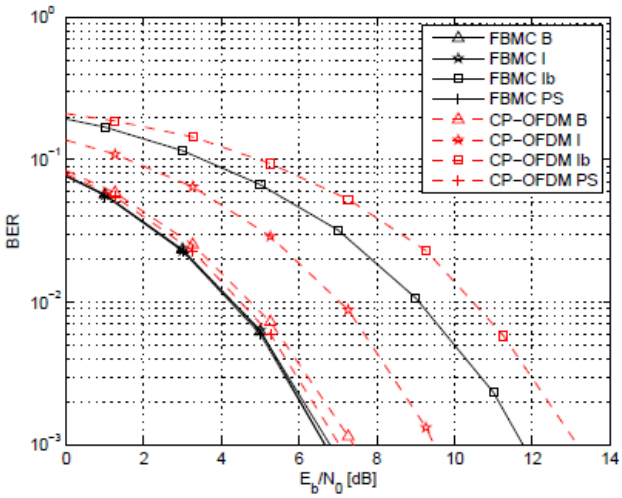

(a) CP length $M/16$

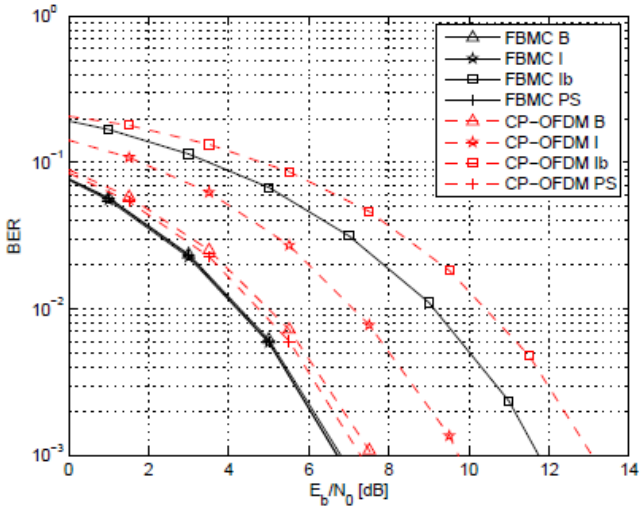

(b) CP length $M/8$

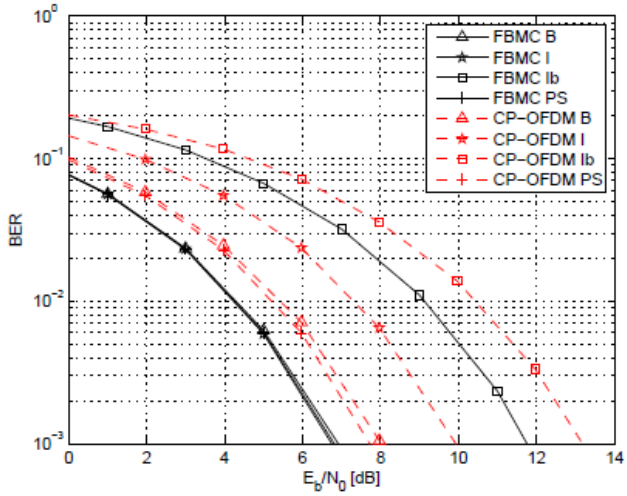

(c) CP length $M/4$

Figure 23: Comparison between FBMC-MA and OFDMA

Furthermore, we have studied the sensitivity of the FBMC system in terms of BER to timing inaccuracy

for the user of interest, under the hypothesis of ideal carrier frequency recovery. The other users are supposed asynchronous with normalized frequency offsets uniformly distributed in the range ± 0.5 and a timing offset uniformly distributed within $\{-T/2,\ldots,T/2-1\}$. In Figure 24, we report the BER of the user of interest with $E_s/N_0 = 20\text{dB}$ as a function of the RTO normalized to the sampling interval $(\hat{\tau}-\tau)/T_s$ in AWGN channel (solid line) and ITU-Vehicular A channel (dashed line) and $U=4$ users. The E_s/N_0 of the other users is equal to $(E_s/N_0)_i = 20\text{dB}$, $i=2,3,4$. Note that the effect of the RTO on the digital data at the output of each subcarrier is an attenuation and a phase rotation proportional to the RTO and to the subcarrier index (see (2.20), (2.21) and (2.24)). This phase rotation incorporated in the channel gain should be compensated by the subcarrier equalizer. It is assumed that on each subcarrier a one-tap equalizer with perfect knowledge of the channel and of the RTO is used. The results show that the interleaved allocation scheme assures the lowest sensitivity to the presence of a RTO, both in AWGN and multipath channel, but on the other hand, it presents a loss of spectral efficiency, since one subcarrier is dropped between two adjacent users. Instead, with the blockwise assignment scheme, an accuracy of ± 100 samples ($\simeq \pm 10\%$ of the FBMC symbol interval) is sufficient to assure an acceptable performance degradation with respect to the case of perfect synchronization (RTO=0). (Note that the

BER corresponding to the interleaved scheme in AWGN is lower than 10^{-5}). We have also analyzed the effect of the presence of a RCFO for the user of interest, for whom RTO is zero, with the other users completely asynchronous. In Figure 25, we report the BER of the user of interest with $E_s / N_0 = 20\text{dB}$ as a function of the RCFO normalized to the subcarrier spacing $\left(\Delta\hat{f} - \Delta f\right)T$ in AWGN channel (solid line) and ITU-Vehicular A channel (dashed line) for an FBMC-MA system with $U = 4$ users. The E_s / N_0 of the other users is also 20 dB. Note that the effect of the RCFO on the digital data at the output of each subcarrier is an attenuation and a phase rotation proportional to the RTO and to the symbol index (see (2.20), (2.21) and (2.24)). This phase rotation incorporated in the channel gain should be compensated by the subcarrier equalizer. It is assumed that on each subcarrier a one-tap equalizer with perfect knowledge of the channel and of the RCFO is used. For blockwise and interleaved allocation schemes an accuracy of ±15% of the subcarrier spacing can provide an acceptable performance degradation with respect to the case of perfect synchronization (RCFO=0).

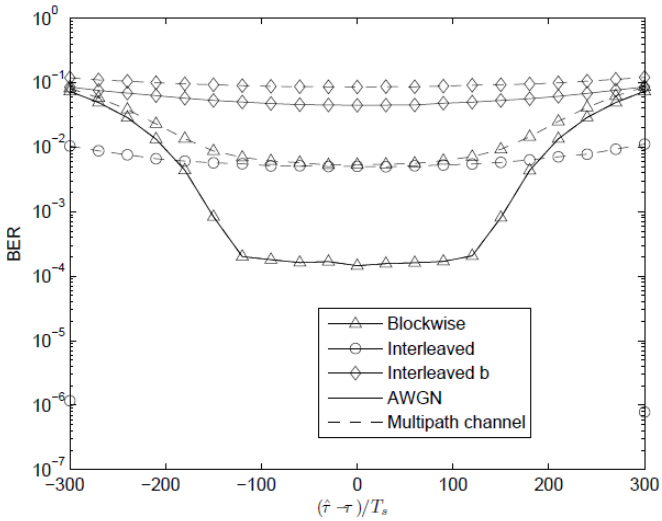

Figure 24: BER as a function of the RTO normalized to the sampling interval for $E_s / N_0 = 20\text{dB}$

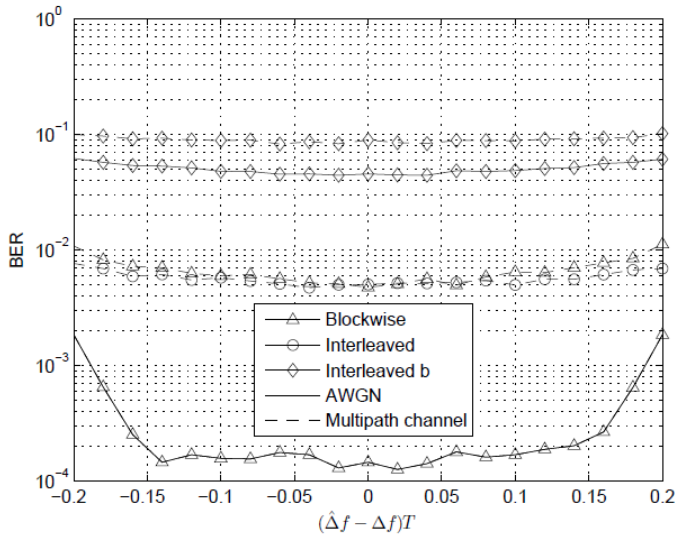

Figure 25: BER as a function of the RCFO normalized to the subcarrier spacing for $E_s / N_0 = 20\text{dB}$

Chapter 3

Data-aided Synchronization Algorithms for FBMC Systems

This chapter deals with the problem of data-aided joint symbol timing and CFO estimation for FBMC systems, both in downlink and uplink transmission. Since FBMC systems are very sensitive to synchronization errors, as shown in chapter 2, accurate synchronization algorithms must be designed. As regards the downlink, it is proposed a new joint symbol timing and CFO synchronization algorithm based on the least squares approach and exploiting the transmission of a training sequence made up of identical parts. Moreover, for the up-link of a multiple access FBMC system, the joint ML phase offset, CFO and symbol timing estimator exploiting a short know preamble embedded in the burst of each of U users is considered. The performance of the derived estimators is assessed by computer simulations both in AWGN and multipath channel.

3.1 Joint Symbol Timing and CFO LS Estimator

In this section we derive a data-aided joint CFO and symbol timing estimator based on the LS approach which exploits the transmission of a training sequence made up of identical blocks. Precisely, by considering the notations introduced in (2.1) and (2.10) for OFDM/OQAM and FMT systems respectively, the training sequence can be obtained by transmitting the sequence of data symbols $a_l(p) = a_l^{TR} \;\; \forall l \in \mathcal{A}$ and $\forall p \in \{0,\ldots,N_{TR}-1\}$. In this way, if we assume that the pulse shaping filter $g(t)$ is different from zero for $t \in \left\{0, T_s, \ldots, \left(N_g - 1\right)T_s\right\}$, where $N_g = \gamma T / T_s$, with γ the overlapping factor, we obtain the training burst

$$
s_{TR}\left(kT_s\right) = \begin{cases} \sqrt{\dfrac{K}{N_u}} \displaystyle\sum_{l\in\mathcal{A}} a_l^{TR} e^{j\frac{2\pi}{N}kl} \sum_{p=0}^{N_{TR}-1} g\left(kT_s - pKT_s\right) \\ \text{FMT} \\ \sqrt{\dfrac{N}{2N_u}} \displaystyle\sum_{p=0}^{N_{TR}-1} \sum_{l\in\mathcal{A}} e^{jl\left(\frac{2\pi}{N}k+\frac{\pi}{2}\right)} \left[a_l^{R,TR} g\left(kT_s - pNT_s\right) \right. \\ \left. + j a_l^{I,TR} g\left(kT_s - NT_s/2 - pNT_s\right)\right] \\ \text{OFDM/OQAM} \end{cases} \tag{3.1}
$$

After a transient of $N_g - 1$ samples and, in particular for $k \in \{N_g - 1, \ldots, N_{TR}N - P - 1\}$, the training sequence in (3.1) satisfies the following relationship

$$s_{TR}(kT_s + PT_s) = s_{TR}(kT_s) \tag{3.2}$$

with $P = lcm\{N, K\}$ for FMT systems and $P = N$ for OFDM/OQAM systems. Thus, the number of identical blocks contained in the training sequence is $N_{rip}^{OFDM/OQAM} = N_{TR} - \gamma$ for OFDM/OQAM systems, while, for FMT systems, the number of identical blocks is $N_{rip}^{FMT} = \left\lfloor \frac{N_{TR}N - \gamma K}{P} \right\rfloor$. Accounting for the relationship (3.2), a joint symbol timing and CFO estimator can be obtained by considering the minimization problem

$$\left(\Delta\hat{f}, \hat{\tau}\right) = \arg\min_{\Delta\tilde{f}, \tilde{\tau}} \left\{ \sum_{k=N_g-1}^{N_{TR}N-P-1} \left| r(kT_s + \tilde{\tau}) - r(kT_s + PT_s + \tilde{\tau}) e^{-j2\pi\Delta\tilde{f}T_s P} \right|^2 \right\} \tag{3.3}$$

where $\Delta\tilde{f}$ and $\tilde{\tau}$ are trial values for CFO and symbol timing, respectively and $r(kT_s)$ is the received signal, defined in (2.2). The minimization in (3.3) (see the algebraic details reported in Appendix B) leads to the following joint CFO and symbol timing estimator referred to as LS estimator

$$\hat{\tau}_{LS} = \arg\max_{\tilde{\tau}} \left\{ 2\left|R(\tilde{\tau})\right| - Q_1(\tilde{\tau}) - Q_2(\tilde{\tau}) \right\} \tag{3.4}$$

$$\Delta\hat{f}_{LS}(\hat{\tau}_{LS}) = \frac{1}{2\pi PT_s} \arg\left\{ R(\hat{\tau}_{LS}) \right\} \tag{3.5}$$

with

$$R(\tilde{\tau}) \triangleq \sum_{k=N_g-1}^{N_{TR}N-P-1} r^*(kT_s+\tilde{\tau})\, r(kT_s+PT_s+\tilde{\tau}) \tag{3.6}$$

and

$$Q_i(\tilde{\tau}) \triangleq \sum_{k=N_g-1}^{N_{TR}N-P-1} \left| r(kT_s+(i-1)PT_s+\tilde{\tau}) \right|^2 \tag{3.7}$$

Let us observe that if we divide the timing metric in (3.4) by the term $Q(\tilde{\tau}) = Q_1(\tilde{\tau}) + Q_2(\tilde{\tau})$ we obtain the modified LS (MLS) joint symbol timing and CFO estimator

$$\hat{\tau}_{MLS} = \arg\max_{\tilde{\tau}} \left\{ \frac{|R(\tilde{\tau})|}{Q(\tilde{\tau})} \right\} \tag{3.8}$$

$$\Delta\hat{f}_{MLS}(\hat{\tau}_{MLS}) = \frac{1}{2\pi PT_s} \arg\{R(\hat{\tau}_{MLS})\} \tag{3.9}$$

that can be used to reduce the false detection probability [27]. The performance of the LS and MSL estimators will be compared with that of the two joint estimators proposed by Tonello and Rossi in [14] and referred in the following as TR1 and TR2. specifically, the joint estimator

$$\hat{\tau}_{TR1} = \arg\max_{\tilde{\tau}} \left\{ \frac{|R(\tilde{\tau})|^2}{Q_2(\tilde{\tau})^2} \right\} \tag{3.10}$$

$$\Delta\hat{f}_{TR1}(\hat{\tau}_{TR1}) = \frac{1}{2\pi PT_s} \arg\{R(\hat{\tau}_{TR1})\} \tag{3.11}$$

exploits only the periodicity of the training burst in (3.1), while the joint estimator

$$\hat{\tau}_{TR2} = \arg\max_{\tilde{\tau}} \left\{ \frac{|S(\tilde{\tau})|^2}{T(\tilde{\tau})^2} \right\} \tag{3.12}$$

$$\Delta\hat{f}_{TR2}\left(\hat{\tau}_{TR2}\right)=\frac{1}{2\pi PT_s}\arg\left\{R\left(\hat{\tau}_{TR2}\right)\right\} \tag{3.13}$$

with

$$S\left(\tilde{\tau}\right)\triangleq\sum_{k=N_g-1}^{N_{TR}N-P-1}\left[r^*\left(kT_s+\tilde{\tau}\right)s_{TR}\left(kT_s\right)\right.$$
$$\left.\times r\left(kT_s+PT_s+\tilde{\tau}\right)s_{TR}^*\left(kT_s+PT_s\right)\right] \tag{3.14}$$

and

$$T\left(\tilde{\tau}\right)\triangleq\sum_{k=N_g-1}^{N_{TR}N-P-1}\left|s_{TR}\left(kT_s+PT_s\right)\right|^2\left|s_{TR}\left(kT_s\right)\right|^2 \tag{3.15}$$

exploits also the knowledge of the periodic training burst. It is worthwhile to note that the considered LS, MLS, TR1 and TR2 CFO estimators in (3.5), (3.9), (3.11) and (3.13), respectively, provide a closed form solution for the CFO estimate and do not require the knowledge of the SNR. Moreover, in the case of OFDM/OQAM systems, they can assure unambiguous CFO estimates if $\left|\Delta fT_s\right|<1/(2N)$, while in the case of FMT systems their acquisition range is reduced to $\left|\Delta fT_s\right|<1/(2P)$. On the other hand, the considered LS, MLS, TR1 and TR2 symbol timing estimators in (3.4), (3.8), (3.10) and (3.12), respectively, do not present a closed form solution but they require a maximization procedure. We underline that in the case of FMT systems the amount of redundancy needed to transmit the training sequence is greater than that exploited in the case of OFDM/OQAM systems. In fact, in the case of OFDM/OQAM systems the training sequence is composed by $N_{rip}^{OFDM/OQAM}=N_{TR}-\gamma$ identical OFDM/OQAM symbols of length N while, in the

case of FMT systems, it is necessary to transmit a training sequence such that $N_{TR}N-\gamma K>P$, where $P=lcm\{N,K\}$ can be much greater than N.

3.2 Cramér – Rao Bound

In this section we derive the expression of the CRVB for joint CFO, phase offset and symbol timing estimation for FBMC systems. Let $\mathbf{v}=[\tau,\Delta f,\phi]^T$ the set of parameters to be estimated and let us consider the observations vector of total length $W=N_{TR}N-N_g+1$

$$\begin{aligned}\mathbf{r}&\triangleq\left[r\left(N_gT_s-T_s\right),\ldots,r\left(N_{TR}NT_s-T_s\right)\right]^T\\&=\boldsymbol{\psi}\left(\Delta f,\phi\right)\mathbf{s}(\tau)+\mathbf{n}\end{aligned}\tag{3.16}$$

with

$$\begin{aligned}&\mathbf{s}(\tau)=\\&=\left[s\left(N_gT_s-T_s-\tau\right),\ldots,s\left(N_{TR}NT_s-T_s-\tau\right)\right]^T\end{aligned}\tag{3.17}$$

the vector of the transmitted training sequence

$$\begin{aligned}&\boldsymbol{\psi}\left(\Delta f,\phi\right)=\\&=\operatorname{diag}\left\{e^{j\left[2\pi(N_g-1)T_s\Delta f+\phi\right]},\ldots,e^{j\left[2\pi(N_{TR}N-1)T_s\Delta f+\phi\right]}\right\}\end{aligned}\tag{3.18}$$

and $\mathbf{n}$ the noise vector with zero mean and covariance matrix $\mathbf{C}_{\mathbf{n}}=\frac{\sigma_n^2}{T_s}\mathbf{I}_W$. The (i,l)th entry of the Fisher Information Matrix (FIM) is equal to

$$\left[\mathbf{F}\right]_{(i,l)} = -\mathrm{E}\left[\frac{\partial \ln p\left(\mathbf{r}\middle|\mathbf{v}\right)}{\partial\left[\mathbf{v}\right]_i \partial\left[\mathbf{v}\right]_l}\right] \quad \forall i,l \in \{1,2,3\} \tag{3.19}$$

where $\ln p\left(\mathbf{r}\middle|\mathbf{v}\right)$ is the logarithm of the probability density function of $\mathbf{r}$ whose expression (up to irrelevant additive factors) is given by

$$\begin{aligned}\ln p\left(\mathbf{r}\middle|\mathbf{v}\right) = &\frac{2T_s}{\sigma_n^2}\Re\left\{\mathbf{r}^*\boldsymbol{\psi}\left(\Delta f,\phi\right)\mathbf{s}(\tau)^T\right\} \\ &-\frac{T_s}{\sigma_n^2}\mathbf{s}(\tau)\mathbf{s}(\tau)^H\end{aligned} \tag{3.20}$$

Substituting (3.19) in (3.20) and taking the statistical expectation we obtain the elements of the FIM

$$\left[\mathbf{F}\right]_{(1,1)} = \frac{2T_2}{\sigma_n^2}\frac{\partial\mathbf{s}(\tau)}{\partial\tau}\frac{\partial\mathbf{s}(\tau)^H}{\partial\tau} \tag{3.21}$$

$$\left[\mathbf{F}\right]_{(1,2)} = \left[\mathbf{F}\right]_{(2,1)} = \frac{2T_s}{\sigma_n^2}\Re\left\{\frac{\partial\mathbf{s}(\tau)}{\partial\tau}\mathbf{D}_{\Delta f}\mathbf{s}(\tau)^H\right\} \tag{3.22}$$

$$\left[\mathbf{F}\right]_{(1,3)} = \left[\mathbf{F}\right]_{(3,1)} = \frac{2T_2}{\sigma_n^2}\Re\left\{\frac{\partial\mathbf{s}(\tau)}{\partial\tau}\mathbf{D}_{\phi}\mathbf{s}(\tau)^H\right\} \tag{3.23}$$

$$\left[\mathbf{F}\right]_{(2,3)} = \left[\mathbf{F}\right]_{(3,2)} = -\frac{2T_s}{\sigma_n^2}\mathbf{s}(\tau)\mathbf{D}_{\Delta f}\mathbf{D}_{\phi}\mathbf{s}(\tau)^H \tag{3.24}$$

$$\left[\mathbf{F}\right]_{(2,2)} = -\frac{2T_s}{\sigma_n^2}\mathbf{s}(\tau)\mathbf{D}_{\Delta f}^2\mathbf{s}(\tau)^H \tag{3.25}$$

$$\left[\mathbf{F}\right]_{(3,3)} = -\frac{2T_s}{\sigma_n^2}\mathbf{s}(\tau)\mathbf{D}_{\phi}^2\mathbf{s}(\tau)^H \tag{3.26}$$

with

$$\mathbf{D}_{\Delta f} = j2\pi T_s \mathrm{diag}\left\{N_g - 1,\ldots,N_{TR}N - 1\right\} \tag{3.27}$$

and

$$\mathbf{D}_{\phi} = j\mathbf{I}_W \tag{3.28}$$

In the case of FMT systems by following the algebraic manipulations reported in Appendix C the CRVBs for symbol timing, CFO and phase offset estimation are given by

$$\mathrm{CRVB}\left(\tau\right)=\left[\mathbf{F}^{-1}\right]_{(1,1)}$$

$$=\frac{\left(NT_s\right)^2}{8\pi^2 W\mathrm{SNR}\left[\frac{1}{N_u}\sum_{l\in\mathcal{A}}\left(l-\frac{1}{N_u}\sum_{l\in\mathcal{A}}l\right)^2\right]} \tag{3.29}$$

$$\mathrm{CRVB}\left(\Delta f\right)=\left[\mathbf{F}^{-1}\right]_{(2,2)}=\frac{3}{2\left(\pi T_s\right)^2\mathrm{SNR}W^3} \tag{3.30}$$

$$\mathrm{CRVB}(\phi)=\left[\mathbf{F}^{-1}\right]_{(3,3)}$$

$$=\frac{3\left[4\beta\frac{1}{N_u}\sum_{l\in\mathcal{A}}l^2-W^2\left(\frac{1}{N_u}\sum_{l\in\mathcal{A}}l\right)^2\right]}{2W^3\mathrm{SNR}\left[\frac{1}{N_u}\sum_{l\in\mathcal{A}}\left(l-\frac{1}{N_u}\sum_{l\in\mathcal{A}}l\right)^2\right]} \tag{3.31}$$

with

$$\beta=\frac{N_{TR}^2N^2+N_{TR}NN_g-4N_{TR}N+N_g^2-5N_g+7}{3} \tag{3.32}$$

From (3.29), (3.30) and (3.31) we can note that the derived CRBVs are inversely proportional to the SNR and depend on the size of the observations window. In particular, the CRVB(τ) is inversely proportional to W and depends on the number and the position of virtual subcarriers while, from (3.30), we can note that the $\mathrm{CRVB}\left(\Delta f\right)$ is inversely proportional to W^3. Into the case of OFDM/OQAM

systems substituting the transmitted signal model (2.1) in the FIM and following the same reasoning reported in Appendix C, we obtain that the $\mathrm{CRVB}(\tau)$, $\mathrm{CRVB}(\Delta f)$ and $\mathrm{CRVB}(\phi)$ coincide with (3.29), (3.30) and (3.31), respectively.

3.3 Numerical Results

In this section the performance of the proposed joint LS and MLS symbol timing and CFO estimators is compared with that of the data-aided synchronization algorithms TR1 and TR2 proposed by Tonello and Rossi in [14]. As stated in section 3.2, all the considered symbol timing estimators require a maximization procedure. In our simulations this maximization is performed in two steps: in the first it is performed a coarse search with a step-size T_s followed, in the second step, by a parabolic interpolation.

A number of 10^4 Monte Carlo trails has been performed under the following conditions:

- The prototype filter is obtained by truncating the sampled version of an SRRC Nyquist filter with a roll-off factor α. Specifically, it is a FIR filter of length $N_g = 8K$ for FMT systems and $N_g = 4N$ for OFDM/OQAM systems.
- The value of the normalized CFO $\Delta\varepsilon = \Delta f T_s N$, of the normalized timing offset

τ / T_s and of the carrier phase ϕ are uniformly distributed in $\left[-N/(4P),...,N/(4P)\right)$, $\left[-N/2,...,N/2\right)$ and $\left[-\pi,.,\pi\right)$, respectively.

- The values of the number of subcarriers and of the roll-off factor parameter for the considered FMT system are $N = 64$ and $\alpha = 0.125$, respectively.
- The values of the number of subcarriers and of the roll-off factor parameter for the considered OFDM/OQAM system are $N = 64$ and $\alpha = 0.6$, respectively.
- The multipath channel has been modelled to consist of $N_m + 1 = 5$ independent Rayleigh-fading taps with an exponentially decaying power delay profile. Specifically, $E\left[\left|h(l)\right|^2\right] = Ce^{-l/4}$, $l \in \{0,\ldots,N_m\}$, where C is a constant such that $\sum_{l=0}^{N_m} E\left[\left|h(l)\right|^2\right] = 1$. Moreover, the channel is fixed in each run but independent from one run to another.
- The complex data symbols $a_p(l)$, when the FMT system is considered, belong to a QPSK constellation.
- The data symbols $a_p^R(l)$ and $a_p^I(l)$, when the OFDM/OQAM system is considered, belong to a BPSK constellation.

3.3.1 OFDM/OQAM System

In the first set of simulations we tested the performance of the considered algorithms for an OFDM/OQAM system in AWGN (solid lines) and multipath channel (dashed lines). Precisely Figure 26 and Figure 27, show the root mean squared error (RMSE) of the considered joint timing and CFO estimators, respectively, as a function of the SNR, for a training sequence with $N_{rip}^{OFDM/OQAM} = 2$ identical bocks each of length N. In Figure 27 we have also shown the theoretical normalized RMSE of the LS CFO estimator whose derivation details are reported in Appendix D. Moreover, in Figure 26 and Figure 27 we have included the previously obtained Cramér-Rao bounds. As shown in Figure 26 the TR2 symbol timing estimator exhibits the best performance for all the considered SNR values both in AWGN and multipath channel. However, in multipath channel and for sufficiently high SNR values, the proposed LS and MLS symbol timing estimators assure an RMSE nearly equal to that achieved by the TR2 estimator. On the other hand, as shown in Figure 27, the TR2 CFO estimator provides the highest RMSE in multipath channel. Specifically, in Figure 28 it is reported the BER of the perfectly synchronized system and that obtained when the considered algorithms are exploited as a function of the SNR. The results show that in AWGN channel the adoption of TR2 synchronization algorithm assures a performance

quite similar to that obtained with perfect synchronization while, in multipath channel, and for sufficiently high SNR values, the proposed LS and MLS algorithms can provide the best performance nearly coincident with that obtained in the absence of synchronization errors. Specifically, the performance cross-over is observed for $\mathrm{SNR} = 20\mathrm{dB}$ and is due to the fact that for $\mathrm{SNR} \geq 20\mathrm{dB}$ the performance of the timing estimators is quite similar while the LS and MLS CFO estimators outperform the TR2 estimator. It is worthwhile to emphasize that the considered LS and MLS estimators exploit only the periodicity of the training burst while the TR2 estimator exploits also the knowledge of the periodic training burst.

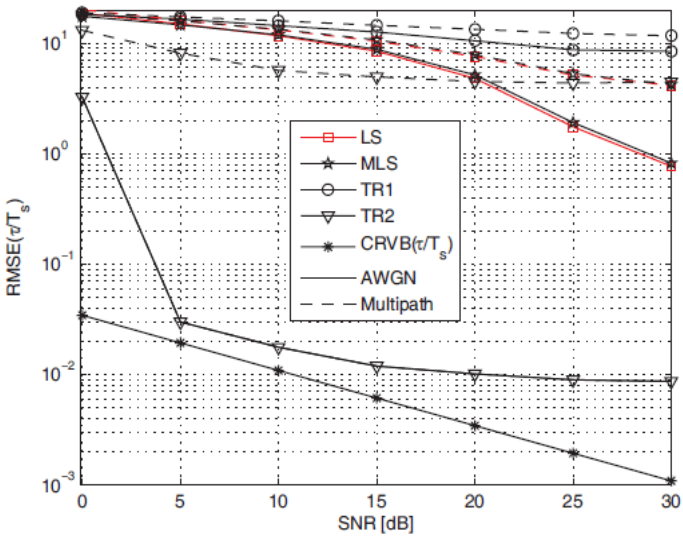

Figure 26: Performance of the considered symbol timing estimators in AWGN channel and multipath channels as a function of SNR for an OFDM/OQAM system.

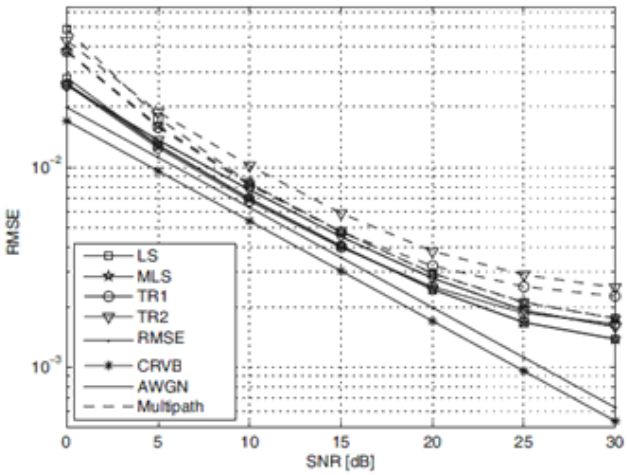

Figure 27: Performance of the considered CFO estimators in AWGN channel and multipath channels as a function of SNR for an OFDM/OQAM system.

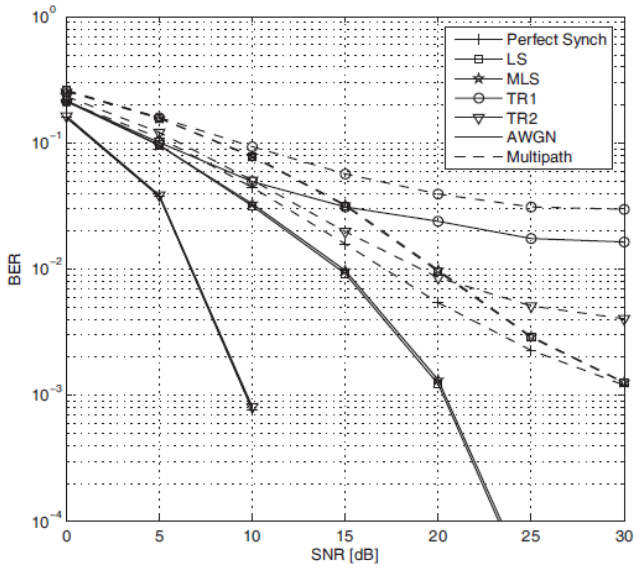

Figure 28: BER of the considered CFO and symbol timing estimators in AWGN and multipath channel as a function of SNR for an OFDM/OQAM system.

3.3.2 FMT System

In this subsection we present the performance of the considered algorithms for an FMT system in AWGN (solid lines) and multipath channel (dashed lines). Precisely, Figure 29 and Figure 30 show the RMSE of the considered symbol timing and CFO estimators, respectively, as a function of the SNR for a training sequence containing two identical blocks of length $P-\gamma K$ where $P=lcm\{64,72\}=576$. We can note that both in AWGN and multipath channel the TR2 symbol timing estimator exhibits the best performance. In particular, in multipath channel the LS and MLS symbol timing estimators are expected to outperform the TR2 estimator only for very high values of SNR. In regard to the performance of the CFO estimators we can note that the LS and MLS estimators assure the lowest RMSE both in AWGN and multipath channel. Moreover, in multipath channel the TR2 CFO estimator provides the highest RMSE. However for $\mathrm{SNR}\geq 10\mathrm{dB}$ the RMSE of the TR2 CFO estimator is lower then 0.1% and this accuracy is sufficient to assure a BER practically coincident with that of the perfectly synchronized system and lower than that obtained when the other considered synchronization algorithms are exploited (see Figure 31).

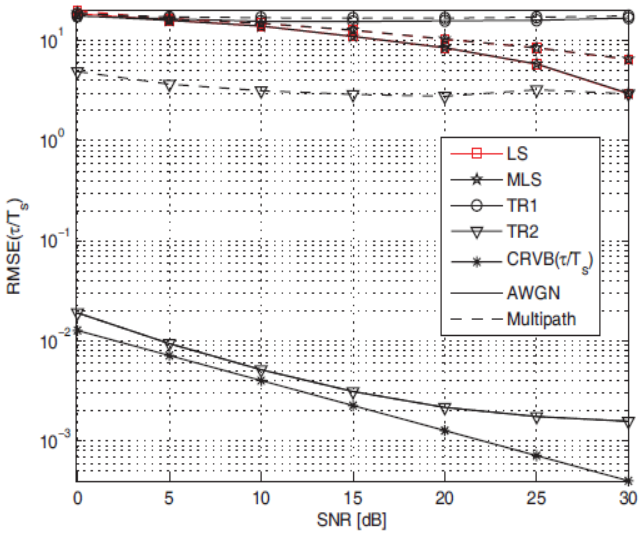

Figure 29: Performance of the considered symbol timing estimators in AWGN and multipath channel as a function of the SNR for an FMT system.

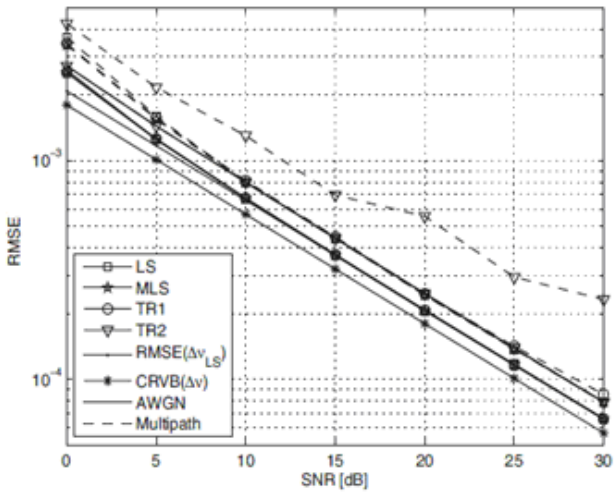

Figure 30: Performance of the considered CFO estimators in AWGN and multipath channel as a function of the SNR for an FMT system.

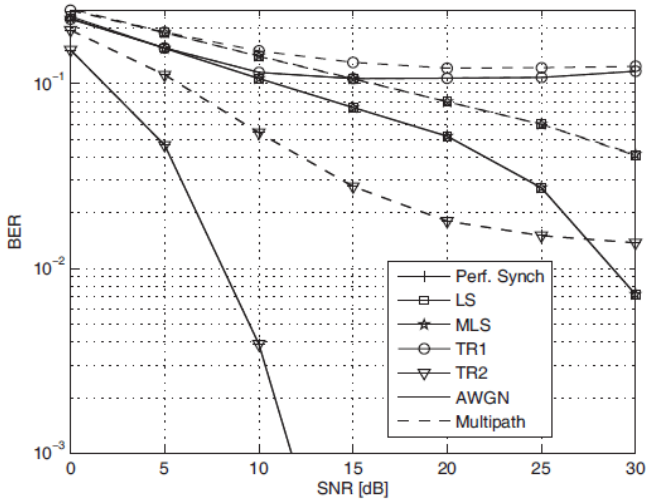

Figure 31: BER of the considered CFO and symbol timing estimators in AWGN and multipath channel as a function of SNR for an FMT system.

3.4 Joint Symbol Timing and CFO Estimation in Multiple Access OFDM/OQAM Systems

In this section, we consider the problem of data-aided synchronization in the up-link of a MA OFDM/OQAM system. In particular, we derive the joint ML symbol timing, CFO and phase offset estimator exploiting a short know preamble embedded in the burst received from each of U users. Let us consider the received signal in the up-link of an AWGN channel, when the information-bearing signal of the ith user $s_i\left(kT_s\right)$ presents a timing offset τ_i, a CFO normalized to the subcarrier

spacing $\varepsilon_i = \Delta f_i T$, a carrier phase offset ϕ_i and an attenuation γ_i can be written as

$$r(kT_s) = \sum_{i=1}^{U} \gamma_i s_i (kT_s - \tau_i) e^{j\left(\frac{2\pi}{N}\varepsilon_i k + \phi_i\right)} + n(kT_s) \quad (3.33)$$

where

$$s_i(kT_s) = \sqrt{\frac{N}{2N_i}} \sum_{p=0}^{S-1} \sum_{l \in \mathcal{A}_i} e^{jl\left(\frac{2\pi}{N}k + \frac{\pi}{2}\right)} \times \left[a_{p,l}^{R} g(kT_s - pT) + j a_{p,l}^{I} g(kT_s - pT - T/2) \right] \quad (3.34)$$

where $T = NT_s$ is the OFDM/OQAM symbol interval, S denotes the number of information-bearing symbols in the burst, while $\mathcal{A}_i$ is the set of subcarriers of size N_i allocated to the ith user.

The known preamble of the ith user is given by

$$z_i(kT_s) = \sqrt{\frac{N}{2N_i}} \sum_{p=0}^{L-1} \sum_{l \in \mathcal{A}_i} e^{jl\left(\frac{2\pi}{N}k + \frac{\pi}{2}\right)} \times \left[a_{p,l}^{R} g(kT_s - pT) + j a_{p,l}^{I} g(kT_s - pT - T/2) \right] \quad (3.35)$$

where $a_{p,l}^{R}$, $a_{p,l}^{I}$, $0 \le p \le L-1$, $\forall l \in \mathcal{A}_i$ denote the known pilot symbols of the ith user. By considering an observations window of total length $N\eta$ containing the non-zero support of the preamble received from each user, the likelihood function in AWGN channel for the unknown parameters ε_i, τ_i and ϕ_i, $i = 1,...,U$, is given by (up to irrelevant multiplicative factor)

$$\Lambda\left(\tilde{\boldsymbol{\varepsilon}},\tilde{\boldsymbol{\tau}},\tilde{\boldsymbol{\phi}}\right)=\exp\left\{-\frac{T_s}{2N_0}\right.$$
$$\left.\times\sum_{k=0}^{N\eta-1}\left|r\left(kT_s\right)-\sum_{i=1}^{U}\gamma_i e^{j\tilde{\phi}_i}e^{j\frac{2\pi}{N}\tilde{\varepsilon}_i k}\tilde{z}_i^{\tilde{\tau}_i}\left(kT_s\right)\right|^2\right\} \tag{3.36}$$

where

$$\tilde{\boldsymbol{\phi}}=\left[\tilde{\phi}_1,...,\tilde{\phi}_U\right]^T,\ \tilde{\boldsymbol{\varepsilon}}=\left[\tilde{\varepsilon}_1,...,\tilde{\varepsilon}_U\right]^T,\ \tilde{\boldsymbol{\tau}}=\left[\tilde{\tau}_1,...,\tilde{\tau}_U\right]^T \tag{3.37}$$

$$z_i^{\tau_i}\left(kT_s\right)=z_i^{\tau_i}\left(kT_s-\tau_i\right)$$
$$=\sqrt{\frac{N}{2N_i}}\sum_{p=0}^{L-1}\sum_{l\in\mathcal{A}_i}e^{jl\left(\frac{2\pi}{T}(kT_s-\tau_i)+\frac{\pi}{2}\right)}$$
$$\times\left[a_{p,l}^{R}g\left(kT_s-pT-\tau_i\right)\right.$$
$$\left.+ja_{p,l}^{I}g\left(kT_s-pT-T/2-\tau_i\right)\right] \tag{3.38}$$

and the notation of the type $\tilde{x}$ indicates trial value of x. By replacing (3.38) in (3.36) and dropping irrelevant multiplicative and additive factors we get

$$\ln\Lambda\left(\tilde{\boldsymbol{\varepsilon}},\tilde{\boldsymbol{\tau}},\tilde{\boldsymbol{\phi}}\right)=\sum_{i=1}^{U}\Re\left[Z_i\left(\tilde{\varepsilon}_i,\tilde{\tau}_i,\tilde{\phi}_i\right)\right] \tag{3.39}$$

where

$$Z_i\left(\tilde{\varepsilon}_i,\tilde{\tau}_i,\tilde{\phi}_i\right)=\gamma_i e^{-j\tilde{\phi}_i}\sum_{k=0}^{N\eta-1}r\left(kT_s\right)e^{-j\frac{2\pi}{N}\tilde{\varepsilon}_i k}$$
$$\times\tilde{z}_i^{\tilde{\tau}_i}\left(kT_s\right)^* \tag{3.40}$$

In the derivation of (3.39) we have neglected the quantity

$$\sum_{k=0}^{N\eta-1}\left|\sum_{i=1}^{U}\gamma_i e^{-j\tilde{\phi}_i}e^{-j\frac{2\pi}{N}\tilde{\varepsilon}_i k}\tilde{z}_i^{\tilde{\tau}_i}\left(kT_s\right)\right|^2\triangleq C_1+C_2 \tag{3.41}$$

Since it is weakly dependent on the parameters to be estimated under the assumptions that the observations window contains the non-zero support

of the preamble received from each user and that the CFO of each user is sufficiently small. In fact, in this case the first contribution in the right hand side (RHS) of (3.41)

$$C_1 = \sum_{i=1}^{U} \gamma_i^2 \sum_{k=0}^{N\eta-1} \left| \tilde{z}_i^{\tilde{\tau}_i}\left(kT_s\right) \right|^2 \tag{3.42}$$

is independent of the phase offset and of the CFO and, moreover, it is weakly dependent on the symbol timing. Furthermore, the second term in the RHS of (3.41)

$$\begin{aligned} C_2 = 2\Re\Bigg\{ & \sum_{i_1=1}^{U} \sum_{i_2=1}^{U-i_1} \sum_{k=0}^{N\eta-1} \gamma_{i_1} \gamma_{i_1+i_2} e^{j\left(\tilde{\phi}_{i_1} - \tilde{\phi}_{i_1+i_2}\right)} \\ & \times e^{j\frac{2\pi}{N}\left(\tilde{\varepsilon}_{i_1} - \tilde{\varepsilon}_{i_1+i_2}\right)k} \tilde{z}_{i_1}^{\tilde{\tau}_{i_1}}\left(kT_s\right) \tilde{z}_{i_1+i_2}^{\tilde{\tau}_{i_1+i_2}}\left(kT_s\right)^* \Bigg\} \end{aligned} \tag{3.43}$$

is negligible since it depends on the scalar product between the signals of the different users whose spectra essentially do not overlap. By substituting (3.38) in (3.40), we get

$$\begin{aligned} Z_i\left(\tilde{\varepsilon}_i, \tilde{\tau}_i, \tilde{\phi}_i\right) = & \sqrt{\frac{N}{2N_i}} \gamma_i e^{-j\tilde{\phi}_i} \sum_{k=0}^{N\eta-1} r\left(kT_s\right) e^{-j\frac{2\pi}{N}\tilde{\varepsilon}_i k} \\ & \times \sum_{l \in \mathcal{A}_i} e^{-jl\left(\frac{2\pi}{T}(kT_s - \tilde{\tau}_i) + \frac{\pi}{2}\right)} \sum_{p=0}^{L-1} \Big[a_{p,l}^R g\left(kT_s - pT - \tilde{\tau}_i\right) \\ & - j a_{p,l}^I g\left(kT_s - pT - T/2 - \tilde{\tau}_i\right) \Big] \end{aligned} \tag{3.44}$$

Hence, (3.44) can be written as

$$Z_i\left(\tilde{\varepsilon}_i, \tilde{\tau}_i, \tilde{\phi}_i\right) = \sqrt{\frac{N}{2N_i}} \gamma_i e^{-j\tilde{\phi}_i} c\left(\tilde{\varepsilon}_i, \tilde{\tau}_i\right) \tag{3.45}$$

where

$$c\left(\tilde{\varepsilon}_i,\tilde{\tau}_i\right)\triangleq\sum_{l\in\mathcal{A}_i}e^{-jl\frac{\pi}{2}}e^{j\frac{2\pi}{T}l\tilde{\tau}_i}$$
$$\times\sum_{p=0}^{L-1}\left[a_{p,l}^{R}w_p^{(l)}\left(\tilde{\varepsilon}_i,\tilde{\tau}_i\right)-ja_{p,l}^{I}w_p^{(l)}\left(\tilde{\varepsilon}_i,\tilde{\tau}_i+T/2\right)\right] \quad (3.46)$$

with

$$w_p^{(l)}\left(\tilde{\varepsilon}_i,\tilde{\tau}_i\right)\triangleq\sum_{k=0}^{N\eta-1}r\left(kT_s\right)e^{-j\frac{2\pi}{N}\tilde{\varepsilon}_i k}e^{-j\frac{2\pi}{N}kl}$$
$$\times g\left(kT_s-\tilde{\tau}_i-pT\right) \quad (3.47)$$

From (3.39) and (3.45), it immediately follows that

$$\hat{\phi}_i^{ML}=\angle\left[c\left(\tilde{\varepsilon}_i,\tilde{\tau}_i\right)\right],\quad i=1,\ldots,U \quad (3.48)$$

and, moreover,

$$\left(\hat{\varepsilon}_i^{ML},\hat{\tau}_i^{ML}\right)=\arg\max_{\tilde{\varepsilon}_i,\tilde{\tau}_i}\left[\left|c\left(\tilde{\varepsilon}_i,\tilde{\tau}_i\right)\right|\right],\quad i=1,\ldots,U \quad (3.49)$$

Therefore, for the *i*th user, the derived joint ML estimator evaluates, for each trial value of the symbol timing $\tilde{\tau}_i$ and of the CFO $\tilde{\varepsilon}_i$, the response of the filter matched to the pulse shaping filter $g(\cdot)$ to the CFO compensated and down-converted signal $r\left(kT_s\right)e^{-j\frac{2\pi}{N}\tilde{\varepsilon}_i k}e^{-j\frac{2\pi}{N}kl}$ at the time instants $\tilde{\tau}_i+pT$ and $\tilde{\tau}_i+pT+T/2$, $0\le p\le L-1$. Specifically, the down-conversion is performed by considering all the frequencies of the subcarrier assigned to the user of interest. Then, exploiting the know pilot symbols, these quantities are combined according to (3.46). The joint ML estimate for the *i*th user is obtained by considering the value of $\left(\tilde{\varepsilon}_i,\tilde{\tau}_i\right)$ that maximizes the magnitude of the statistic in (3.46).

The two-dimensional maximization required by the joint ML estimator in (3.49) undertakes heavy

computational burden. Therefore, to obtain a more feasible synchronization scheme, let us exploit the assumption that the CFO of each user is sufficiently small. Specifically, if each CFO is sufficiently small that within a time ΔQ, comparable with the length of the prototype filter, $e^{-j(2\pi/N)\tilde{\varepsilon}_i \Delta Q} \simeq 1$, for $i = 1,\ldots,U$, it follows that

$$\begin{aligned} w_p^{(l)}\left(\tilde{\varepsilon}_i, \tilde{\tau}_i\right) &= e^{-j2\pi\tilde{\varepsilon}_i p} e^{-j\frac{2\pi}{N}\tilde{\varepsilon}_i\tilde{\theta}_i} e^{-j\frac{2\pi}{N}l\tilde{\theta}_i} \\ &\times \sum_{k=0}^{N\rho-1} r\left[\left(k + pN + \tilde{\theta}_i\right)T_s\right] e^{-j\frac{2\pi}{N}\tilde{\varepsilon}_i k} e^{-j\frac{2\pi}{N}kl} g\left(kT_s\right) \quad (3.50) \\ &\simeq e^{-j2\pi\tilde{\varepsilon}_i p} e^{-j\frac{2\pi}{N}\tilde{\varepsilon}_i\tilde{\theta}_i} w_p^{(l)}\left(0, \tilde{\tau}_i\right) \end{aligned}$$

where $N\rho$ is the length of the prototype filter and the integer θ_i is the ith timing offset normalized to the sampling interval $\theta_i = \tau_i / T_s$. Moreover,

$$\begin{aligned} w_p^{(l)}\left(\tilde{\varepsilon}_i, \tilde{\tau}_i + T/2\right) \simeq\ & e^{-j2\pi\tilde{\varepsilon}_i\left(p+\frac{1}{2}\right)} e^{-j\frac{2\pi}{N}\tilde{\varepsilon}_i\tilde{\theta}_i} \\ & \times w_p^{(l)}\left(0, \tilde{\tau}_i + T/2\right) \end{aligned} \quad (3.51)$$

Therefore, under the assumption that the CFO of each user is sufficiently small it results that

$$c\left(\tilde{\varepsilon}_i,\tilde{\tau}_i\right)\simeq e^{-j\frac{2\pi}{N}\tilde{\varepsilon}_i\tilde{\theta}_i}\sum_{p=0}^{L-1}e^{-j2\pi\tilde{\varepsilon}_i p}$$
$$\times\sum_{p=0}^{L-1}\left[a_{p,l}^{R}w_p^{(l)}\left(0,\tilde{\tau}_i\right)-ja_{p,l}^{I}w_p^{(l)}\left(0,\tilde{\tau}_i+T/2\right)\right]$$
$$=e^{-j\frac{2\pi}{N}\tilde{\varepsilon}_i\tilde{\theta}_i}\left\{\underbrace{\sum_{l\in\mathcal{A}_i}e^{-jl\frac{\pi}{2}}a_{0,l}^{R}w_0^{(l)}\left(0,\tilde{\tau}_i\right)}_{P_i(\tilde{\tau}_i)}\right. \tag{3.52}$$
$$\left.+e^{-j\pi\tilde{\varepsilon}_i}\underbrace{\sum_{l\in\mathcal{A}_i}e^{-j(l+1)\frac{\pi}{2}}a_{0,l}^{I}w_0^{(l)}\left(0,\tilde{\tau}_i+T/2\right)}_{Q_i(\tilde{\tau}_i)}\right\}$$

Hence, under the assumption $\left|\varepsilon_i\right|\ll N/\Delta Q$ and in the case of a training sequence with $L=1$ OFDM/OQAM symbol, the approximate ML (AML) estimator of the CFO of the *i*th user, obtained by maximizing the magnitude of $c\left(\tilde{\varepsilon}_i,\tilde{\tau}_i\right)$ in (3.52), is given by

$$\hat{\varepsilon}_i^{AML}\left(\tilde{\tau}_i\right)=\frac{1}{\pi}\angle\left\{P_i^{*}\left(\tilde{\tau}_i\right)Q_i\left(\tilde{\tau}_i\right)\right\} \tag{3.53}$$

By substituting the closed form AML CFO estimate (3.53) in (3.52), the AML estimator of the timing offset of the *i*th user results to be

$$\begin{aligned}\hat{\tau}_i^{AML}&=\arg\max_{\tilde{\tau}_i}\left[\left|c\left(\hat{\varepsilon}_i^{AML}\left(\tilde{\tau}_i\right),\tilde{\tau}_i\right)\right|\right]\\&=\arg\max_{\tilde{\tau}_i}\left[\left|P_i\left(\tilde{\tau}_i\right)\right|+\left|Q_i\left(\tilde{\tau}_i\right)\right|\right]\end{aligned} \tag{3.54}$$

In Figure 33 we report the AML cost function of the symbol timing estimator of the first user in AWGN. An MA OFDM/OQAM system with $N=1024$

subcarriers and $U = 4$ users, each with $E_s / N_0 = 13\text{dB}$ and with delays $\tau_1 = 0$, $\tau_2 = 20T_s$, $\tau_3 = 50T_s$ and $\tau_4 = 100T_s$, is considered. Moreover, three different kinds of allocation schemes, blockwise, interleaved and interleaved b, are taken into account. As shown in Figure 32, in the blockwise scheme, a block of $N_i = 256$, $i = 1,\ldots,4$ adjacent subcarriers is assigned to the *i*th user. On the contrary, in the interleaved and interleaved b schemes, groups of adjacent subcarriers are allocated to different users and in particular, in the former case, one subcarrier is dropped between two users. The results show that the behaviour of the cost function depends on the adopted allocation scheme. In particular, in the cases of interleaved and interleaved b allocation schemes, the cost function presents local maxima that can interfere with the absolute maximum especially for low E_s / N_0 values, while in the case of blockwise allocation the considered ML cost function exhibits only one sharp peak at the actual value of the symbol timing of the first user $\tau_1 = 0$.

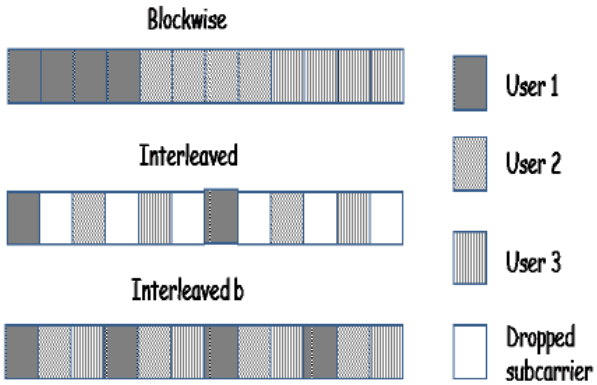

Figure 32: Subcarrier allocation schemes

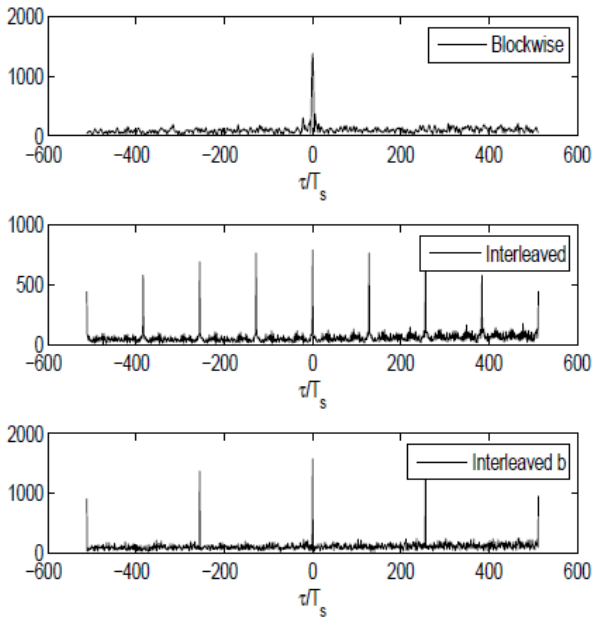

Figure 33: Cost function of the proposed AML symbol timing estimator in AWGN for $N = 1024$.

3.5 Numerical Results

In this section the performance of the proposed joint AML estimator in (3.53) and (3.54) is assessed via computer simulations. A number of 500 Monte Carlo trials has been performed under the following conditions (unless otherwise stated)

- The considered MA OFDM/OQAM system has a bandwidth $B = 1/T_s = 11.2\text{MHz}$ and a number of subcarriers $N = 1024$.
- The data symbols $a_{p,l}^R$ and $a_{p,l}^I$ are the real and imaginary part of QPSK symbols.
- The number of users is $U = 4$ each with 256 subcarriers.
- The prototype filter is obtained by truncating a SRRC Nyquist filter with a roll-off parameter $\alpha = 0.75$ and a length ρN, where the overlap parameter ρ is fixed at $\rho = 4$. Specifically, the filter $g(t)$ is truncated in the interval $\left[-\frac{\rho N}{2}T_s, \frac{\rho N}{2}T_s\right]$ and it is delayed by $\frac{\rho N - 1}{2}T_s$ time units to get a causal prototype filter [28].
- The value of E_s / N_0 for users 2,3 and 4 has been fixed at $E_s / N_0 = 20\text{dB}$. Moreover, the carrier phase, the CFO and the symbol timing (assumed to be an integer multiple of the sampling period T_s) of each user are

uniformly distributed in $[-\pi,\pi)$, $[-0.5,0.5)$ and $\{-NT_s/2, NT_s/2-1\}$, respectively.

- The length of the training sequence is $L=1$ OFDM/OQAM symbol.
- The considered multipath channel is the ITU Vehicular A [26], which has six independent Rayleigh fading taps with delays 0, 0.31, 071, 1.09, 1.73 and 2.51 μs and relative power 0, -1, -9, -10, -15 and -20dB. Moreover, the channel is fixed in each run but it is independent from one run to another.

Notice that although the proposed estimator has been derived by considering only the preamble of each user, in the simulations the burst of each user contains the exploited preamble and the information bearing data.

In the simulations, we have tested the performance of the derived joint estimator both in AWGN (solid line) and multipath channel (dashed line) when the three considered allocation schemes are adopted. Figure 34 displays the RMSE, normalized to the OFDM/OQAM symbol interval T, of the AML symbol timing estimator for the first user as a function of E_s/N_0. In AWGN channel and, for sufficiently high E_s/N_0 values , the interleaved and interleaved b schemes assure better estimates than blockwise scheme. However, the presence of the local maxima in the cost functions for the interleaved and interleaved b schemes leads to a severe performance degradation as E_s/N_0

decreases. The effect of local maxima in the cost function is also evident from the performance of the interleaved b scheme in multipath channel. Figure 35 shows the RMSE, normalized to the intercarrier spacing $1/T$, of the AML CFO estimator for the first user as a function of E_s/N_0. Both in AWGN and multipath, for sufficiently high E_s/N_0 values, the lowest RMSE is obtained when the interleaved b scheme is adopted. Finally, in Figure 36 it is reported the BER obtained in multipath channel by exploiting the proposed joint AML algorithm followed by a one-tap equalizer with perfect knowledge of the channel and of the residual synchronization errors. For all considered allocation schemes, a contained performance loss is observed with respect to the case of one-tap equalization with perfect channel knowledge and perfect synchronization.

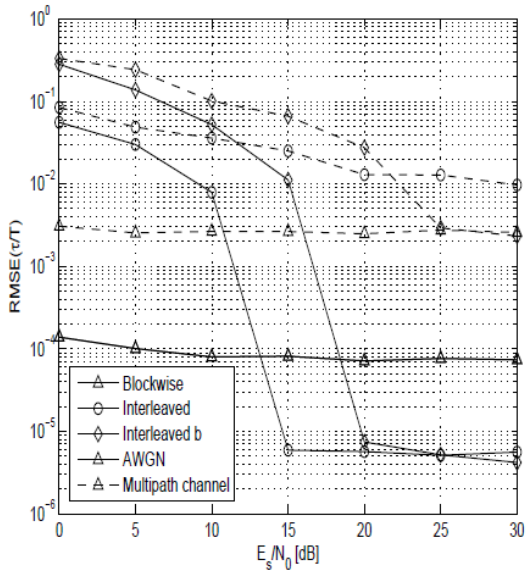

Figure 34: Performance of the proposed AML symbol timing estimator in AWGN and multipath channel.

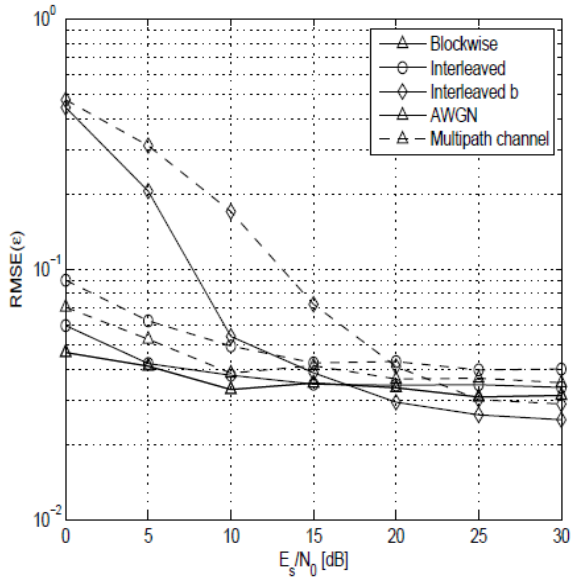

Figure 35: Performance of the proposed AML CFO estimator in AWGN and multipath channel.

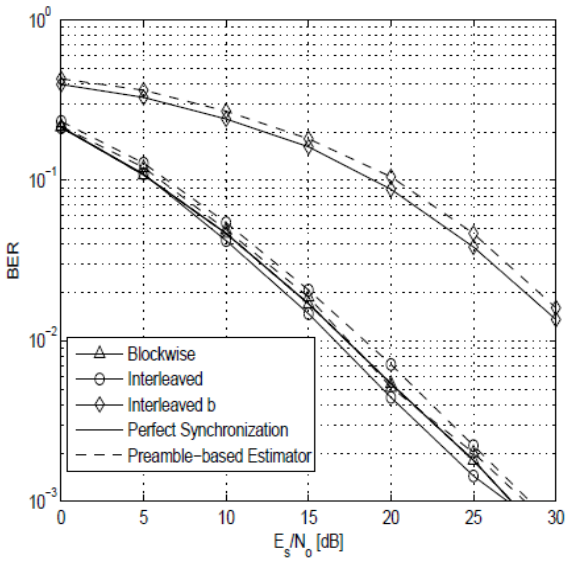

Figure 36: BER of the proposed joint estimator in multipath channel.

Chapter 4

Blind Synchronization Algorithms for FBMC Systems

In this chapter the problem of blind CFO and symbol timing estimation for FBMC systems is considered. Specifically, by exploiting the statistical properties of the received FMT signal in the presence of multipath channels, a closed-form blind CFO estimator is derived. Moreover as regards OFDM/OQAM systems, under the assumptions of low SNR values, three ML CFO estimators for non dispersive channels are derived. Due to their significant computational complexity a more feasible CFO synchronization algorithm is proposed. Finally, under the assumptions of low SNR values, the joint ML symbol timing and phase offset estimator for AWGN channel is considered. The performance of the derived estimators is assessed via computer simulations both in AWGN and multipath channel.

4.1 Blind CFO Estimation for Noncritically Sampled FMT Systems

Let us consider a lightly modified version of the digitalized FMT system model described in (2.10)

$$s(l)=\sigma_s\sqrt{\frac{K}{N_u}} \times\sum_{n=-\infty}^{+\infty}\sum_{k\in\mathcal{A}}a_n(k)g\left(l-nK\right)e^{j\frac{2\pi}{N}lk} \tag{4.1}$$

where $s(l)=s\left(lT_s\right)$. It is assumed that the data symbols are statistically independent and identically distributed (i.i.d.) random variables with zero mean and unit variance (assumption A1). Moreover in (4.1), $g(l)$ is the unit energy prototype filter assumed to be a SRRC Nyquist filter with a roll-off factor α, $0\le\alpha\le 1$ (assumption A2) and $\sigma_s^2=\left\langle E\left[\left|s(l)\right|^2\right]\right\rangle$. Therefore, the expression of the received signal in the presence of CFO ε (normalized to the intercarrier spacing), a carrier phase ϕ and a timing offset τ, is given by

$$r(l)=e^{j\left(\frac{2\pi}{N}\varepsilon l+\phi\right)}s(l-\tau)+n(l) \tag{4.2}$$

where the additive noise $n(l)$ is zero-mean, circular white Gaussian process with variance $\sigma_n^2=E\left[\left|n(l)\right|^2\right]$ and statistically independent of the transmitted signal $s(l)$ (assumption A3). Let us

observe that from assumptions (A1) and (A2) we can easily derive the following result.

Result 1: The unconjugate correlation function of the transmitted FMT signal is equal to

$$\begin{aligned} R_s(m) &= \left\langle E\left[s^*(l)s(l+m) \right] \right\rangle \\ &= \sigma_s^2 R_g(m) \frac{1}{N_u} \sum_{k \in \mathcal{A}} e^{j\frac{2\pi}{N}km} \end{aligned} \tag{4.3}$$

where $R_g(m) = g(m) \otimes g(-m)$ is the autocorrelation function of the prototype filter.

Proof: Accounting for the expression of the transmitted FMT signal (4.1) and by exploiting the assumptions (A1) and (A2), it can be shown that

$$\begin{aligned} &\left\langle E\left[s^*(l)s(l+m) \right] \right\rangle \\ &= \frac{\sigma_s^2 K}{N_u} \sum_{k \in \mathcal{A}} e^{j\frac{2\pi}{N}km} \left\langle \sum_{n=-\infty}^{+\infty} g^*(l-nK)g(l+m-nK) \right\rangle \\ &= \frac{\sigma_s^2 K}{N_u} \sum_{k \in \mathcal{A}} e^{j\frac{2\pi}{N}km} \\ &\times \frac{1}{K} \sum_{l=0}^{K-1} \sum_{n=-\infty}^{+\infty} g^*(l-nK)g(l+m-nK) \\ &= \frac{\sigma_s^2}{N_u} R_g(m) \sum_{k \in \mathcal{A}} e^{j\frac{2\pi}{N}km} \end{aligned} \tag{4.4}$$

From Result 1, we can note that the unconjugate correlation function of the received FMT signal depends on the autocorrelation function of the prototype filter and, on the number N_u and of the position of the useful subcarriers. In particular if $K = N$ (critical sampling) the roll-off factor α of the prototype filter $g(n)$ is zero,

$$g(n)=\frac{1}{\sqrt{N}}\operatorname{sinc}\left(n/N\right)=\frac{1}{\sqrt{N}}\frac{\sin\left(\pi n/N\right)}{\pi n/N} \tag{4.5}$$

and then $R_g(m)=\operatorname{sinc}(m/N)$. Hence, in the case of critical sampling, Result 1 can be written as

Result 1b:

$$R_s(m)=\frac{\sigma_s^2}{N_u}\operatorname{sinc}\left(\frac{m}{N}\right)\sum_{k\in\mathcal{A}}e^{j\frac{2\pi}{N}km} \tag{4.6}$$

4.1.1 Proposed Best Linear Unbiased Algorithm

In this subsection, by exploiting the Result 1 presented in the section 4.1, we derive a new blind closed-form CFO synchronization algorithm for the considered multicarrier system.

Let us consider an observation window of length QN and let us estimate the autocorrelation function of the received signal at $m=\eta N$

$$\begin{aligned}B(\eta)&=\hat{R}_r\left(\eta N\right)\\&=\frac{1}{N\left(Q-\eta\right)}\sum_{k=0}^{N(Q-\eta)-1}r^*\left(k\right)r\left(\eta N+k\right)\end{aligned} \tag{4.7}$$

$\forall\eta\in\left\{L_1,\ldots,L_2-1\right\}$, with $1\le L_1<L_2<Q$.

Substituting the expression of the received signal (4.2) into (4.7) and neglecting the noise × noise term $n^*\left(k\right)n\left(k+\eta N\right)$, we have

$$
\begin{aligned}
B(\eta) &= \frac{1}{N(Q-\eta)} e^{j2\pi\varepsilon\eta} \\
&\times \sum_{k=0}^{N(Q-\eta)-1} \Big[s^*(k-\tau)\, s(k-\tau+\eta N) \\
&\qquad + w^*(k) s(k-\tau+\eta N) \\
&\qquad + s^*(k-\tau)\, w(k+\eta N) \Big] \\
&= e^{j2\pi\varepsilon\eta} \Bigg\{ \zeta(\eta) + \frac{1}{N(Q-\eta)} \\
&\times \sum_{k=0}^{N(Q-\eta)-1} \Big[w^*(k) s(k-\tau+\eta N) \\
&\qquad + s^*(k-\tau)\, w(k+\eta N) \Big] \Bigg\}
\end{aligned}
\tag{4.8}
$$

where, under the hyphotesis of a zero mean circular noise, the random variable $w(k) = n(k) e^{-j\left[(2\pi/N)\varepsilon k + \phi\right]}$ is statistically coincident with $n(k)$. Moreover, the quantity $\zeta(\eta)$ in (4.8), defined as

$$
\begin{aligned}
\zeta(\eta) &= \frac{1}{N(Q-\eta)} \\
&\times \sum_{k=0}^{N(Q-\eta)-1} s^*(k-\tau)\, s(k-\tau+\eta N)
\end{aligned}
\tag{4.9}
$$

for $N(Q-\eta) \gg 1$ can be approximated by [29]

$$
\zeta(\eta) \simeq R_s(\eta N) = \sigma_s^2 R_g(\eta N) \tag{4.10}
$$

Let us now consider the vector $\mathbf{y} \in \mathbb{R}^{(L_2-L_1)\times 1}$ whose elements are defined as

$$
\begin{aligned}
&y(\eta) \triangleq \arg\left\{ \operatorname{sgn}\left[R_g(\eta N) \right] B(\eta) \right\}, \\
&\eta \in \{ L_1, \ldots, L_2 - 1 \}
\end{aligned}
\tag{4.11}
$$

At high SNR values and under the constraint $|\varepsilon| < 1/\left[2\left(L_2 - 1\right)\right]$, the quantity $y(\eta)$ can be approximated by

$$\begin{aligned} y(\eta) &\simeq 2\pi\varepsilon\eta + \arctan\left\{\frac{\Im\left[1+\beta(\eta)\right]}{\Re\left[1+\beta(\eta)\right]}\right\} \\ &\simeq 2\pi\varepsilon\eta + \Im\left[\beta(\eta)\right] \end{aligned} \tag{4.12}$$

with

$$\begin{aligned} \beta(\eta) \triangleq & \frac{1}{\zeta(\eta)N(Q-\eta)} \\ & \times \sum_{k=0}^{N(Q-\eta)-1} \Big[w^*(k)s\left(k-\tau+\eta N\right) \\ & \qquad + s^*\left(k-\tau\right)w\left(k+\eta N\right)\Big] \end{aligned} \tag{4.13}$$

Using a vectorial notation, the scalar equation (4.12) can be rewritten as

$$\mathbf{y} = 2\pi\varepsilon\boldsymbol{\eta}_{L_2-L_1} + \boldsymbol{\mu} \tag{4.14}$$

where

$$\boldsymbol{\eta}_{L_2-L_1} \triangleq \left[L_1, \ldots, L_2 - 1\right]^T \tag{4.15}$$

while

$$\boldsymbol{\mu} \triangleq \left[\Im\left[\beta\left(L_1\right)\right], \ldots, \Im\left[\beta\left(L_2-1\right)\right]\right]^T \tag{4.16}$$

is the noise-related vector with zero mean and covariance matrix $\mathbf{C}_\mu \in \mathbb{R}^{(L_2-L_1)\times(L_2-L_1)}$. Then, by the Gauss-Markov theorem (see [31, p.136]), the linear unbiased CFO estimator with minimum variance is given by

$$\hat{\varepsilon}_{BLU} = \frac{1}{2\pi}\left[\frac{\boldsymbol{\eta}_{L_2-L_1}^T \mathbf{C}_\mu^{-1}\mathbf{y}}{\boldsymbol{\eta}_{L_2-L_1}^T \mathbf{C}_\mu^{-1}\boldsymbol{\eta}_{L_2-L_1}}\right] \tag{4.17}$$

where the (m,l)th element of the matrix $\mathbf{C}_{\mu}$, defined as

$$\left[\mathbf{C}_{\mu}\right]_{(m,l)} = E\left\{\Im\left[\beta\left(L_1+m-1\right)\right]\Im\left[\beta\left(L_1+l-1\right)\right]\right\} \quad (4.18)$$

$$\forall\left(m,l\right)\in\left\{1,\ldots,L_2-L_1\right\}$$

is equal to (see Appendix E for derivation details)

$$\left[\mathbf{C}_{\mu}\right]_{(m,l)} = \frac{1}{N\left(Q-L_1-l+1\right)\left(Q-L_1-m+1\right)} \times \frac{1}{R_g\left(\left(L_1+l-1\right)N\right)R_g\left(\left(L_1+m-1\right)N\right)\mathrm{SNR}} \quad (4.19)$$

$$\times\left[\left(Q-m-l-2L_1+2\right)R_g\left(\left(2L_1+m+l-2\right)N\right) + \left(Q-\max\left\{m,l\right\}-L_1+1\right)R_g\left(\left(m-l\right)N\right)\right]$$

where $\mathrm{SNR}\triangleq\sigma_s^2/\sigma_n^2$ is the signal-to-noise-ratio. The considered BLU CFO estimator, whose acquisition range is given by $\left|\varepsilon\right|<1/\left[2\left(L_2-1\right)\right]$, provides an explicit expression for the estimate $\hat{\varepsilon}$ and it is independent of the knowledge of the timing parameter. Moreover, its variance for $Q\gg L_1+L_2$ and under the assumption of high SNR is given by

$$\mathrm{var}\left\{\hat{\varepsilon}_{BLU}\right\} = \frac{1}{4\pi^2\boldsymbol{\eta}_{L_2-L_1}^{T}\mathbf{C}_{\mu}^{-1}\boldsymbol{\eta}_{L_2-L_1}} \quad (4.20)$$

It is important to note that in the case of critical sampling (i.e. $K=N$), accounting for Result 1b, the autocorrelation function of the transmitted FMT signal evaluated at $m=\eta N$ results to be

$$R_s\left(\eta N\right)=\sigma_s^2R_g\left(\eta N\right)=\sigma_s^2\mathrm{sinc}\left(\eta\right)=\sigma_s^2\delta\left(\eta\right) \quad (4.21)$$

In this case, accounting for (4.7) the term $B(\eta)$ does not depend on the CFO ε. Thus, it follows that the proposed BLU algorithm does not work for $\alpha = 0$ and its performance degrades with small roll-off factors.

In the case of $L_1 = 1$ and $L_2 = 2$, the BLU estimator is equal to

$$\hat{\varepsilon}_{MAT} = \frac{1}{2\pi} \arg\{B(1)\} \tag{4.22}$$

while for $L_1 = 2$ and $L_2 = 3$ we obtain

$$\hat{\varepsilon}_{BLU23} = \frac{1}{4\pi} \arg\{-B(2)\} \tag{4.23}$$

The estimator in (4.22) is labelled as modified Assalini and Tonello (MAT) estimator, since it is a modified version of the joint symbol timing and CFO algorithm proposed in [10], while the estimator in (4.23), referred to as BLU23, has been proposed in [21]. Accounting for (4.20), we can obtain, for $Q \gg L_1 + L_2$ and under the assumption of high SNR values, the theoretical variance of the MAT and the BLU23 estimators, in particular

$$\mathrm{var}\{\hat{\varepsilon}_{MAT}\} = \frac{R_g(0) - R_g(2N)}{4\pi^2 NQ\mathrm{SNR}R_g^2(N)} \tag{4.24}$$

$$\mathrm{var}\{\hat{\varepsilon}_{\mathrm{BLU23}}\} = \frac{R_g(0) - R_g(4N)}{16\pi^2 NQ\mathrm{SNR}R_g^2(2N)} \tag{4.25}$$

From (4.24) and (4.25), for the considered prototype filter, it follows that $\mathrm{var}\{\hat{\varepsilon}_{MAT}\} > \mathrm{var}\{\hat{\varepsilon}_{\mathrm{BLU23}}\}$.

In the next section, the performance of the closed-form estimators (4.17), (4.22) and (4.23) is

compared with that of the estimator derived in [8], labelled as LLSS estimator, whose expression is

$$\hat{\varepsilon}_{\mathrm{LLSS}} = \arg\max_{\tilde{\varepsilon}} \left\{ \sum_{q=0}^{Q-1} \sum_{k \in \mathcal{A}} \left| z_q^{(k)}\left(\tilde{\varepsilon}\right) \right|^2 \right\} \tag{4.26}$$

where $\tilde{\varepsilon}$ is a trial value of the CFO,

$$z_q^{(k)}\left(\tilde{\varepsilon}\right) \triangleq \sum_{n=0}^{N-1} \sum_{l} r_l(n) g_l^*\left(n - qK\right) e^{-j\frac{2\pi}{N}\left[\tilde{\varepsilon}\left(n+lN\right)+kn\right]} \tag{4.27}$$

is the DFT of $\sum_{l} r_l(n) g_l^*\left(n - qK\right) e^{-j\left(2\pi/N\right)\tilde{\varepsilon}\left(n+lN\right)}$, with $r_l(n) \triangleq r\left(n+lN\right)$ and $g_l(n) \triangleq g\left(n+lN\right)$.

Note that the LLSS estimator (4.26) requires, unlike the considered closed-form estimators (4.17), (4.22) and (4.23), a maximization procedure with respect to the continuous variable ε.

4.1.2 Numerical Results and Comparisons

In this subsection, the performance of the proposed BLU estimator (4.17) is assessed via computer simulations and compared with that of the MAT estimator (4.22), the BLU23 estimator (4.23), the LLSS estimator (4.26) and the synchronization algorithm proposed by Bölcskei in [11]. A number of 10^4 Monte Carlo trails has been performed under the following conditions (unless otherwise stated)

- The prototype filter $g\left(n\right)$ is obtained by truncating an SRRC Nyquist filter. Specifically, it is a FIR filter of length γK

(see [2] for implementation details), where the overlap parameter γ is fixed at $\gamma = 8$.

- The values of the normalized CFO and of the carrier phase are fixed at $\varepsilon = 0.1$ and $\phi = \pi / 8$, respectively.
- The multipath channel has been modelled to consist of $N_m + 1 = 15$ independent Rayleigh-fading taps with a maximum delay spread $N_m = 14$ and an exponentially decaying power delay profile. Specifically, $E\left[\left|h(l)\right|^2\right] = Ce^{-l/4}$, $l \in \{0, \ldots, N_m\}$, where C is a constant such that $\sum_{l=0}^{N_m} E\left[\left|h(l)\right|^2\right] = 1$. Moreover, either a static channel or a time-varying channel with normalized Doppler bandwidth $B_d T = 0.1$ have been considered.
- The data symbols $a_n(k)$ belong to a QPSK constellation.
- The size of the set of subcarriers of the considered FMT system is $N = 128$ while the number of virtual subcarriers is $N_v = 16$.
- The parameters L_1 and L_2 of the proposed BLU estimator (4.17) are equal to $L_1 = 1$ and $L_2 = 3$.

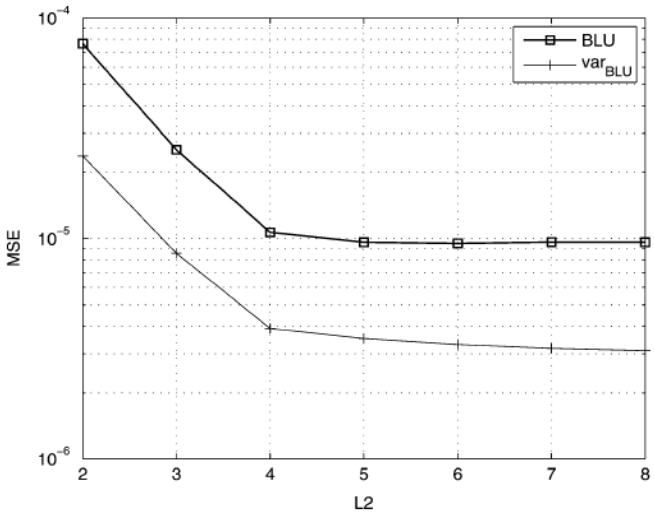

Figure 37: MSE of the BLU estimator in AWGN channel as a function of the parameter L_2, in the case of ideal timing for $\mathrm{SNR} = 5\mathrm{dB}$, $N = 128$ subcarriers and $\alpha = 0.125$.

In Figure 37, we compare numerical and theoretical performance of the proposed BLU estimator for $L_1 = 1$ as a function of the parameter L_2. In particular, the results have been obtained in the case of AWGN channel with $\mathrm{SNR} = 5\mathrm{dB}$, $\alpha = 0.125$, $\varepsilon = 0.01$ and $Q = 40$. We can note that, accounting for (4.18), the value of the parameter L_2 is limited by the overlap factor γ, in fact, for $L_2 > \gamma$ the covariance matrix $\mathbf{C}_\mu$ is singular and the derived BLU estimator cannot be exploited. For this reason in Figure 37 we take $2 \le L_2 \le \gamma$. From Figure 37, we can see that for $L_2 > 4$ theoretical and numerical performance of the proposed BLU estimator do not improve significantly.

Figure 38 and Figure 39 display the mean-squared error (MSE) of the proposed BLU estimator for $L_1 = 1$ and $L_2 \in \{2,3,4\}$ as a function of the parameter Q, in the case of AWGN channel with $\mathrm{SNR} = 5\mathrm{dB}$ and $\mathrm{SNR} = 20\mathrm{dB}$, respectively. In particular, the results have been obtained for $\alpha = 0.25$, $\varepsilon = 0.05$ and in the case of perfect timing synchronization. In the figure, it is also included for comparison the theoretical performance of the considered estimator. We can note that the performance of the proposed BLU estimator improves as the values of the parameter L_2 and Q increase. Moreover, as the SNR value increases, the gap between numerical and theoretical variance increases since the actual performance of the BLU estimator presents a floor (see Figure 40). Figure 40 shows the MSE of the considered CFO estimators as a function of SNR. Precisely, the results are obtained in the case of perfect timing recovery for $Q = 40$, $\alpha = 0.125$ and $\alpha = 0.25$. In the figure are also included the theoretical variance of the BLU estimator, whose expression is reported in (4.20) and the modified Cramér-Rao bound [31] for CFO estimation, derived in Appendix F. The results show that the LLSS estimator provides the lowest MSE while the proposed BLU estimator assures the best performance among the considered closed-form estimators. In Figure 41, we compare the performance of the considered estimators in the case of QPSK and 16-QAM constellations. As indicated in the figure, by varying the signal constellation, the performance of all considered estimators is

practically the same. Figure 42 shows the MSE of the considered CFO estimators as a function of the SNR in the case of perfect timing recovery for $Q = 40$, $\alpha = 0.125$ and $\alpha = 0.25$. We can note that, although all the considered estimators have been derived in AWGN channel, in the presence of multipath channel they assure a performance nearly equal to that obtained in the case of a non dispersive channel (see Figure 40). In Figure 43, we report the performance of the considered estimators in the case of a non ideal timing recovery. Specifically, we evaluate the MSE of the considered CFO estimators as a function of the normalized timing offset τ / K for $\mathrm{SNR} = 10\mathrm{dB}$, $Q = 40$, $N = 128$ subcarriers and for $\alpha = 0.125$ and $\alpha = 0.25$. The results show that the LLSS estimator, derived under the assumption of ideal timing, assures the best performance for $\tau / K < 0.25$, while its accuracy rapidly deteriorates in the presence of larger timing offsets. Moreover, its sensitivity to the timing offset is higher for larger values of the roll-off factor α. On the other hand, the MSE of the BLU, BLU23, MAT and Bölcskei's estimators is practically independent of the actual value of the timing offset. Finally, in Figure 44, we compare the MSE of the considered CFO estimators as a function of the SNR in the case of perfect timing recovery for $Q = 40$, $\alpha = 0.25$, $B_d T = 0.0$ and $B_d T = 0.1$. We can note that, in the presence of a time varying scenario, all considered estimators exhibit for low and moderate SNR values a performance loss with respect to the case of static channel. However, the BLU, BLU23 and MAT

estimators attain for $B_dT = 0.1$ and high SNR values the same floor exhibited in the case of $B_dT = 0.0$.

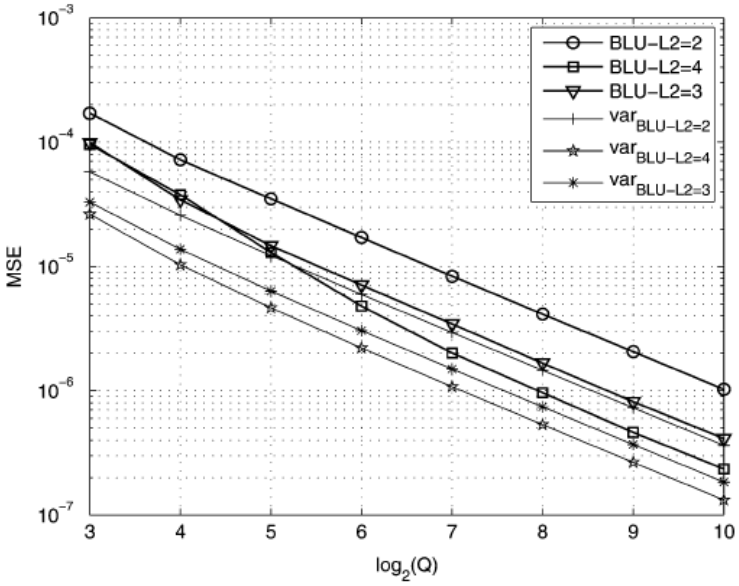

Figure 38: MSE of the considered CFO estimators in AWGN channel as a function of the parameter Q, in the case of ideal timing for $\mathrm{SNR} = 5\mathrm{dB}$, $N = 128$ subcarriers and for $\alpha = 0.25$.

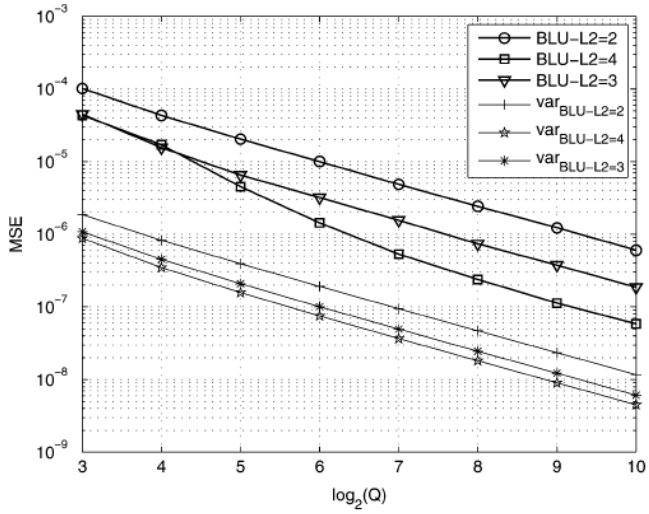

Figure 39: MSE of the considered CFO estimators in AWGN channel as a function of the parameter Q, in the case of ideal timing for $\mathrm{SNR} = 20\mathrm{dB}$, $N = 128$ subcarriers and for $\alpha = 0.25$.

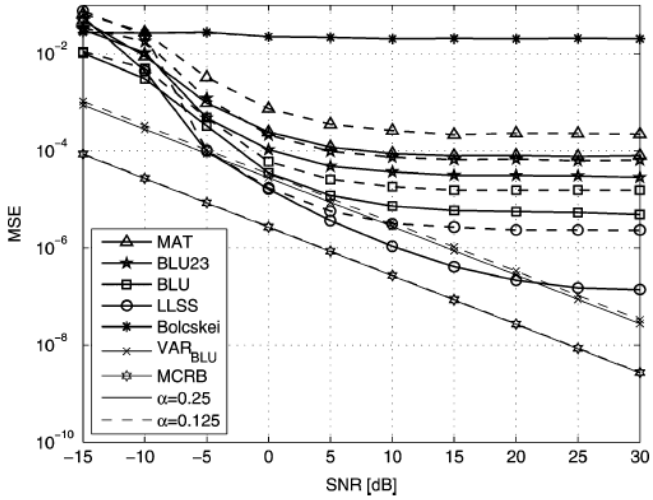

Figure 40: MSE of the considered CFO estimators in AWGN channel as a function of the SNR, in the case of ideal timing for $Q = 40$, $N = 128$ subcarriers and for $\alpha = 0.125$ and $\alpha = 0.25$.

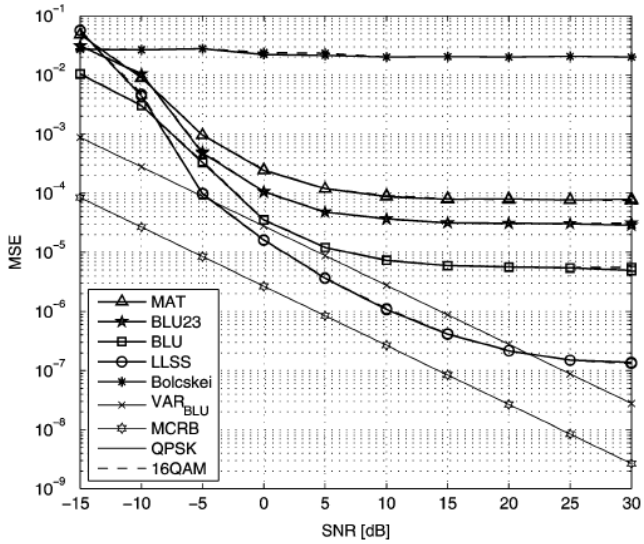

Figure 41: MSE of the considered CFO estimators in AWGN channel as a function of the SNR, in the case of ideal timing for $Q = 40$, $N = 128$ subcarriers, $\alpha = 0.25$ and for 16QAM and QPSK constellation.

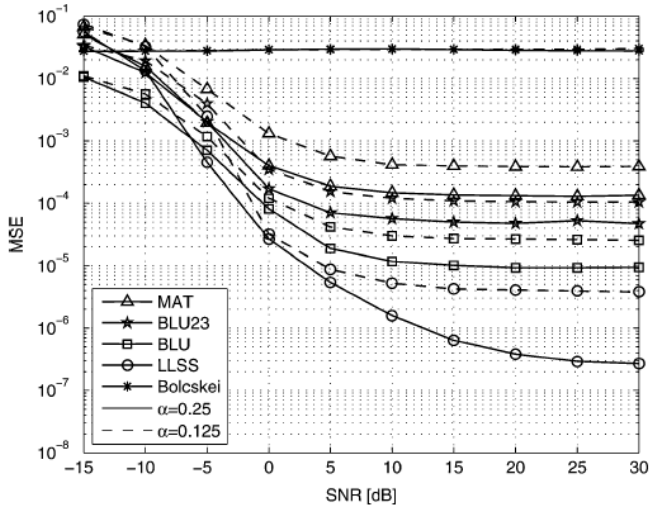

Figure 42: MSE of the considered CFO estimators in multipath channel as a function of the SNR, in the case of ideal timing for $Q = 40$, $N = 128$ subcarriers and for $\alpha = 0.125$ and $\alpha = 0.25$.

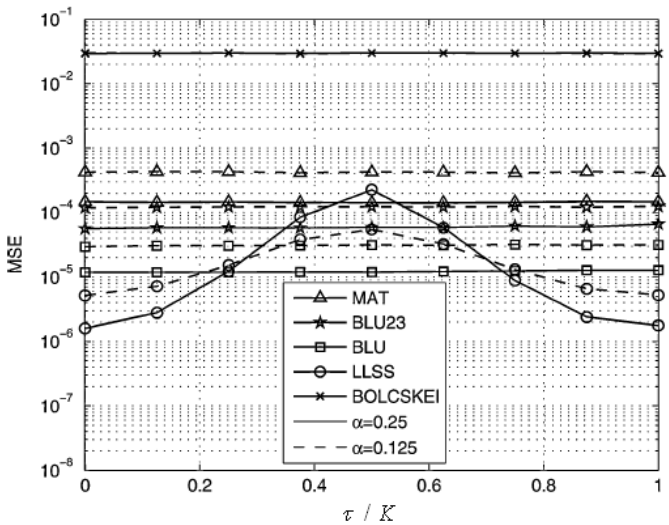

Figure 43: MSE of the considered CFO estimators in multipath channel as a function of the timing offset τ / K for $\mathrm{SNR} = 10\mathrm{dB}$, $Q = 40$, $N = 128$ subcarriers, for $\alpha = 0.125$ and $\alpha = 0.25$.

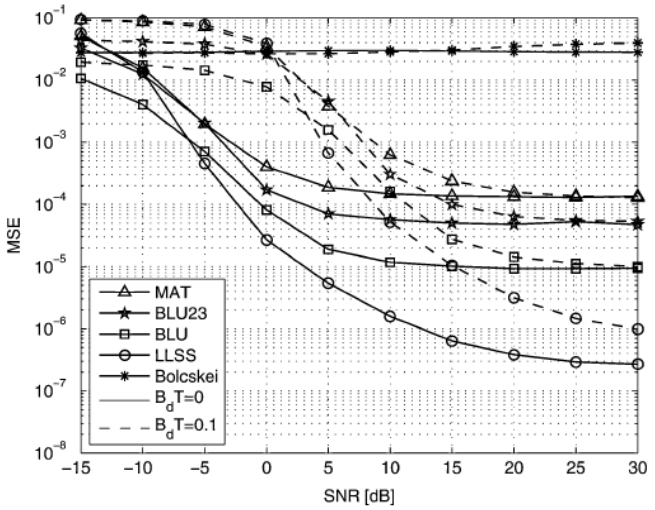

Figure 44: MSE of the considered CFO estimators in multipath channel as a function of the SNR, in the case of ideal timing for $Q = 40$, $N = 128$ subcarriers, $\alpha = 0.25$ and for $B_d T = 0$ and $B_d T = 0.1$.

4.2 Non Data-Aided CFO Estimation for Pulse Shaping OFDM/OQAM Systems

Let us consider the transmitted OFDM/OQAM signal described in (2.1). In particular, by assuming that $E\left[\left|s(kT_s)\right|^2\right]=\sigma_s^2$, (2.1) can be written as

$$\begin{aligned} s(k) = \sigma_s \sqrt{\frac{N}{2N_u}} \sum_{p=-\infty}^{+\infty} \sum_{l\in\mathcal{A}} e^{jl\left(\frac{2\pi}{N}k+\frac{\pi}{2}\right)} \\ \times\left[a_l^R(p)g\left(k-pN\right)\right. \\ \left. + ja_l^I(p)g\left(k-pN-N/2\right)\right] \end{aligned} \tag{4.28}$$

where $s(k)\triangleq s\left(kT_s\right)$.

In the following we assume that

AS1) The data symbols $\left\{a_l^R(p)\right\}_{p=-\infty}^{\infty}$ and $\left\{a_l^I(p)\right\}_{p=-\infty}^{\infty}$, $\forall l\in\mathcal{A}$ belonging to a PAM constellation, are statistically independent and identically distributed random variables with zero mean and unit variance.

AS2) The pulse-shaping filter $g(k)$ is an unit energy SRRC pulse, with a roll-of parameter α, satisfying the orthogonality condition (see [11], [26])

$$\begin{aligned} \sum_{p=-\infty}^{\infty} g\left(k-pN/2\right)g\left(k+\beta N-pN/2\right) \\ = \frac{2}{N}\delta(\beta) \end{aligned} \tag{4.29}$$

From Assumptions (AS1) and (AS2) we can easily derive the following results:

Result 1. The unconjugate correlation function of the transmitted OFDM/OQAM signal $s(k)$ at time k and lag m is equal to

$$\begin{aligned} R_s(k;m) &\triangleq E\left[s^*(k)s(k+m)\right] \\ &= \frac{N\sigma_s^2}{2N_u}\sum_{l\in\mathcal{A}} e^{j\frac{2\pi}{N}lm}\sum_{p=-\infty}^{\infty} g\left(k-p\frac{N}{2}\right) \\ &\times g\left(k+m-p\frac{N}{2}\right) \\ &= \frac{\sigma_s^2}{N_u}\sum_{l\in\mathcal{A}} e^{j\frac{2\pi}{N}lm}\int_{-1/2}^{1/2}\left|G(\mu)\right|^2 e^{-j2\pi\mu m}\mathrm{d}\mu \end{aligned} \tag{4.30}$$

where the last inequality follows from AS2 on the pulse-shaping filter and, moreover

$$G(\mu) = \sum_{k=-\infty}^{\infty} g(k)e^{-j2\pi k\mu} \tag{4.31}$$

is the DFT of the real pulse-shaping filter $g(k)$.

Result 2. The relation function (or the conjugate correlation function) of the transmitted signal $s(k)$ is given by

$$\begin{aligned} C_s(k;m) &\triangleq E\left[s(k)s(k+m)\right] \\ &= \frac{N\sigma_s^2}{2N_u}\sum_{l\in\mathcal{A}} e^{j\frac{2\pi}{N}l(2k+m)}e^{jl\pi} \\ &\times\sum_{p=-\infty}^{\infty}(-1)^p g\left(k-p\frac{N}{2}\right)g\left(k+m-p\frac{N}{2}\right) \\ &= \frac{2\sigma_s^2}{N_u}\sum_{l\in\mathcal{A}} e^{j\frac{2\pi}{N}l(2k+m)}e^{jl\pi}\Re\left\{e^{j\frac{2\pi}{N}(k+m)}\right. \\ &\left.\times\int_{-1/2}^{1/2} G(\mu)G^*\left(\mu-\frac{1}{N}\right)e^{-j2\pi\mu m}\mathrm{d}\mu\right\} \end{aligned} \tag{4.32}$$

From Result 1 we can deduce that for the considered pulse-shaping filter, the OFDM/OQAM signal is

stationary with respect to its unconjugate correlation function. On the other hand, from Result 2 we can note that the conjugate correlation function results to be conjugate second-order cyclostationary with period N.

In the absence of virtual subcarriers (that is for $N = N_u$) the unconjugate correlation function of the transmitted OFDM/OQAM signal $s(k)$ at time k and lag m is equal to (see [32])

$$\begin{aligned} R_s(k;m) &= \frac{N\sigma_s^2}{2}\delta\left(m-\beta N\right) \\ &\times \sum_{p=-\infty}^{\infty} g\left(k-p\frac{N}{2}\right)g\left(k+m-p\frac{N}{2}\right) \\ &= \sigma_s^2\delta\left(m-\beta N\right) \end{aligned} \tag{4.33}$$

Moreover, the conjugate correlation function results to be

$$\begin{aligned} C_s(k;m) &= \frac{N\sigma_s^2}{2}\delta\left(2k+m+N\left(\frac{1}{2}-\beta\right)\right) \\ &\times \sum_{p=-\infty}^{\infty} (-1)^p g\left(k-p\frac{N}{2}\right)g\left(k+m-p\frac{N}{2}\right) \end{aligned} \tag{4.34}$$

4.2.1 ML CFO Estimators for Low SNR Conditions

In this subsection, we derive three ML CFO estimators for OFDM/OQAM systems under the assumption of low SNR conditions.

The discrete-time received signal in AWGN channel, in the presence of a CFO normalized to the

intercarrier spacing ε and a carrier phase offset ϕ can be written as

$$r(k) = e^{j\left(\frac{2\pi}{N}\varepsilon k+\phi\right)} s(k) + n(k) \tag{4.35}$$

where $s(k)$ is the transmitted OFDM/OQAM signal and $n(k)$ denotes the zero-man circular complex white Gaussian noise with $E\left[\left|n(k)\right|^2\right] = \sigma_n^2$ and statistically independent of $s(k)$.

Let us consider an observations window of total length $W = \eta N$, the likelihood function in AWGN channel, for the transmitted symbol sequence

$$\mathbf{a}^R = \left\{a_l^R(p); l \in \mathcal{A}, p \in \mathbb{Z}\right\} \tag{4.36}$$

$$\mathbf{a}^I = \left\{a_l^I(p); l \in \mathcal{A}, p \in \mathbb{Z}\right\} \tag{4.37}$$

and for the two unknown parameters ε and ϕ is given by (up to irrelevant multiplicative factor)

$$\Lambda\left(\tilde{\varepsilon}, \tilde{\phi}, \tilde{\mathbf{a}}^R, \tilde{\mathbf{a}}^I\right) = \exp\left\{-\frac{1}{\sigma_n^2}\sum_{k=0}^{\eta-1}\sum_{m=0}^{N-1}\left|r_k(m) - e^{j\left[\frac{2\pi}{N}\tilde{\varepsilon}(m+kN)+\tilde{\phi}\right]}\tilde{s}_k(m)\right|^2\right\} \tag{4.38}$$

where

$$\begin{aligned} s_k(m) &\triangleq s\left(m+kN\right) \\ &= \sigma_s\sqrt{\frac{N}{2N_u}}\sum_{p=-\infty}^{+\infty}\sum_{l\in\mathcal{A}} e^{jl\left(\frac{2\pi}{N}m+\frac{\pi}{2}\right)} \\ &\times\left[a_l^R(p)g\left(m+kN-pN\right)\right. \\ &\left.+ja_l^I(p)g\left(m+kN-pN-N/2\right)\right] \end{aligned} \tag{4.39}$$

is the transmitted OFDM/OQAM signal and the notation of type $\tilde{x}$ indicates trial value of x.

Replacing (4.39) in (4.38) and dropping factors independent of the unknown parameters we get

$$\Lambda\left(\tilde{\varepsilon},\tilde{\phi},\tilde{\mathbf{a}}^{R},\tilde{\mathbf{a}}^{I}\right)=\exp\left\{\frac{2}{\sigma_n^2}\Re\left[\sum_{k=0}^{\eta-1}\sum_{m=0}^{N-1}r_k(m)\,\tilde{s}_k^{*}(m)\times e^{-j\left[\frac{2\pi}{N}\tilde{\varepsilon}(m+kN)+\tilde{\phi}\right]}\right]\right\} \tag{4.40}$$

By developing in series the likelihood function until the second-order we obtain

$$\Lambda\left(\tilde{\varepsilon},\tilde{\phi},\tilde{\mathbf{a}}^{R},\tilde{\mathbf{a}}^{I}\right)=1+\frac{2}{\sigma_n^2}\Re\left[\sum_{k=0}^{\eta-1}\sum_{m=0}^{N-1}y_k(m)\,\tilde{s}_k^{*}(m)\right]+\frac{1}{2}\left(\frac{2}{\sigma_n^2}\Re\left[\sum_{k=0}^{\eta-1}\sum_{m=0}^{N-1}y_k(m)\,\tilde{s}_k^{*}(m)\right]\right)^2 \tag{4.41}$$

with $y_k(m)=r_k(m)e^{-j\left[2\pi/N\tilde{\varepsilon}(m+kN)+\tilde{\phi}\right]}$. Moreover, by averaging function (4.41) with respect to the data symbols and accounting for assumption AS1, we obtain the marginal likelihood function

$$\begin{aligned}\Lambda\left(\tilde{\varepsilon},\tilde{\phi}\right)=1+\frac{1}{\sigma_n^4}\Re\Bigg\{&\sum_{k_1=0}^{\eta-1}\sum_{m_1=0}^{N-1}\sum_{k_2=0}^{\eta-1}\sum_{m_2=0}^{N-1}y_{k_1}^{*}\left(m_1\right)\\&\times y_{k_2}^{*}\left(m_2\right)E\left[\tilde{s}_{k_1}\left(m_1\right)\tilde{s}_{k_2}\left(m_2\right)\right]\Bigg\}\\&+\frac{1}{\sigma_n^4}\sum_{k_1=0}^{\eta-1}\sum_{m_1=0}^{N-1}\sum_{k_2=0}^{\eta-1}\sum_{m_2=0}^{N-1}y_{k_1}\left(m_1\right)\\&\times y_{k_2}^{*}\left(m_2\right)E\left[\tilde{s}_{k_1}^{*}\left(m_1\right)\tilde{s}_{k_2}\left(m_2\right)\right]\end{aligned} \tag{4.42}$$

We can note that the marginal likelihood function (4.42) depends on both the conjugate and unconjugate correlation functions of the OFDM/OQAM signal. Moreover, accounting for

Result 1 and Result 2, likelihood function (4.42) can be rewritten as

$$\Lambda\left(\tilde{\varepsilon},\tilde{\phi}\right)=1+\frac{\gamma^2}{4}$$
$$\times\Re\left\{e^{-j2\tilde{\phi}}\sum_{p=0}^{\eta-1}\sum_{l\in\mathcal{A}}e^{-jl\pi}\left[\left(z_{p,l}^{R}\left(\tilde{\varepsilon}\right)\right)^2-\left(z_{p,l}^{I}\left(\tilde{\varepsilon}\right)\right)^2\right]\right\} \quad (4.43)$$
$$+\frac{\gamma^2}{4}\sum_{p=0}^{\eta-1}\sum_{l\in\mathcal{A}}\left[\left|z_{p,l}^{R}\left(\tilde{\varepsilon}\right)\right|^2+\left|z_{p,l}^{I}\left(\tilde{\varepsilon}\right)\right|^2\right]$$

where

$$\gamma\triangleq\frac{2\sigma_s}{\sigma_n^2}\sqrt{\frac{N}{2N_u}} \quad (4.44)$$

while the quantities

$$z_{p,l}^{R}\left(\tilde{\varepsilon}\right)=\sum_{m=0}^{N-1}\left[\sum_{k=-\infty}^{\infty}r_{k+p}\left(m\right)e^{-j\frac{2\pi}{N}\tilde{\varepsilon}\left(m+kN+pN\right)}\times g_k\left(m\right)\right]e^{-j\frac{2\pi}{N}ml} \quad (4.45)$$

and

$$z_{p,l}^{I}\left(\tilde{\varepsilon}\right)=\sum_{m=0}^{N-1}\left[\sum_{k=-\infty}^{\infty}r_{k+p}\left(m\right)e^{-j\frac{2\pi}{N}\tilde{\varepsilon}\left(m+kN+pN\right)}\times g_k\left(m-N/2\right)\right]e^{-j\frac{2\pi}{N}ml} \quad (4.46)$$

can be interpreted as the DFT of the response of the receiver polyphase filterbanks $g_k\left(m\right)$ and $g_k\left(m-N/2\right)$ to the input signal $r_{k+p}\left(m\right)e^{-j2\pi/N\tilde{\varepsilon}\left(m+kN+pN\right)}$.

The joint ML estimator is obtained by searching the values of the parameters ε and ϕ that maximize likelihood function (4.42). To proceed we keep the parameter ε fixed and let ϕ vary. Under these

conditions the function $\Lambda\left(\tilde{\varepsilon},\tilde{\phi}\right)$ in (4.42) achieves a maximum for

$$\hat{\phi}_{\mathrm{MLLS}} = \frac{1}{2}\arg\left\{\sum_{p=0}^{\eta-1}\sum_{l\in\mathcal{A}} e^{-jl\pi}\left[\left(z_{p,l}^{R}\left(\tilde{\varepsilon}\right)\right)^2-\left(z_{p,l}^{I}\left(\tilde{\varepsilon}\right)\right)^2\right]\right\} \quad (4.47)$$

Hence, accounting for (4.42) and (4.47), the ML CFO estimator for low SNR values is given by

$$\hat{\varepsilon}_{\mathrm{MLLS}} = \arg\max_{\tilde{\varepsilon}}\left\{\left|\sum_{p=0}^{\eta-1}\sum_{l\in\mathcal{A}} e^{-jl\pi}\left[\left(z_{p,l}^{R}\left(\tilde{\varepsilon}\right)\right)^2-\left(z_{p,l}^{I}\left(\tilde{\varepsilon}\right)\right)^2\right]\right| + \sum_{p=0}^{\eta-1}\sum_{l\in\mathcal{A}}\left[\left|z_{p,l}^{R}\left(\tilde{\varepsilon}\right)\right|^2+\left|z_{p,l}^{I}\left(\tilde{\varepsilon}\right)\right|^2\right]\right\} \quad (4.48)$$

Note that if we consider the carrier phase as random nuisance parameter uniformly distributed in $[0,2\pi)$ and average (4.40) with respect to ϕ we obtain

$$\Lambda\left(\tilde{\varepsilon},\tilde{\mathbf{a}}^{R},\tilde{\mathbf{a}}^{I}\right) = \frac{1}{2\pi}\int_{0}^{2\pi}\Lambda\left(\tilde{\varepsilon},\tilde{\phi},\tilde{\mathbf{a}}^{R},\tilde{\mathbf{a}}^{I}\right)\mathrm{d}\tilde{\phi} = I_0\left(|\mu|\right) \quad (4.49)$$

where

$$\mu = \frac{2}{\sigma_n^2}\Re\left[\sum_{k=0}^{\eta-1}\sum_{m=0}^{N-1} y_k(m)\tilde{s}_k^{*}(m)\right] \quad (4.50)$$

and $I_0(\cdot)$ is the modified Bessel function of the first kind and order zero. Under the assumption of low SNR values the Bessel function can be approximated as

$$I_0\left(|\mu|\right) \simeq 1+\frac{|\mu|^2}{4} \quad (4.51)$$

Moreover, under the assumption AS1, by averaging function (4.51) with respect to the data symbols and neglecting additive and multiplicative parameters independent of the CFO $\tilde{\varepsilon}$, we obtain

$$\begin{aligned}\Lambda(\tilde{\varepsilon}) &= \sum_{k_1=0}^{\eta-1}\sum_{m_1=0}^{N-1}\sum_{k_2=0}^{\eta-1}\sum_{m_2=0}^{N-1} y_{k_1}(m_1)\, y_{k_2}^{*}(m_2) \\ &\quad \times E\left[\tilde{s}_{k_1}^{*}(m_1)\,\tilde{s}_{k_2}(m_2)\right] \\ &= \frac{\gamma^2}{4}\sum_{p=0}^{\eta-1}\sum_{l\in\mathcal{A}}\left[\left|z_{p,l}^{R}(\tilde{\varepsilon})\right|^2 + \left|z_{p,l}^{I}(\tilde{\varepsilon})\right|^2\right]\end{aligned} \tag{4.52}$$

and the corresponding blind ML CFO estimator is given by

$$\begin{aligned}&\hat{\varepsilon}_{\mathrm{UMLLS}} \\ &= \arg\max_{\tilde{\varepsilon}}\left\{\sum_{k_1=0}^{\eta-1}\sum_{m_1=0}^{N-1}\sum_{k_2=0}^{\eta-1}\sum_{m_2=0}^{N-1} y_{k_1}(m_1)\, y_{k_2}^{*}(m_2)\right. \\ &\left.\times E\left[\tilde{s}_{k_1}^{*}(m_1)\,\tilde{s}_{k_2}(m_2)\right]\right\} \\ &= \arg\max_{\tilde{\varepsilon}}\left\{\sum_{p=0}^{\eta-1}\sum_{l\in\mathcal{A}}\left[\left|z_{p,l}^{R}(\tilde{\varepsilon})\right|^2 + \left|z_{p,l}^{I}(\tilde{\varepsilon})\right|^2\right]\right\}\end{aligned} \tag{4.53}$$

Thus, ML estimator (4.53) is coincident with the second term of the cost function in (4.48), depending on the unconjugate correlation function. Therefore, it is referred to as unconjugate MLLS estimator (UMLLS estimator). However, as demonstrated in Appendix G, it cannot be used in the case of a fully loaded OFDM/OQAM system ($N = N_u$).

If we do not consider the second term of the cost function in (4.48), we obtain the CFO estimator

$$\begin{aligned}\hat{\varepsilon}_{\mathrm{CMLLS}} &= \arg\max_{\tilde{\varepsilon}} \left\{ \sum_{k_1=0}^{\eta-1} \sum_{m_1=0}^{N-1} \sum_{k_2=0}^{\eta-1} \sum_{m_2=0}^{N-1} y_{k_1}^{*}(m_1) \right. \\ &\left. \times y_{k_2}^{*}(m_2) E\left[\tilde{s}_{k_1}(m_1) \tilde{s}_{k_2}(m_2) \right] \right\} \\ &= \arg\max_{\tilde{\varepsilon}} \left\{ \left| \sum_{p=0}^{\eta-1} \sum_{l \in \mathcal{A}} e^{-jl\pi} \right. \right. \\ &\left. \left. \times \left[\left(z_{p,l}^{R}(\tilde{\varepsilon}) \right)^2 - \left(z_{p,l}^{I}(\tilde{\varepsilon}) \right)^2 \right] \right| \right\}\end{aligned} \tag{4.54}$$

Note that in the case of a fully loaded OFDM/OQAM system the CFO estimator in (4.54), exploiting the conjugate correlation function of the OFDM/OQAM signal, is coincident with the ML estimator for low SNR, then in the following it will be referred to as conjugate MLLS estimator (CMLLS estimator).

4.2.2 LS CFO Estimator

Let us consider the following statistics:

$$\hat{R}(m) = \frac{1}{N-m} \sum_{k=0}^{N-m-1} r^{*}(k) r(k+m) \tag{4.55}$$

and

$$\hat{R}(N-m) = \frac{1}{m} \sum_{k=0}^{m-1} r^{*}(k) r(k+N-m) \tag{4.56}$$

Under assumptions AS1 and AS2, for $1 \le m \le N-1$, it follows that

$$\hat{R}(m) = e^{j\frac{2\pi}{N}\varepsilon m} \frac{\sigma_s^2 z(m)}{N_u} \sum_{l \in \mathcal{A}} e^{j\frac{2\pi}{N}ml} + e_1(m) \tag{4.57}$$

where

$$e_1(m) \triangleq \hat{R}(m) - E\left[\hat{R}(m)\right] \tag{4.58}$$

and

$$z(m) \triangleq \int_{-1/2}^{1/2} \left|G(\mu)\right|^2 e^{j2\pi\mu m} \mathrm{d}\mu \tag{4.59}$$

is a real function since

$$\left|G(\mu)\right| \triangleq \left|\sum_{k=-\infty}^{\infty} g(k) e^{j2\pi k\mu}\right| \tag{4.60}$$

is an even function. Specifically, accounting for assumption AS2, $z(m)$ is the raised cosine pulse. Moreover, for $1 \le m \le N-1$, we have

$$\begin{aligned} \hat{R}(N-m) = e^{j\frac{2\pi}{N}\varepsilon(N-m)} \frac{\sigma_s^2 z(N-m)}{N_u} \\ \times \sum_{l\in\mathcal{A}} e^{-j\frac{2\pi}{N}ml} + e_2(m) \end{aligned} \tag{4.61}$$

where

$$e_2(m) \triangleq \hat{R}(N-m) - E\left[\hat{R}(N-m)\right] \tag{4.62}$$

It is shown in Appendix H that, under assumptions AS1 and AS2, the zero mean "noise" terms in (4.58) and (4.62) have a variance $\mathcal{O}\left(\left(N-m\right)^{-1}\right)$ and $\mathcal{O}\left(m^{-1}\right)$, respectively. Moreover, it is worthwhile to emphasize that, since under assumption AS2 $z(l)$ is the raised cosine pulse (see (4.59)), for $1 \le m \le N-1$, it follows that

$$z(m) > 0 \tag{4.63}$$

and

$$z(N-m) > 0 \tag{4.64}$$

Taking into account (4.55), (4.61), (4.63) and (4.64) it follows that a CFO estimate can be obtained by minimizing the norm

$$J(\varepsilon)=\left|\sum_{m=L_1}^{L_2-1}\hat{R}(m)\hat{R}(N-m)-\frac{\sigma_s^4 e^{j2\pi\varepsilon}}{N_u^2}\right. \\ \left.\times\sum_{m=L_1}^{L_2-1}z(m)z(N-m)\left|\sum_{l\in\mathcal{A}}e^{j\frac{2\pi}{N}ml}\right|^2\right|^2 \tag{4.65}$$

where L_1 and L_2 are design parameters selected so that the conditions $N-m\gg 1$ and $m\gg 1$ are satisfied. The minimization of the least square error in (4.65) with respect to ε leads to the proposed closed-form LS CFO estimator

$$\hat{\varepsilon}_{\mathrm{LS}}=\frac{1}{2\pi}\arg\left\{\sum_{m=L_1}^{L_2-1}\hat{R}(m)\hat{R}(N-m)\right\} \tag{4.66}$$

It is worthwhile to emphasize that the CFO estimator in (4.66), whose acquisition range is $|\varepsilon|<1/2$, does not require the knowledge of the SNR. Moreover, in the case of an observations window composed by η OFDM/OQAM symbols, estimator (4.66) can be generalized as

$$\hat{\varepsilon}_{\mathrm{LS}}=\frac{1}{2\pi\eta}\sum_{p=0}^{\eta-1}\arg\left\{\sum_{m=L_1}^{L_2-1}\hat{R}_p(m)\hat{R}_p(N-m)\right\} \tag{4.67}$$

with

$$\hat{R}_p(m)=\frac{1}{N-m}\times\sum_{k=0}^{N-m-1}r^*(k+pN)r(k+m+pN) \tag{4.68}$$

and

$$\hat{R}_p(N-m)=\frac{1}{m}\times\sum_{k=0}^{m-1}r^*(k+pN)r(k+N-m+pN) \tag{4.69}$$

4.2.3 Simulation Results

In this subsection the performance of the proposed MLLS, UMLLS, CMLLS and LS CFO estimators in (4.48), (4.53), (4.54) and (4.67) respectively, is assessed via computer simulations and compared with that of the blind algorithm proposed in [12], labelled as CS estimator. Note that the blind CFO estimator based on the unconjugate cyclostationary proposed in [11] is not considered in the following experiments since, as previously stated, under assumptions AS1 and AS2 the OFDM/OQAM signal is stationary with respect to its unconjugate correlation function.

A number of 10^3 Monte Carlo trials has been performed under the following conditions (unless otherwise stated):

- The prototype filter $g(k)$ is obtained by truncating a SRRC Nyquist filter with a roll-off parameter $\alpha=0.6$. Specifically, it is a FIR filter of length γN, where the overlap parameter γ is fixed at $\gamma=8$.
- The values of the normalized CFO and of the carrier phase are uniformly distributed in $[-1/4,1/4)$ and in $[-\pi,\pi)$, respectively.

- The multipath channel has been modelled to consist of $N_m+1=5$ independent Rayleigh-fading taps with a maximum delay spread $N_m=4$ and an exponentially decaying power delay profile. Specifically, $E\left[\left|h(l)\right|^2\right]=Ce^{-l/4}$, $l\in\{0,\ldots,N_m\}$, where C is a constant such that $\sum_{l=0}^{N_m}E\left[\left|h(l)\right|^2\right]=1$. Moreover, the channel is fixed in each run but it is independent from one run to another.
- The size of the set of subcarriers of the considered OFDM/OQAM system is $N=64$ while the number of virtual subcarriers is $N_v=16$.
- The parameters L_1 and L_2 of the proposed LS estimator (4.67) are equal to $L_1=N/4$ and $L_2=N/2$.
- The signal-to-noise ratio is defined as $\text{SNR}\triangleq\sigma_s^2/\sigma_n^2$.

Note that the considered MLLS, UMLLS, CMLLS and CS estimators require a maximization procedure with respect a continuous parameter $\tilde{\varepsilon}$. This maximization is performed exploiting a two step procedure. In the first step it is performed a coarse search with a step size $1/(16\eta)$ followed, in the second step, by a parabolic interpolation.

To obtain some insights about the acquisition range of the considered CFO estimators, Figure 45 shows the behaviour in a single run of the MLLS, UMLLS

and CMLLS cost functions for $\tilde{\varepsilon} \in \left[-N/2, N/2\right)$ and in the case of a fully loaded OFDM/OQAM system. By investigating these results, we can deduce that in this case the acquisition range of the MLLS and CMLLS estimators is $|\varepsilon| < 1/2$ and, moreover, the UMLLS cost function is weakly dependent on the CFO (see Appendix G).

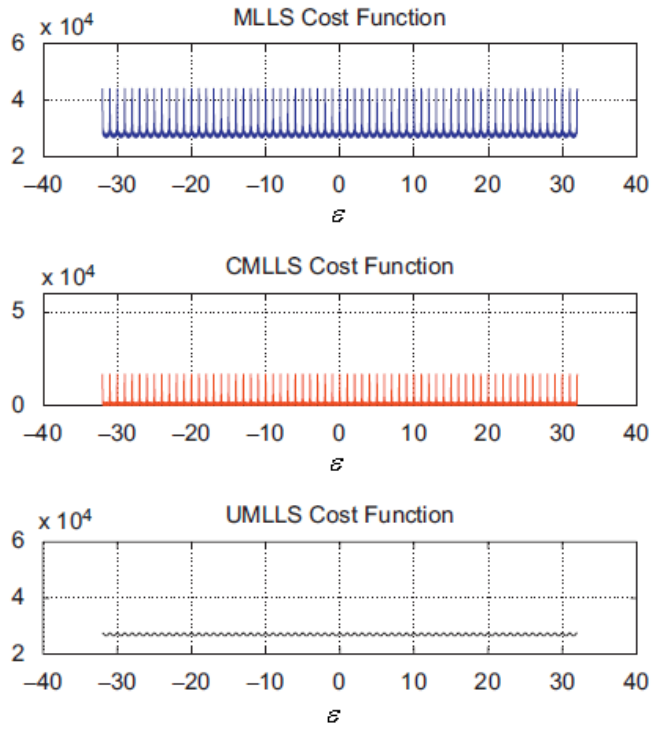

Figure 45: Cost functions of the considered ML CFO estimators in a single run and in AWGN channel with $\mathrm{SNR} = 10\mathrm{dB}$**,** $\eta = 16$**,** $N = 64$ **and** $N_v = 0$**.**

In Figure 46 we present the MLLS, CMLLS and UMLLS cost functions in the case of an OFDM/OQAM system with $N_v = 16$ virtual subcarriers. As illustrated in the figure, by inserting

virtual subcarriers, the acquisition range of the MLLS, CMLLS and UMLLS estimators is $|\varepsilon| < N/2$. However, the MLLS, UMLLS and CMLLS cost functions present local maxima located at $k/2 \quad \forall k \in \mathbb{Z}$ that can interfere with the absolute maximum especially at low SNR values or in dispersive channels leading to outliers. This observation is corroborated by numerical results shown in Figure 47. Precisely, in Figure 47 we report the outlier probability $P_e \triangleq P\left\{\left|\hat{\varepsilon} - \varepsilon\right| \geq 1/2\right\}$ for the MLLS, UMLLS and CMLLS estimators in AWGN channel (solid line) and multipath channel (dashed line) as a function of the SNR. As indicated in the figure, in AWGN channel the MLLS, UMLLS and CMLLS estimators provide, for $\mathrm{SNR} > 5\mathrm{dB}$, CFO estimates without ambiguity, while in dispersive channel the outlier probability is quite high in the whole range of SNR values.

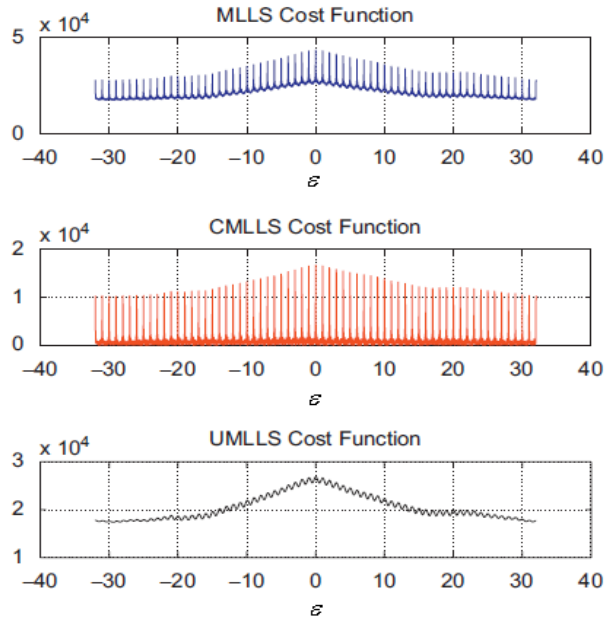

Figure 46: Cost functions of the considered ML CFO estimators in a single run and in AWGN channel with $\mathrm{SNR} = 10\mathrm{dB}$, $\eta = 16$, $N = 64$ **and** $N_v = 16$.

In this first set of simulations we have tested the performance of the proposed algorithms in AWGN channel. Precisely, Figure 48 shows the RMSE of the considered CFO estimators as a function of the actual value of the normalized CFO ε in AWGN channel for $\eta = 16$ OFDM/OQAM symbols. As indicated in the figure, the performance of the MLLS, UMLLS and CMLLS estimators is nearly the same for almost all the considered CFO values, while the RMSE of the CS and LS synchronization algorithms depend on the actual value of the normalized CFO. Figure 49 and Figure 50 show the RMSE of the considered CFO estimators as a

function of the SNR in AWGN channel for $\eta = 16$ OFDM/OQAM symbols. In particular, in Figure 49 we consider the performance of the considered estimators in the case of perfect timing synchronization while in Figure 50 we report numerical results in the presence of timing errors uniformly distributed in $\{0,\ldots,N-1\}T_s$. Moreover, in Figure 49 we also include the MCRB [31] for CFO estimation, derived in Appendix F. The results show that in the case of perfect timing synchronization the MLLS and CMLLS estimators provide the lowest RMSE, while the closed-form LS synchronization algorithm outperforms the much more complex UMLLS and CS estimators. Moreover, the UMLLS, LS and CS estimators are particularly robust to the presence of timing errors, while the MLLS and CMLLS estimators present a severe performance degradation in the presence of timing errors. In Figure 51 we report the RMSE of the considered blind CFO estimators as a function of the number of observed OFDM/OQAM symbols for an SNR value fixed at $\text{SNR} = 10\text{dB}$ and in the case of perfect timing synchronization. As indicated in the figure, the MLLS and CMLLS estimators assure the best performance among all the considered estimators.

Figure 52 displays the RMSE of the MLLS, UMLLS, CMLLS, LS and CS algorithms as a function of the observed OFDM/OQAM symbols and in the presence of multipath channel. As we can see, the MLLS and CMLLS algorithms in multipath channel present a performance degradation with

respect to that achieved in AWGN channel, due to the poor estimate in the coarse search caused by the model mismatch. Instead, the CS, UMLLS and LS estimators exhibit a contained performance loss with respect to the AWGN channel case. However, the closed form LS algorithm assures the best performance among all the considered estimators for a low number of observed OFDM/OQAM symbols. Finally, the results reported in Figure 53 show the RMSE of the considered CFO estimators as a function of the SNR. We can note that for the considered number of OFDM/OQAM symbols $\eta = 16$ the feasible-computational LS CFO estimator provides the most accurate estimates in the whole range of the considered SNR values.

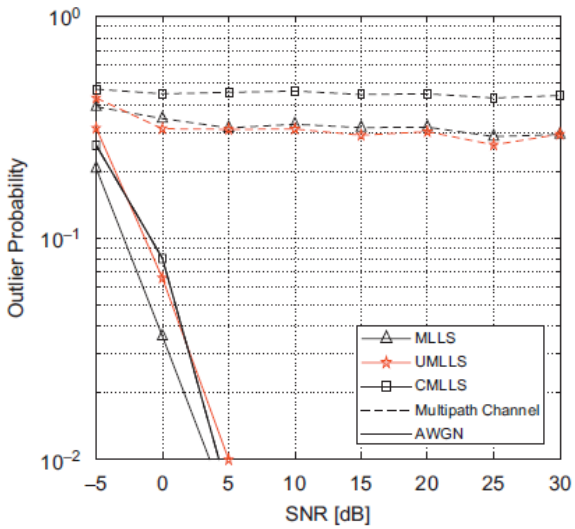

Figure 47: Outlier probability for the considered ML CFO estimators in AWGN (solid lines) and multipath channel (dashed lines) as a function of the SNR for $\eta = 16$, $N = 64$ and $N_v = 16$.

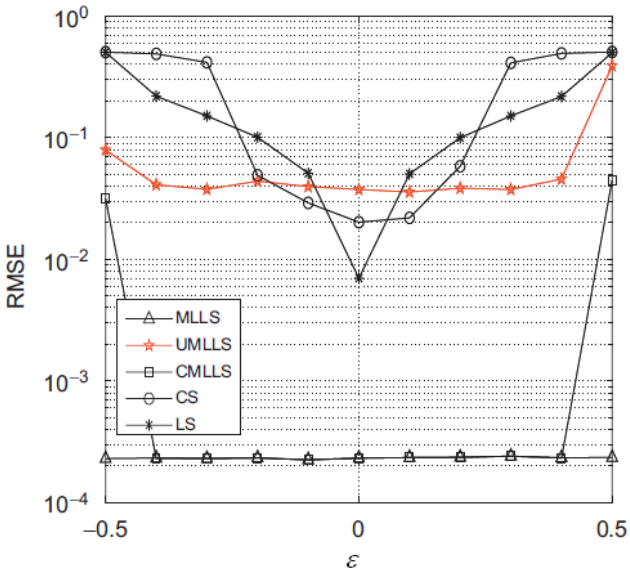

Figure 48: Performance of the considered CFO estimators in AWGN channel as a function of the normalized CFO value ε for $\mathrm{SNR} = 10\mathrm{dB}$, $\eta = 16$, $N = 64$ and $N_v = 16$.

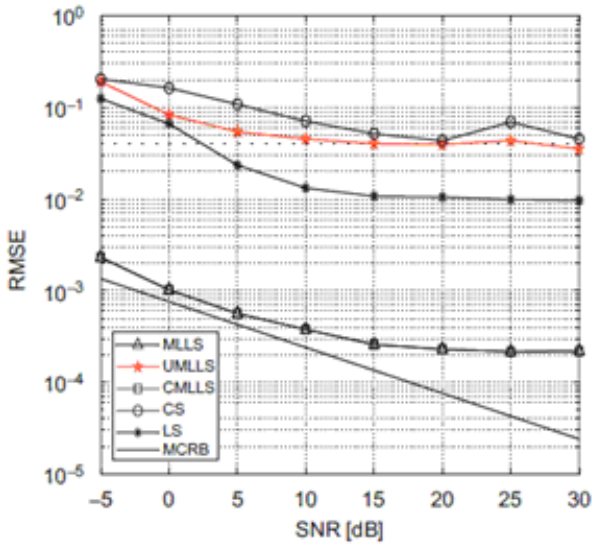

Figure 49: Performance of the considered CFO estimators in AWGN channel as a function of the SNR for $\eta = 16$, $N = 64$ and $N_v = 16$.

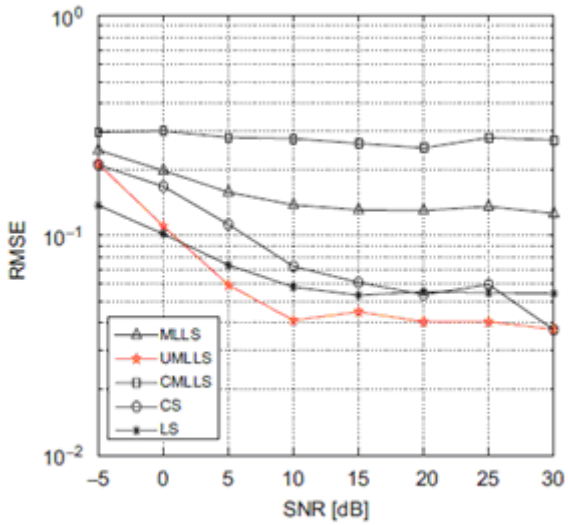

Figure 50: Performance of the considered CFO estimators in AWGN channel as a function of the SNR in the presence of timing errors for $\eta = 16$, $N = 64$ and $N_v = 16$.

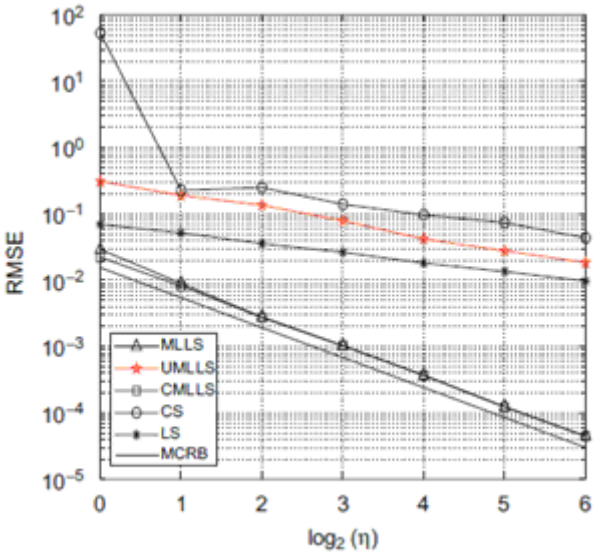

Figure 51: Performance of the considered CFO estimators in AWGN channel as a function of the logarithm of OFDM/OQAM symbols η for $\mathrm{SNR} = 10\mathrm{dB}$, $N = 64$ and $N_v = 16$.

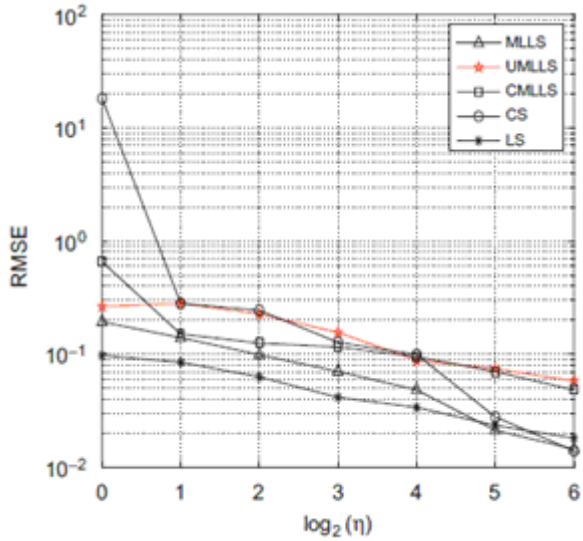

Figure 52: Performance of the considered CFO estimators in multipath channel as a function of the logarithm of OFDM/OQAM symbols η for $\mathrm{SNR} = 10\mathrm{dB}$, $N = 64$ and $N_v = 16$.

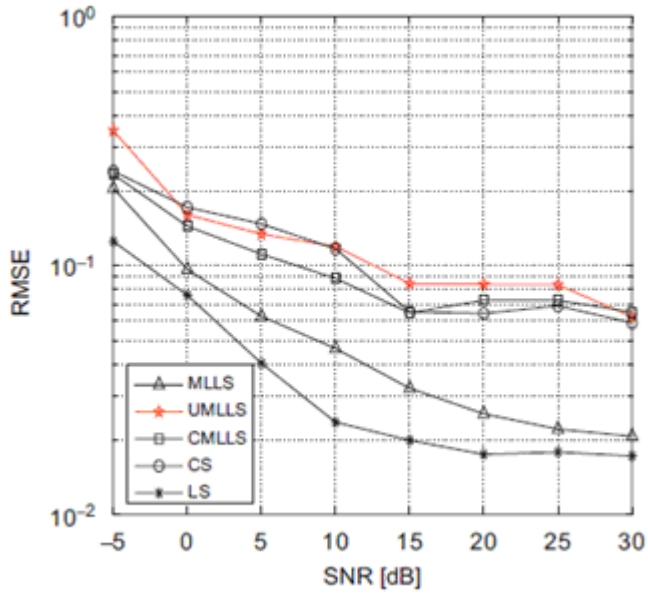

Figure 53: Performance of the considered CFO estimators in AWGN channel as a function of the SNR in the presence of timing errors for $\eta = 16$, $N = 64$ and $N_v = 16$.

4.3 Blind Symbol Timing Estimation for OFDM/OQAM Systems

In this section we derive the ML symbol timing estimator for OFDM/OQAM systems with perfect CFO synchronization and under the assumptions of low SNR values.

Let us consider an OFDM/OQAM system with N subcarriers and no virtual subcarriers, the digitalized received signal in AWGN channel, in the presence of a timing offset τ, a CFO Δf, a carrier phase offset ϕ and an attenuation γ can be written as

$$r\left(kT_s\right)=\gamma s\left(kT_s\right)e^{j\left(2\pi k\Delta fT_s+\phi\right)}+n\left(kT_s\right) \tag{4.70}$$

where $s\left(kT_s\right)$ is the transmitted OFDM/OQAM signal, while $n\left(kT_s\right)$ denotes the zero-mean circular complex white Gaussian noise with a variance σ_n^2/T_s.

In the following we assume that

ASS1) The data symbols $\left\{a_l^R\left(p\right)\right\}_{p=-\infty}^{\infty}$ and $\left\{a_l^I\left(p\right)\right\}_{p=-\infty}^{\infty}$, $\forall l\in\left\{0,\ldots,N-1\right\}$ belonging to a PAM constellation are statistically independent and identically distributed random variables with zero mean and variance a_2.

ASS2) The real-valued and unit-energy pulse-shaping filter $g(t)$ is bandlimited within $\left[-1/T,1/T\right]$.

Under the assumptions ASS1 and ASS2 we can rewrite the results (4.33) and (4.34) as

$$R_s\left(kT_s;mT_s\right)=\frac{a_2}{2}\sum_{l=0}^{N-1}e^{j\frac{2\pi}{N}lm}$$
$$\times\sum_{p=-\infty}^{+\infty}\left[g\left(kT_s-pT\right)g\left(kT_s+mT_s-pT\right)\right. \quad (4.71)$$
$$\left.+g\left(kT_s-pT-\frac{T}{2}\right)g\left(kT_s+mT_s-pT-\frac{T}{2}\right)\right]$$

and

$$C_s\left(kT_s;mT_s\right)=\frac{a_2}{2}\sum_{l=0}^{N-1}e^{j\frac{2\pi}{N}l(2k+m)}e^{jl\pi}$$
$$\times\sum_{p=-\infty}^{+\infty}\left[g\left(kT_s-pT\right)g\left(kT_s+mT_s-pT\right)\right. \quad (4.72)$$
$$\left.-g\left(kT_s-pT-\frac{T}{2}\right)g\left(kT_s+mT_s-pT-\frac{T}{2}\right)\right]$$

respectively. Moreover, it is worthwhile to emphasize that in the presence of a CFO, the unconjugate correlation function of the signal $\overline{s}\left(kT_s\right)=s\left(kT_s\right)e^{j2\pi\Delta fT_s}$ is equal to

$$R_{\overline{s}}\left(kT_s;mT_s\right)=R_s\left(kT_s;mT_s\right)e^{-j2\pi\Delta fT_sm} \quad (4.73)$$

while the conjugate correlation function is given by

$$C_{\overline{s}}\left(kT_s;mT_s\right)=C_s\left(kT_s;mT_s\right)e^{j2\pi\Delta fT_s(2k+m)} \quad (4.74)$$

From (4.73) and (4.74) it follows that the presence of the CFO does not change the unconjugate cyclostationarity period while it affects the conjugate cyclostationarity period. In fact, the term $e^{-j2\pi\Delta fT_sm}$ in (4.73) is a constant for each lag value mT_s while the term $e^{j2\pi\Delta fT_s(2k+m)}$ in (4.74) is a periodic function for each lag value mT_s. For

example, in the presence of a CFO normalized to the intercarrier spacing fixed at $\Delta fT = 0.1$, the conjugate cyclostationarity period is changed from T to $5T$.

4.3.1 ML Symbol Timing Estimator for Low SNR Conditions

By considering an observations window of length $N\eta$, the likelihood function in AWGN channel, for the transmitted symbol sequences

$$\mathbf{a}^R = \left\{ a_l^R(p); l \in \{0, N-1\}, p \in \mathbb{Z} \right\}$$

and

$$\mathbf{a}^I = \left\{ a_l^I(p); l \in \{0, N-1\}, p \in \mathbb{Z} \right\}$$

and for the two unknown parameters τ and ϕ is given by (up to irrelevant multiplicative factors)

$$\Lambda\left(\tilde{\tau}, \tilde{\phi}, \tilde{\mathbf{a}}^R, \tilde{\mathbf{a}}^I\right) = \exp\left\{ -\frac{T_s}{\sigma_n^2} \sum_{k=0}^{\eta-1} \sum_{m=0}^{N-1} \left| r_k\left(mT_s\right) - \gamma e^{j\tilde{\phi}} \tilde{s}_k^{\tilde{\tau}}\left(mT_s\right) \right|^2 \right\} \tag{4.75}$$

where

$$\begin{aligned} & s_k^{\tau}\left(mT_s\right) \triangleq s\left(kT + mT_s - \tau\right) \\ & = \sqrt{\frac{1}{2}} \sum_{p=-\infty}^{+\infty} \sum_{l=0}^{N-1} e^{jl\left(\frac{2\pi}{T}(mT_s - \tau) + \frac{\pi}{2}\right)} \\ & \times \left[a_l^R(p) g\left(mT_s + kT - pT - \tau\right) \right. \\ & \left. + j a_l^I(p) g\left(mT_s + kT - pT - T/2 - \tau\right) \right] \end{aligned} \tag{4.76}$$

By replacing (4.76) in (4.75) and dropping irrelevant factors we get

$$\Lambda\left(\tilde{\tau},\tilde{\phi},\tilde{\mathbf{a}}^{R},\tilde{\mathbf{a}}^{I}\right)=\exp\left\{\frac{2\gamma T_s}{\sigma_n^2}\Re\left[\sum_{k=0}^{\eta-1}\sum_{m=0}^{N-1}r_k\left(mT_s\right)\times e^{-j\tilde{\phi}}\tilde{s}_k^{\tilde{\tau}}\left(mT_s\right)^*\right]\right\} \tag{4.77}$$

since the quantity $\sum_{k=0}^{\eta-1}\sum_{m=0}^{N-1}\left|\tilde{s}_k^{\tilde{\tau}}\left(mT_s\right)\right|^2$ is weakly dependent on the parameter τ. By developing in series the likelihood function until the second-order, by averaging with respect to the data symbols and, finally, by using the relationship $\Re^2(A)=\left(\Re\left(A^2\right)+\left|A\right|^2\right)/2$, we obtain (up to irrelevant additive terms)

$$\Lambda\left(\tilde{\tau},\tilde{\phi}\right)=\frac{\gamma^2T_s^2}{\sigma_n^4}\times E\left[\Re\left\{\left(e^{-j\tilde{\phi}}\sum_{k=0}^{\eta-1}\sum_{m=0}^{N-1}r_k\left(mT_s\right)\tilde{s}_k^{\tilde{\tau}}\left(mT_s\right)^*\right)^2\right\}+\left|\sum_{k=0}^{\eta-1}\sum_{m=0}^{N-1}r_k\left(mT_s\right)e^{-j\tilde{\phi}}\tilde{s}_k^{\tilde{\tau}}\left(mT_s\right)^*\right|^2\right] \tag{4.78}$$

The joint MLLS estimator is obtained by searching the values of the parameters τ and ϕ that maximize the likelihood function in (4.78). To proceed we keep the parameter τ fixed and let ϕ vary. Under these conditions the function $\Lambda\left(\tilde{\tau},\tilde{\phi}\right)$ in (4.78) achieves a maximum for

$$\hat{\phi}_{\mathrm{MLLS}} = \frac{1}{2}\angle\left\{\sum_{k_1=0}^{\eta-1}\sum_{m_1=0}^{N-1}\sum_{k_2=0}^{\eta-1}\sum_{m_2=0}^{N-1} r_{k_1}\left(m_1 T_s\right) \times r_{k_2}\left(m_2 T_s\right) E\left[\tilde{s}_{k_1}^{\tilde{\tau}}\left(m_1 T_s\right)^{*}\tilde{s}_{k_2}^{\tilde{\tau}}\left(m_2 T_s\right)^{*}\right]\right\} \tag{4.79}$$

Hence, accounting for (4.78) and (4.79), the MLLS symbol timing estimator is given by

$$\hat{\tau}_{\mathrm{MLLS}} = \arg\max_{\tilde{\tau}}\left[uc\left(\tilde{\tau}\right) + \left|c\left(\tilde{\tau}\right)\right|\right] \tag{4.80}$$

where

$$uc\left(\tilde{\tau}\right) = \sum_{k_1=0}^{\eta-1}\sum_{m_1=0}^{N-1}\sum_{k_2=0}^{\eta-1}\sum_{m_2=0}^{N-1} r_{k_1}\left(m_1 T_s\right) r_{k_2}^{*}\left(m_2 T_s\right) \times E\left[\tilde{s}_{k_1}^{\tilde{\tau}}\left(m_1 T_s\right)^{*}\tilde{s}_{k_2}^{\tilde{\tau}}\left(m_2 T_s\right)\right] \tag{4.81}$$

and

$$c\left(\tilde{\tau}\right) = \sum_{k_1=0}^{\eta-1}\sum_{m_1=0}^{N-1}\sum_{k_2=0}^{\eta-1}\sum_{m_2=0}^{N-1} r_{k_1}\left(m_1 T_s\right) r_{k_2}\left(m_2 T_s\right) \times E\left[\tilde{s}_{k_1}^{\tilde{\tau}}\left(m_1 T_s\right)^{*}\tilde{s}_{k_2}^{\tilde{\tau}}\left(m_2 T_s\right)^{*}\right] \tag{4.82}$$

From (4.81) and (4.82), it follows that the term $uc\left(\tilde{\tau}\right)$ is the contribution to the cost function exploiting the unconjugate correlation function of the transmitted OFDM/OQAM signal, while the term $c\left(\tilde{\tau}\right)$ is the contribution exploiting the conjugate correlation function. Since under the assumption ASS2 on the pulse-shaping filter the transmitted OFDM/OQAM signal results to be stationary with respect to its unconjugate correlation function, the term $uc\left(\tilde{\tau}\right)$ in (4.81) does not depend on the symbol timing and, then in this case we obtain

$$\hat{\tau}_{\mathrm{MLLS}} = \arg\max_{\tilde{\tau}} \left[\left| c\left(\tilde{\tau}\right) \right| \right] \tag{4.83}$$

Therefore, the conjugate correlation function can bring additional information which can be used for bind symbol timing estimation.

By substituting (4.72) in (4.82) and putting $q_i = k_i N + m_i$, $i = 1, 2$, we get

$$\begin{aligned} c\left(\tilde{\tau}\right) &= \frac{a_2}{2} \sum_{q_1=0}^{N\eta-1} \sum_{q_2=0}^{N\eta-1} r\left(q_1 T_s\right) r\left(q_2 T_s\right) \\ &\times \sum_{l=0}^{N-1} e^{j\frac{2\pi}{T} l\left(q_1 T_s + q_2 T_s - 2\tilde{\tau}\right)} e^{jl\pi} \\ &\times \sum_{p=-\infty}^{+\infty} \left[g\left(q_1 T_s - pT - \tilde{\tau}\right) g\left(q_2 T_s - pT - \tilde{\tau}\right) \right. \\ &\left. - g\left(q_1 T_s - pT - \frac{T}{2} - \tilde{\tau}\right) g\left(q_2 T_s - pT - \frac{T}{2} - \tilde{\tau}\right) \right] \end{aligned} \tag{4.84}$$

Hence, (4.84) becomes

$$c\left(\tilde{\tau}\right) = \sum_{l=0}^{N-1} e^{-jl\pi} e^{j\frac{4\pi}{T} l\tilde{\tau}} \sum_{p=-\infty}^{+\infty} \left[z_p^{(l)}\left(\tilde{\tau}\right)^2 - \hat{z}_p^{(l)}\left(\tilde{\tau}\right)^2 \right] \tag{4.85}$$

with

$$z_p^{(l)}\left(\tilde{\tau}\right) = \sum_{q=0}^{N\eta-1} r\left(qT_s\right) e^{-j\frac{2\pi}{N} ql} g\left(qT_s - pT - \tilde{\tau}\right) \tag{4.86}$$

and

$$\begin{aligned} &\hat{z}_p^{(l)}\left(\tilde{\tau}\right) \\ &= \sum_{q=0}^{N\eta-1} r\left(qT_s\right) e^{-j\frac{2\pi}{N} ql} g\left(qT_s - pT - \tilde{\tau} - \frac{T}{2}\right) \end{aligned} \tag{4.87}$$

From (4.85) it follows that $c\left(\tilde{\tau} + T/2\right) = -c\left(\tilde{\tau}\right)$ and, then, the MLLS symbol timing cost function in (4.83) is a periodic function of period $T/2$, that is the acquisition range is $\left|\tau\right| < T/4$. To obtain some

insight about the lower bound on the performance of the considered estimator in Appendix F and with reference to a SRRC Nyquist filter it is derived the MCRB [31]. Specifically, the MCRB for symbol timing normalized to the OFDM/OQAM symbol interval, for CFO normalized to the intercarrier spacing and for phase, is given by

$$MCRB\left(\frac{\tau}{T}\right)=\frac{1}{8\pi^2\mathrm{SNR}\eta N\left[\frac{N^2-1}{12}+\xi\right]} \underset{N\gg 1}{\cong} \frac{3}{2\pi^2\mathrm{SNR}\eta N^3} \tag{4.88}$$

$$MCRB\left(\Delta fT\right)=\frac{3N}{2\mathrm{SNR}\pi^2\eta\left(N^2\eta^2-1\right)} \underset{N\gg 1}{\cong} \frac{3}{2\pi^2\mathrm{SNR}\eta^3 N} \tag{4.89}$$

$$MCRB\left(\phi\right)=\frac{1}{2\mathrm{SNR}\eta N\left[1-\frac{3\left(\eta N-1\right)}{2\left(2\eta N-1\right)}\right]}+\frac{\left(N-1\right)^2}{8\mathrm{SNR}\eta N\left[\frac{N^2-1}{12}+\xi\right]} \underset{N\gg 1}{\cong} \frac{7}{2\mathrm{SNR}\eta N} \tag{4.90}$$

where $\mathrm{SNR}\triangleq\frac{\gamma^2 a_2}{\sigma_n^2}$. From (4.88), (4.89) and (4.90) it follows that the MCRB for symbol timing normalized to the OFDM/OQAM symbol interval and for phase decrease at the rate $1/\eta$, while the MCRB for CFO normalized to the intercarrier

spacing decreases at the rate $1/\eta^3$. Moreover, for large values of the number of subcarriers the MCRB for normalized CFO and for phase decrease at the rate $1/N$, while the MCRB for normalized symbol timing decreases at the rate $1/N^3$.

4.3.2 Numerical Results

The performance of the MLLS estimator in (4.83) has been assessed via computer simulations by performing a number of 10^3 Monte Carlo trials under the following conditions (unless otherwise stated):
The considered OFDM/OQAM system has a bandwidth $B = 1/T_s = 11.2\text{MHz}$.

- The data symbols $a_l^R(p)$ and $a_l^I(p)$ are the real and imaginary part of QPSK symbols.
- The prototype filter is obtained by truncating an SRRC Nyquist filter with a roll-off parameter $\alpha = 0.75$ and a length ρN where the overlap parameter ρ is fixed at $\rho = 4$. Moreover, the prototype filter $g(t)$ is truncated in the interval $\left[-\frac{\rho N}{2}T_s, -\frac{\rho N}{2}T_s\right[$ and is delayed by $\frac{\rho N - 1}{2}T_s$ time units to get a causal prototype filter [28].

- The carrier phase is uniformly distributed in $[-\pi, \pi)$.
- The symbol timing in uniformly distributed in $\{-N/4, N/4-1\}T_s$.
- The considered multipath channel is the ITU Vehicular A [26], which has six independent Rayleigh fading taps with delays 0, 0.31, 071, 1.09, 1.73 and 2.51 μs and relative power 0, -1, -9, -10, -15 and -20dB. Moreover, the channel is fixed in each run but it is independent from one run to another.

Figure 54 displays the RMSE (normalized to the OFDM/OQAM interval T) of the considered symbol timing estimator as a function of the logarithm of the number of subcarriers N and for one OFDM/OQAM symbol. It results that in AWGN channel (solid line) the proposed estimator provides accurate estimates and, moreover, the asymptotic ($N \gg 1$) performance presents a slope similar to that predicted by the MCRB. In the considered multipath channel (dashed line), the ML estimator exhibits a performance degradation due to the mismatch with respect to the considered model. However, the estimates result to be quite accurate for a sufficiently large number of subcarriers. In Figure 55 we report the RMSE of the proposed symbol timing estimator as a function of the logarithm of the number of OFDM/OQAM symbols in the case of $N = 8$ subcarriers. In this case the multipath channel has been modelled to consist of two independent Rayleigh fading taps with delays $[0,1]T_s$ and relative

power $[0,-8.7]$dB. The numerical results show that in AWGN channel the performance of the proposed estimator presents, for a sufficiently large number of OFDM/OQAM symbols, the same asymptotic ($\eta \gg 1$) slope as the MCRB. However, for the considered number of subcarriers the performance in multipath is satisfactory only for a relatively high number of OFDM/OQAM symbols. Therefore, the proposed algorithm should be exploited in a multipath channel when the number of subcarriers is much higher than the maximum delay spread of the channel. In fact, in this case the proposed algorithm can provide accurate estimates also when only one OFDM/OQAM symbol is used. This statement is corroborated by the results reported in Figure 56 where it is shown the performance of the proposed estimator s a function of the SNR for $N = 2048$ subcarriers and, moreover, only one OFDM/OQAM symbol is exploited. As shown in Figure 57, the adoption of the proposed symbol timing estimator assures a negligible performance degradation with respect to the case of one-tap channel equalization with perfect channel knowledge and perfect synchronization. Finally, in Figure 58 we have analyzed the performance of the MLLS estimator as a function of the CFO. It results that in the case of a low number of subcarriers and a large number of OFDM/OQAM symbols, the presence of the CFO leads to a severe performance degradation, while when a large number of subcarriers is used and only one symbol OFDM/OQAM is exploited, the accuracy of the estimates is not affected by the CFO.

The high sensitivity of the proposed estimation algorithm to the presence of a CFO when a large number of OFDM/OQAM symbols is used can be explained by considering that in this case the symbol timing estimator exploits the second-order conjugate cyclostationarity of the OFDM/OQAM signal and, moreover, the period of the conjugate cyclostationarity is changed by the presence of a CFO (see (4.74)). Therefore, in this case the problem of joint CFO, symbol timing and phase estimation should be considered to obtain accurate estimates. Of course, the joint ML estimator for low SNR values results to be highly complex since, as it can be easily shown, it requires a two-dimensional maximization procedure with respect to two continuous parameters. On the other hand, when only one OFDM/OQAM symbol is exploited, the estimator does not exploit the conjugate cyclostationarity and its performance is essentially unaffected by the CFO.

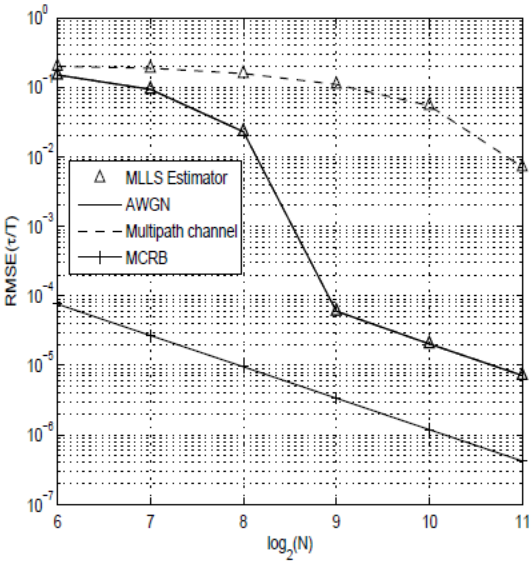

Figure 54: RMSE of the MLLS estimator as a function of the logarithm of the number of subcarriers for $\mathrm{SNR} = 20\mathrm{dB}$ **and** $\eta = 1$**.**

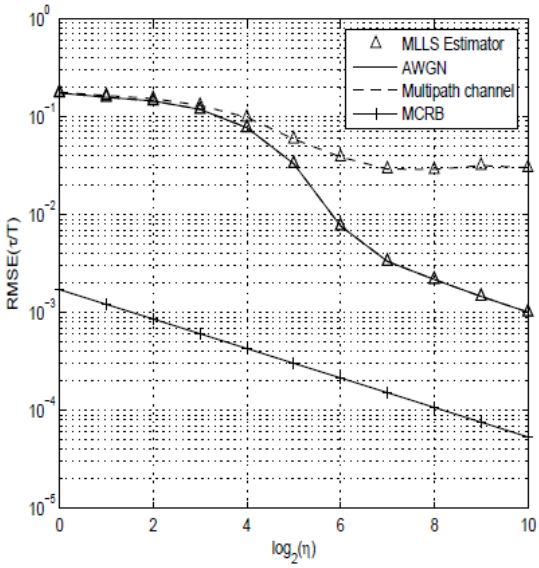

Figure 55: RMSE of the MLLS estimator as a function of the logarithm of the number of OFDM/OQAM symbols for $\mathrm{SNR} = 20\mathrm{dB}$ **and** $N = 8$**.**

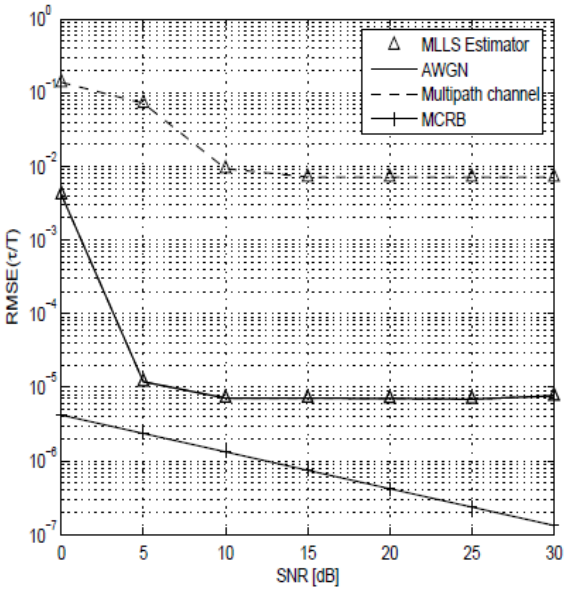

Figure 56: RMSE of the MLLS estimator as a function of the SNR for $\eta = 1$ and $N = 2048$.

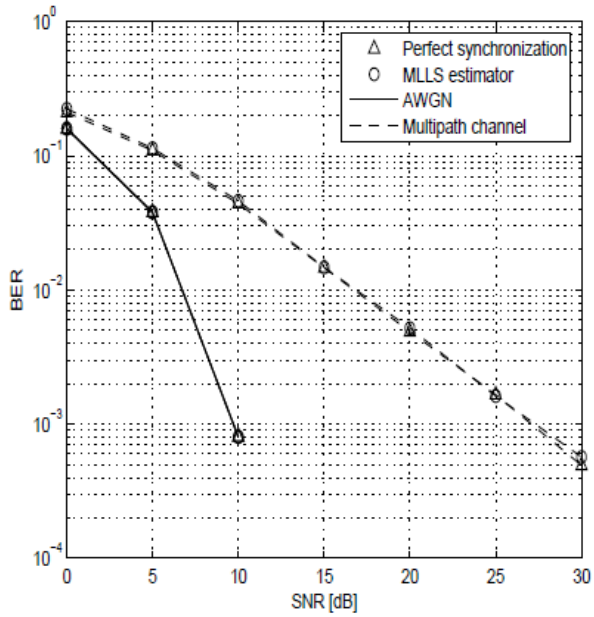

Figure 57: BER as a function of the SNR for $N = 2048$.

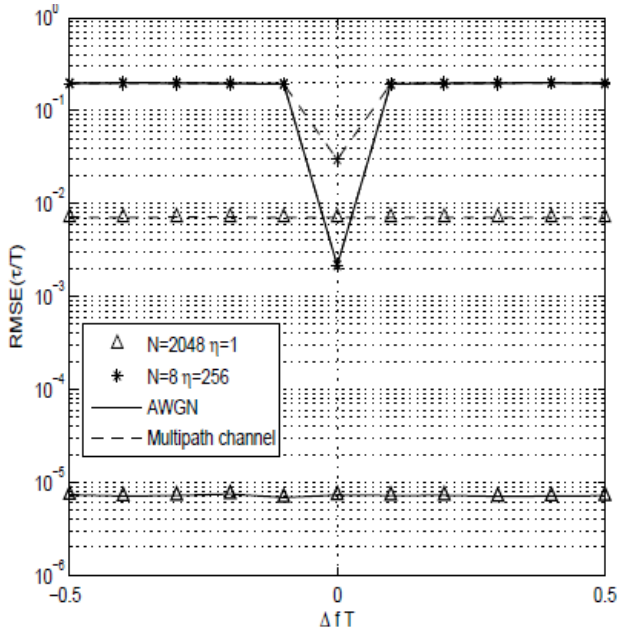

Figure 58: RMSE of the MLLS estimator as a function of the CFO for SNR = 20dB**.**

Chapter 5

Conclusions

In this thesis, issues related to symbol timing and CFO synchronization for FBMC systems are discussed. After the description of FMT and OFDM/OQAM system models, we have investigated their sensitivity to synchronization errors. We have shown that the considered filter-bank based multicarrier systems are very sensitive to synchronization errors, in fact as proved analytically, ISI and ICI can arise at the output of the subchannel matched filters at the receiver. Moreover, it has been shown that in asynchronous uplink FMT and OFDM/OQAM systems are more robust than OFDMA systems to misalignments among users. Successively new data-aided and blind synchronization algorithm have been derived and analyzed.

A synchronization scheme based on a training sequence made up of identical parts has been considered. The proposed method is based on the LS approach, it operates in the time domain before running the receiver filter bank, and, moreover, it does not require the knowledge of the channel impulse response and of the SNR. The performance of the derived estimator has been assessed via computer simulation and compared with that of two joint symbol timing and CFO estimators previously

proposed by Tonello and Rossi in [14] and referred to as TR1 and TR2. Specifically, the proposed estimators and the TR1 estimator exploit only the periodicity of the training burst while the TR2 joint estimator exploits also the knowledge of the periodic training burst. The numerical results have shown that the LS CFO estimator can outperform the TR2 estimator while the knowledge of the shape of the periodic training burst can be exploited by the TR2 to provide more accurate symbol timing estimates. We have also considered the problem of data-aided synchronization for MA OFDM/OQAM systems. In particular, we have derived the joint ML estimator for the phase offset, the CFO and the symbol timing of each of U users and, moreover, we have shown that this approach, when the CFO of each user is sufficiently small leads to U different AML joint phase offset, CFO and symbol timing estimators. Specifically, for each user the phase estimate and the CFO estimate are in closed form while the symbol timing estimate requires a one-dimensional maximization procedure. The performance of the proposed AML joint estimator has been assessed via computer simulations both in AWGN and in multipath channel, and for three different allocation schemes. The numerical results have shown that with only one training symbol and for all the considered allocation schemes, the adoption of the AML estimation scheme can assure a contained performance degradation with respect to the case of one tap equalization with perfect channel knowledge and perfect synchronization.

Afterwards, we have considered the problem of blind feed forward CFO estimation for noncritically sampled FMT systems. In particular, a closed-form CFO estimator based on the statistical properties of the received FMT signal in the presence of non dispersive channel is derived. The performance of the proposed estimator has been compared with that of the ML-based LLSS estimator proposed in [8], that of a modified version of the estimators proposed in [10] and with the estimators considered in [11] and [21]. Computer simulation results have shown that the proposed BLU CFO estimator outperforms the MAT estimator and those derived in [11] and [21] and these present a remarkable robustness in the presence of non ideal timing recovery. In particular, the proposed estimator can outperform the LLSS estimator for large values of the timing offset.

As regards OFDM/OQAM systems, we have dealt with the problem of blind CFO and symbol timing estimation. Specifically, under the hypothesis of low SNR values, the joint ML CFO and carrier phase estimator (MLLS estimator) and its particularization to the case of fully loaded OFDM/OQAM system (CMLLS estimator) have been derived. Moreover, the ML CFO estimator for low SNR values and a carrier phase modeled as a random nuisance parameter uniformly distributed in $[0, 2\pi)$ (UMLLS estimator) has been obtained. Since their implementation complexity is high, a simpler estimation algorithm termed LS estimator has been proposed. The performance of the considered synchronization algorithms has been compared with that of the CS estimator derived in [12]. As

illustrated by computer simulations, in AWGN channel the MLLS and CMLLS estimators can assure the lowest RMSE, however, they are particularly sensitive to the presence of timing errors. Moreover, in multipath channel the closed-form LS CFO estimator can provide the best performance for a relatively low number of OFDM/OQAM symbols.

Finally, the ML phase offset and symbol timing estimator for OFDM/OQAM systems in AWGN channel and under the hypothesis of low SNR values has been proposed. Since the phase estimate is in closed form, the symbol timing estimate requires only a one-dimensional maximization procedure. Specifically, the derived proposed estimator presents an acquisition range equal to $|\tau| < T/4$. The numerical results show that the ML estimator can assure accurate estimates both in AWGN and multipath channel in the case of sufficiently large number of subcarriers and only one OFDM/OQAM symbol. Furthermore, in this case its performance is essentially unaffected by the CFO and, then, it can be exploited before CFO correction. On the other hand, when a large number of OFDM/OQAM symbols is exploited, the proposed estimator demonstrates a severe performance degradation when a CFO is present. This is due to the fact that the ML symbol timing estimator exploits the second-order conjugate cyclostationarity of the OFDM/OQAM signal and, moreover, the period of conjugate cyclostationarity is changed by the presence of the CFO.

Appendix A

Orthogonality Conditions

In this Appendix we derive the conditions that the prototype filter has to satisfy in order to verify the orthogonality conditions (1.47) and (1.48).

At the receiver side, the filter $f(t)$ is matched to the transmission filter $g(t)$, that is $f(t) = g^*(-t)$. Under the hypothesis that $g(t)$ is even and real, then it results $f(t) = g(t)$. Therefore (1.47) and (1.48) can be rewritten as

$$\begin{aligned}
&\Re\left\{\int_{-\infty}^{+\infty} g(\tau) f\left(nT-\tau\right) e^{j\left(\frac{2\pi}{T}\tau+\frac{\pi}{2}\right)k} \mathrm{d}\tau\right\} \\
&= \int_{-\infty}^{+\infty} g(\tau) g\left(nT-\tau\right) \cos\left[\left(\frac{2\pi}{T}\tau+\frac{\pi}{2}\right)k\right] \mathrm{d}\tau \qquad \text{(A.1)} \\
&= \delta\left(k\right)\delta\left(n\right)
\end{aligned}$$

and

$$\begin{aligned}
&\Im\left\{\int_{-\infty}^{+\infty} g(\tau) f\left(nT-\tau-\frac{T}{2}\right) e^{j\left(\frac{2\pi}{T}\tau+\frac{\pi}{2}\right)k} \mathrm{d}\tau\right\} \\
&= \int_{-\infty}^{+\infty} g(\tau) g\left(nT-\tau-\frac{T}{2}\right) \sin\left[\left(\frac{2\pi}{T}\tau+\frac{\pi}{2}\right)k\right] \mathrm{d}\tau \quad \text{(A.2)} \\
&= 0
\end{aligned}$$

respectively.

After the change of variables $\tau = \lambda + \alpha$, where $\alpha = \frac{1}{2}\left(nT - \frac{T}{2}\right)$, (A.2) becomes

$$\int_{-\infty}^{+\infty} g(\lambda+\alpha)g\left(\lambda-\alpha\right)\sin\left(\frac{2\pi}{T}\lambda k + nk\pi\right)\mathrm{d}\lambda$$

$$= \int_{-\infty}^{+\infty} g(\lambda+\alpha)g\left(\lambda-\alpha\right)\sin\left(\frac{2\pi}{T}\lambda k\right)(-1)^{nk}\,\mathrm{d}\lambda \qquad \text{(A.3)}$$

$$= 0, \qquad \forall k$$

Let us consider now the change of variables $\tau = \lambda + n\frac{T}{2}$. Hence (A.1) can be rewritten as

$$\int_{-\infty}^{+\infty} g\left(\lambda + n\frac{T}{2}\right)g\left(\lambda - n\frac{T}{2}\right)\cos\left[\frac{2\pi}{T}\lambda k + \pi nk + \frac{\pi}{2}k\right]\mathrm{d}\lambda$$

$$= \begin{cases} \int_{-\infty}^{+\infty} g\left(\lambda + n\frac{T}{2}\right)g\left(\lambda - n\frac{T}{2}\right)\cos\left[\frac{2\pi}{T}\lambda k\right]\mathrm{d}\lambda \\ = \delta(k)\delta(n) \qquad k \ \ even \\ -\sin\left(\frac{\pi}{2}k\right) \\ \times\int_{-\infty}^{+\infty} g\left(\lambda + n\frac{T}{2}\right)g\left(\lambda - n\frac{T}{2}\right)\sin\left[\frac{2\pi}{T}\lambda k + \pi nk\right]\mathrm{d}\lambda \\ = \delta(k)\delta(n) \qquad k\,odd \end{cases} \qquad \text{(A.4)}$$

By analyzing the term for k odd, we obtain

$$
\begin{aligned}
&-\sin\left(\frac{\pi}{2}k\right) \\
&\times\int_{-\infty}^{+\infty} g\left(\lambda+n\frac{T}{2}\right)g\left(\lambda-n\frac{T}{2}\right)\sin\left[\frac{2\pi}{T}\lambda k+\pi nk\right]\mathrm{d}\lambda \\
&=-\sin\left(\frac{\pi}{2}k\right)\cos\left(\pi nk\right) \\
&\times\int_{-\infty}^{+\infty} g\left(\lambda+n\frac{T}{2}\right)g\left(\lambda-n\frac{T}{2}\right)\sin\left[\frac{2\pi}{T}\lambda k\right]\mathrm{d}\lambda=0 \quad \forall k
\end{aligned}
\tag{A.5}
$$

Therefore, the only condition to be imposed in order to verify the orthogonality conditions (1.47) and (1.48) is given by (A.4) for k even

$$
\begin{aligned}
&\int_{-\infty}^{+\infty} g\left(\lambda+n\frac{T}{2}\right)g\left(\lambda-n\frac{T}{2}\right)\cos\left[\frac{2\pi}{T}\lambda k\right]\mathrm{d}\lambda \\
&=\delta(k)\delta(n)
\end{aligned}
\tag{A.6}
$$

Appendix B

Derivation of the Joint Symbol Timing and CFO LS Estimator

In this Appendix, we illustrate how to derive the expression of the joint symbol timing and CFO LS estimator in (3.4) and (3.5). Let us consider the minimization problem in (3.3)

$$\left(\Delta\hat{f},\hat{\tau}\right)=\arg\min_{\Delta\tilde{f},\tilde{\tau}}\left\{\sum_{k=N_g-1}^{N_{TR}N-P-1}\left|r\left(kT_s+\tilde{\tau}\right)-r\left(kT_s+PT_s+\tilde{\tau}\right)e^{-j2\pi\Delta\tilde{f}T_sP}\right|^2\right\} \tag{B.1}$$

after simple algebraic manipulation, we obtain

$$\left(\Delta\hat{f},\hat{\tau}\right)=\arg\min_{\Delta\tilde{f},\tilde{\tau}}\left\{Q_1\left(\tilde{\tau}\right)+Q_2\left(\tilde{\tau}\right)-2\left|R\left(\tilde{\tau}\right)\right|\cos\left(-2\pi\Delta\tilde{f}T_sP+\angle R\left(\tilde{\tau}\right)\right)\right\} \tag{B.2}$$

with

$$Q_1\left(\tilde{\tau}\right)+Q_2\left(\tilde{\tau}\right)=\sum_{k=N_g-1}^{N_{TR}N-P-1}\left(\left|r\left(kT_s+\tilde{\tau}\right)\right|^2+\left|r\left(kT_s+PT_s+\tilde{\tau}\right)\right|^2\right) \tag{B.3}$$

and

$$R\left(\tilde{\tau}\right)=\sum_{k=N_g-1}^{N_{TR}N-P-1}r^*\left(kT_s+\tilde{\tau}\right)r\left(kT_s+PT_s+\tilde{\tau}\right) \tag{B.4}$$

The maximum with respect to the CFO is obtained when the cosine term in (B.2) is equal to one. This yields the CFO estimator

$$\Delta\hat{f}\left(\tilde{\tau}\right)=\frac{1}{2\pi PT_s}\arg\left\{R\left(\tilde{\tau}\right)\right\} \tag{B.5}$$

In this case the cost function in (B.2) can be written as

$$\Gamma\left(\tilde{\tau},\Delta\tilde{f}\left(\tilde{\tau}\right)\right)=Q_1\left(\tilde{\tau}\right)+Q_2\left(\tilde{\tau}\right)-2\left|R\left(\tilde{\tau}\right)\right| \tag{B.6}$$

and the joint LS symbol timing and CFO estimator is given by

$$\hat{\tau}_{LS}=\arg\max_{\tilde{\tau}}\left\{2\left|R\left(\tilde{\tau}\right)\right|-Q_1\left(\tilde{\tau}\right)-Q_2\left(\tilde{\tau}\right)\right\} \tag{B.7}$$

and

$$\Delta\hat{f}_{LS}\left(\hat{\tau}_{LS}\right)=\frac{1}{2\pi PT_s}\arg\left\{R\left(\hat{\tau}_{LS}\right)\right\}. \tag{B.8}$$

Appendix C

CRVB of Joint Symbol Timing, CFO and Phase Offset Estimation for FMT Systems

In this Appendix, we present some algebraic details to derive the expression of the CRVB of joint symbol timing, CFO and phase offset estimation for FMT systems shown in (3.29), (3.30) and (3.31). Accounting for the expression of the transmitted FMT signal (2.10), the (1,1) entry of FIM can be rewritten as

$$
\begin{aligned}
\left[\mathbf{F}\right]_{(1,1)} &= \frac{2T_s K}{\sigma_n^2} \\
&\times \sum_{k=N_g-1}^{N_{TR}N-1} \frac{1}{N_u} \Bigg[\sum_{l_1,l_2 \in \mathcal{A}} a_{l_1} a_{l_2}^{*} \, e^{j\frac{2\pi(1+\alpha)}{T}\left[(kT_s-\tau)(l_1-l_2)\right]} \\
&\times \sum_{p_1,p_2=-\infty}^{\infty} \frac{\partial g\left(kT_s - p_1 K T_s - \tau\right)}{\partial \tau} \frac{\partial g\left(kT_s - p_2 K T_s - \tau\right)}{\partial \tau} \\
&+ \frac{1}{N_u} \sum_{l_1,l_2 \in \mathcal{A}} a_{l_1} a_{l_2}^{*} e^{j\frac{2\pi(1+\alpha)}{T}\left[(kT_s-\tau)(l_1-l_2)\right]} \frac{4\pi^2 l_1 l_2 \left(1+\alpha\right)^2}{T^2} \\
&\times \sum_{p_1,p_2=-\infty}^{\infty} g\left(kT_s - p_1 K T_s - \tau\right) g\left(kT_s - p_2 K T_s - \tau\right) \Bigg]
\end{aligned}
\tag{C.1}
$$

Under the assumption of a pulse shaping filter assumed to be an SRRC Nyquist filter with a signalling interval T, we obtain

$$\begin{aligned}
&\sum_{p_1,p_2=-\infty}^{\infty} g\left(kT_s - p_1 kT_s - \tau\right) g\left(kT_s - p_2 kT_s - \tau\right) \\
&= \left(\sum_{p=-\infty}^{\infty} g\left(kT_s - pT - \tau\right) \right)^2 \\
&= \left(\int_{-\infty}^{+\infty} G(f) e^{j2\pi f\left(kT_s - \tau\right)} \sum_{p=-\infty}^{\infty} e^{-j2\pi fpT} \mathrm{d}f \right)^2 \\
&= \left(\frac{1}{T} \sum_{q=-\infty}^{+\infty} G\left(\frac{q}{T}\right) e^{j\frac{2\pi}{T}q\left(kT_s - \tau\right)} \right)^2 = \frac{1}{T}
\end{aligned} \tag{C.2}$$

and

$$\begin{aligned}
&\sum_{p_1,p_2=-\infty}^{\infty} \frac{\partial g\left(kT_s - p_1 KT_s - \tau\right)}{\partial \tau} \\
&\times \frac{\partial g\left(kT_s - p_2 KT_s - \tau\right)}{\partial \tau} = 0
\end{aligned} \tag{C.3}$$

Therefore, we have

$$\begin{aligned}
\left[\mathbf{F}\right]_{(1,1)} &= \frac{2}{\sigma_n^2} \sum_{k=N_g-1}^{N_{TR}N-1} \frac{1}{N_u} \\
&\times \sum_{l_1,l_2 \in \mathcal{A}} a_{l_1} a_{l_2}^* e^{j\frac{2\pi(1+\alpha)}{T}\left[\left(kT_s - \tau\right)\left(l_1 - l_2\right)\right]} \frac{4\pi^2 l_1 l_2 \left(1+\alpha\right)^2}{T^2}
\end{aligned} \tag{C.4}$$

By exploiting the following result [33]

$$\begin{aligned}&\frac{1}{W^q}\sum_{k=N_g-1}^{N_{TR}N-1}k^q\frac{1}{N_u}\sum_{l_1,l_2\in\mathcal{A}}a_{l_1}a_{l_2}^{*}e^{j\frac{2\pi(1+\alpha)}{T}\left[(kT_s-\tau)(l_1-l_2)\right]}l_1l_2\\&=\frac{1}{q+1}\frac{1}{N_u}\sum_{l\in\mathcal{A}}\left|a_l\right|^2l^2\\&+\mathcal{O}\left(\frac{1}{W^q}\right)\frac{1}{N_u}\sum_{\substack{l_1,l_2\in\mathcal{A}\\l_1\neq l_2}}a_{l_1}a_{l_2}^{*}e^{j\frac{2\pi(1+\alpha)}{T}\left[(kT_s-\tau)(l_1-l_2)\right]}l_1l_2\\&\cong\frac{1}{q+1}\frac{1}{N_u}\sum_{l\in\mathcal{A}}\left|a_l\right|^2l^2\end{aligned}\tag{C.5}$$

and for a training sequence with $\left|a_l\right|^2=1\quad\forall l\in\mathcal{A}$, the expression (C.4) can be approximated by

$$\left[\mathbf{F}\right]_{(1,1)}=\frac{2W}{\sigma_n^2}\frac{1}{N_u}\sum_{l\in\mathcal{A}}\left(\frac{2\pi l\left(1+\alpha\right)}{T}\right)^2\tag{C.6}$$

Analogously, we obtain

$$\begin{aligned}&\left[\mathbf{F}\right]_{(1,2)}=\left[\mathbf{F}\right]_{(2,1)}=-\frac{4\pi^2\mathrm{SNR}}{N_uN}\\&\times\left(N_{TR}N-N_g+1\right)\left(N_{TR}N+N_g-3\right)\sum_{l\in\mathcal{A}}l\end{aligned}\tag{C.7}$$

$$\begin{aligned}&\left[\mathbf{F}\right]_{(1,3)}=\left[\mathbf{F}\right]_{(3,1)}\\&=-\frac{4\pi\mathrm{SNR}}{N_uT}\left(N_{TR}N-N_g+1\right)\sum_{l\in\mathcal{A}}l\end{aligned}\tag{C.8}$$

$$\begin{aligned}&\left[\mathbf{F}\right]_{(2,3)}=\left[\mathbf{F}\right]_{(3,2)}=\frac{2\pi}{\sigma_n^2}T_s\\&\times\left(N_{TR}N-N_g\right)\left(N_{TR}N+N_g-1\right)\end{aligned}\tag{C.9}$$

$$\begin{aligned}&\left[\mathbf{F}\right]_{(2,2)}=\frac{\left(2\pi T_s\right)^2}{\sigma_n^2}\frac{\left(N_{TR}N-N_g\right)}{3}\left(2N_{TR}^2N^2\right.\\&\left.+2N_g^2-3N_{TR}N-3N_g+1+2N_gN_{TR}N\right)\end{aligned}\tag{C.10}$$

$$\left[\mathbf{F}\right]_{(3,3)} = \frac{2}{\sigma_n^2}\left(N_{TR}N - N_g\right) \tag{C.11}$$

The CRVB for symbol timing, CFO and phase is given by the corresponding diagonal element of inverse of FIM, that is

$$\mathrm{CRVB}\left(\tau\right) = \left[\mathbf{F}^{-1}\right]_{(1,1)}$$

$$= \frac{\left(NT_s\right)^2}{8\pi^2 W \mathrm{SNR}\left[\frac{1}{N_u}\sum_{l\in\mathcal{A}}\left(l - \frac{1}{N_u}\sum_{l\in\mathcal{A}} l\right)^2\right]} \tag{C.12}$$

$$\mathrm{CRVB}\left(\Delta f\right) = \left[\mathbf{F}^{-1}\right]_{(2,2)} = \frac{3}{2\left(\pi T_s\right)^2 \mathrm{SNR} W^3} \tag{C.13}$$

$$\mathrm{CRVB}(\phi) = \left[\mathbf{F}^{-1}\right]_{(3,3)}$$

$$= \frac{3\left[4\beta\frac{1}{N_u}\sum_{l\in\mathcal{A}} l^2 - W^2\left(\frac{1}{N_u}\sum_{l\in\mathcal{A}} l\right)^2\right]}{2W^3 \mathrm{SNR}\left[\frac{1}{N_u}\sum_{l\in\mathcal{A}}\left(l - \frac{1}{N_u}\sum_{l\in\mathcal{A}} l\right)^2\right]} \tag{C.14}$$

where β is defined in (3.32).

Appendix D

Theoretical Variance of the LS, MLS, TR1 and TR2 CFO Estimators

In this Appendix, we derive the theoretical variance of the LS, MLS, TR1 and TR2 CFO estimators reported in (3.5), (3.9), (3.11) and (3.13), respectively, in the case of perfect symbol timing synchronization. Let us observe that in the case of perfect symbol timing synchronization the LS and the TR1 CFO estimators are coincident and, moreover, for $\left|\Delta\hat{f}_{LS}-\Delta f\right| \ll 1/\left(2\pi PT_s\right)$ we can approximate their estimation as (see [34])

$$\Delta\hat{f}_{LS}-\Delta f \cong \frac{1}{\left(2\pi PT_s\right)} \times \left\{ \frac{\sum_{k=N_g-1}^{N_{TR}N-P-1} \Im\left[e^{-j2\pi\Delta fPT_s} r^*\left(kT_s\right) r\left(kT_s+PT_s\right)\right]}{\sum_{k=N_g-1}^{N_{TR}N-P-1} \Re\left[e^{-j2\pi\Delta fPT_s} r^*\left(kT_s\right) r\left(kT_s+PT_s\right)\right]} \right\} \quad \text{(D.1)}$$

Substituting the signal model (2.2) in (D.1), under the assumption of high SNR conditions, we obtain

$$\Delta\hat{f}_{LS} - \Delta f \cong \frac{1}{2\pi P T_s \sum_{k=N_g-1}^{N_{TR}N-P-1} \left|s\left(kT_s\right)\right|^2} \sum_{k=N_g-1}^{N_{TR}N-P-1} \Im\left[w^*\left(kT_s\right) s\left(kT_s\right) + w\left(kT_s + PT_s\right) s^*\left(kT_s\right)\right] \tag{D.2}$$

where, under the hypothesis of a zero-mean circular noise, the random variable

$$w\left(kT_s\right) \triangleq n\left(kT_s\right) e^{-j\left[2\pi\Delta f k T_s + \phi\right]} \tag{D.3}$$

is statistically coincident with $n\left(kT_s\right)$ and has a variance $E\left[\left|w\left(kT_s\right)\right|^2\right] = \sigma_n^2 / T_s$.

From (D.1) we obtain $E\left[\Delta\hat{f}_{LS} - \Delta f\right] = 0$, that is, for high SNR values, the CFO LS estimate is unbiased. Moreover, the mean squared error is given by

$$E\left[\left(\Delta\hat{f}_{LS} - \Delta f\right)^2\right] = \frac{\sigma_n^2}{4\pi^2 P^2 T_s^3 \sum_{k=N_g-1}^{N_{TR}N-P-1} \left|s\left(kT_s\right)\right|^2} \tag{D.4}$$

Note that, using the result (C.2) and the approximation (C.5), we have

$$\sum_{k=N_g-1}^{N_{TR}N-P-1} \left|s\left(kT_s\right)\right|^2 \simeq \frac{N_{TR}N - P - N_g + 1}{T_s} \tag{D.5}$$

Therefore, the MSE in (D.4) can be approximated by

$$E\left[\left(\Delta\hat{f}_{LS} - \Delta f\right)^2\right] = \frac{\sigma_n^2}{4\pi^2 P^2 T_s^2 \mathrm{SNR}\left(N_{TR}N - P - N_g + 1\right)} \tag{D.6}$$

From (D.6) we can observe that, into the case of AWGN channel and perfect symbol timing synchronization the TR1 and LS CFO estimators have the same theoretical variance, whose

expression depends on the length $N_{TR}N$ of the training sequence and it is inversely proportional to the SNR and P^2.

Appendix E

Derivation of the Matrix $\mathbf{C}_{\mu}$

In this Appendix, we report some details to derive the (m,l)th element of the covariance matrix (4.19). Substituting the expression of the received signal in (4.18) and accounting for the result (4.3), we obtain

$$\begin{aligned}
\left[\mathbf{C}_{\mu}\right]_{(m,l)} &= \frac{K}{2N^2\left(Q-L_1-l+1\right)\left(Q-L_1-m+1\right)} \\
&\times \frac{1}{R_g\left(\left(L_1+l-1\right)N\right)R_g\left(\left(L_1+m-1\right)N\right)\mathrm{SNR}} \\
&\times \Bigg[-\sum_{k=(L_1+l-1)N}^{(Q-L_1-m+1)N-1}\sum_{n=-\infty}^{+\infty}\tilde{g}_n\left(k-\left(L_1+l-1\right)N\right) \\
&\times \tilde{g}_n\left(k+\left(L_1+m-1\right)N-nK\right) \\
&- \sum_{k=(L_1+l-1)N}^{(Q-L_1-m+1)N-1}\sum_{n=-\infty}^{+\infty}\tilde{g}_n\left(k+\left(L_1+l-1\right)N\right) \\
&\times \tilde{g}_n\left(k-\left(L_1+m-1\right)N\right) \\
&+ \sum_{k=0}^{(Q-L_1-\max\{l,m\}+1)N-1}\sum_{n=-\infty}^{+\infty}\tilde{g}_n\left(k+\left(L_1+l-1\right)N\right) \\
&\times \tilde{g}_n\left(k+\left(L_1+m-1\right)N\right) \\
&+ \sum_{k=\left(L_1+\max\{l,m\}-1\right)N}^{QN-1}\sum_{n=-\infty}^{+\infty}\tilde{g}_n\left(k-\left(L_1+l-1\right)N\right) \\
&\times \tilde{g}_n\left(k-\left(L_1+m-1\right)N\right) \Bigg]
\end{aligned} \tag{E.1}$$

with $\tilde{g}_n(k) = g\left(k - \tau - nK\right)$. Moreover, taking into account that for $k_1 - k_2 \gg K$

$$\begin{aligned}
&\frac{1}{k_1 - k_2} \sum_{k=k_2}^{k_1 - 1} \sum_{n=-\infty}^{+\infty} g\left(k - \tau - nK\right) g\left(k - \tau + m - nK\right) \\
&\cong \left\langle \sum_{n=-\infty}^{+\infty} g\left(k - \tau - nK\right) g\left(k - \tau + m - nK\right) \right\rangle \qquad \text{(E.2)} \\
&= \frac{R_g(m)}{K}
\end{aligned}$$

the (m,l)th element of the covariance matrix for $Q \gg L_1 + L_2$ can be approximated as

$$\begin{aligned}
\left[\mathbf{C}_{\mu}\right]_{(m,l)} &= \frac{1}{N\left(Q - L_1 - l + 1\right)\left(Q - L_1 - m + 1\right)} \\
&\times \frac{1}{R_g\left(\left(L_1 + l - 1\right)N\right) R_g\left(\left(L_1 + m - 1\right)N\right) \mathrm{SNR}} \qquad \text{(E.3)} \\
&\times \Big[\left(Q - m - l - 2L_1 + 2\right) R_g\left(\left(2L_1 + m + l - 2\right)N\right) \\
&+ \left(Q - \max\left\{m,l\right\} - L_1 + 1\right) R_g\left(\left(m - l\right)N\right)\Big]
\end{aligned}$$

Appendix F

Derivation of the MCRB

In this Appendix, we derive the expression of the MCRB for FMT and OFDM/OQAM systems. As regards FMT systems, we analyze the case of perfect timing synchronization, while for OFDM/OQAM systems we report the MCRB for timing, CFO and phase.

F.1 MCRB for FMT Systems

Let $\mathbf{r}$ the observation vector and $\mathbf{v}=\left[\varepsilon,\phi\right]^T$ the vector of the parameters to be estimated in the presence of random nuisance vector $\mathbf{a}=\left[a_1(n),\ldots,a_{\mathcal{A}}(n)\right]^T$, the (i,l)th entry of the MFIM under the assumptions A1, A2 and A3 (see section 4.1) and in the case of perfect timing synchronization is equal to

$$\left[\mathbf{F}\right]_{(i,l)}=-E_{\mathbf{r},\mathbf{a}}\left\{\frac{\partial \ln p_{\mathbf{r},\mathbf{a}}\left(\mathbf{r}|\mathbf{a},\mathbf{v}\right)}{\partial\left[\mathbf{v}\right]_i\,\partial\left[\mathbf{v}\right]_l}\right\},\forall i,l\in\{1,2\} \quad \text{(F.1)}$$

where

$$\ln p_{\mathbf{r},\mathbf{a}}\left(\mathbf{r}\middle|\mathbf{a},\mathbf{v}\right)=\frac{2}{\sigma_n^2}$$
$$\times\sum_{q=0}^{Q-1}\sum_{m=0}^{N-1}\Re\left\{r_q^*(m)s_q(m)e^{j\left[\frac{2\pi}{N}\varepsilon(qN+m)+\phi\right]}\right\} \tag{F.2}$$

After some calculations, we obtain

$$\left[\mathbf{F}\right]_{(1,1)}=\frac{2K\sigma_s^2}{\sigma_n^2}\sum_{l=0}^{QN-1}\left(\frac{2\pi l}{N}\right)^2\sum_{n=-\infty}^{+\infty}g^2\left(l-nK\right) \tag{F.3}$$

$$\left[\mathbf{F}\right]_{(1,2)}=\left[\mathbf{F}\right]_{(2,1)}$$
$$=\frac{2K\sigma_s^2}{\sigma_n^2}\sum_{l=0}^{QN-1}\frac{2\pi l}{N}\sum_{n=-\infty}^{+\infty}g^2\left(l-nK\right) \tag{F.4}$$

$$\left[\mathbf{F}\right]_{(2,2)}=\frac{2K\sigma_s^2}{\sigma_n^2}\sum_{l=0}^{QN-1}\sum_{n=-\infty}^{+\infty}g^2\left(l-nK\right) \tag{F.5}$$

The MCRB for CFO and the carrier phase estimation is given by the corresponding diagonal element of the inverse of MFIM, whose expression is

$$\mathrm{MCRB}\left(\varepsilon\right)=\left[\mathbf{F}^{-1}\right]_{(1,1)}=\frac{1}{2\mathrm{SNR}K}$$
$$\times\frac{\displaystyle\sum_{l=0}^{QN-1}\left(\frac{2\pi l}{N}\right)^2\sum_{n=-\infty}^{+\infty}g^2\left(l-nK\right)}{\displaystyle\sum_{l_1,l_2=0}^{QN-1}\frac{2\pi l_1}{N}\left(\frac{2\pi l_1}{N}-\frac{2\pi l_2}{N}\right)\sum_{n_1,n_2=-\infty}^{+\infty}g^2\left(l_1-n_1K\right)g^2\left(l_2-n_2K\right)} \tag{F.6}$$

$$\mathrm{MCRB}(\phi)=\left[\mathbf{F}^{-1}\right]_{(2,2)}=\frac{1}{2\mathrm{SNR}K}$$
$$\times\frac{\sum_{l=0}^{QN-1}\sum_{n=-\infty}^{+\infty}g^2(l-nK)}{\sum_{l_1,l_2=0}^{QN-1}\frac{2\pi l_1}{N}\left(\frac{2\pi l_1}{N}-\frac{2\pi l_2}{N}\right)\sum_{n_1,n_2=-\infty}^{+\infty}g^2(l_1-n_1K)\,g^2(l_2-n_2K)} \tag{F.7}$$

F.2 MCRB for OFDM/OQAM Systems

Let $\mathbf{r}$ the observation vector and $\mathbf{v}=\left[\tau,\Delta f,\phi\right]^T$ the vector of the parameters to be estimated in the presence of random nuisance vector $\mathbf{a}=\left[\mathbf{a}^R,\mathbf{a}^I\right]^T$, the (i,l)th entry of the MFIM under the assumptions ASS1 (see section 4.3) is equal to

$$\left[\mathbf{F}\right]_{(i,l)}=-E_{\mathbf{r},\mathbf{a}}\left\{\frac{\partial\ln p_{\mathbf{r},\mathbf{a}}\left(\mathbf{r}\middle|\mathbf{a},\mathbf{v}\right)}{\partial\left[\mathbf{v}\right]_i\,\partial\left[\mathbf{v}\right]_l}\right\}, \tag{F.8}$$

$\forall i,l\in\{1,2,3\}$

where (up to irrelevant additive factors)

$$\ln p_{\mathbf{r},\mathbf{a}}\left(\mathbf{r}\middle|\mathbf{a},\mathbf{v}\right)$$
$$=\frac{2\gamma T_s}{\sigma_n^2}\sum_{m=0}^{N-1}\Re\left\{r^*(kT_s)\,s(kT_s-\tau)\,e^{j[2\pi\Delta fkT_s+\phi]}\right\} \tag{F.9}$$
$$-\frac{\gamma^2T_s}{\sigma_n^2}\sum_{k=0}^{N\eta-1}\left|s(kT_s-\tau)\right|^2$$

It results that

$$\left[\mathbf{F}\right]_{(1,1)} = \frac{\gamma^2 a_2 T_s}{\sigma_n^2} \sum_{k=0}^{\eta N-1} \sum_{p=-\infty}^{+\infty} \sum_{l=0}^{N-1} \left(\frac{2\pi l}{T}\right)^2$$
$$\times \left[g^2\left(kT_s - \tau - pT\right) + g^2\left(kT_s - \tau - pT - \frac{T}{2}\right)\right]$$
$$+ \frac{\gamma^2 a_2 T_s}{\sigma_n^2} N \sum_{k=0}^{\eta N-1} \sum_{p=-\infty}^{+\infty} \left[\dot{g}^2\left(kT_s - \tau - pT\right)\right. \quad \text{(F.10)}$$
$$\left. + \dot{g}^2\left(kT_s - \tau - pT - \frac{T}{2}\right)\right.$$

$$\left[\mathbf{F}\right]_{(1,2)} = \left[\mathbf{F}\right]_{(2,1)} = -\frac{\gamma^2 a_2 T_s}{\sigma_n^2} \frac{4\pi^2}{N} \sum_{k=0}^{\eta N-1} k \sum_{l=0}^{N-1} l$$
$$\times \sum_{p=-\infty}^{+\infty} \left[g^2\left(kT_s - \tau - pT\right) + g^2\left(kT_s - \tau - pT - \frac{T}{2}\right)\right] \quad \text{(F.11)}$$

$$\left[\mathbf{F}\right]_{(1,3)} = \left[\mathbf{F}\right]_{(3,1)} = -\frac{\gamma^2 a_2 T_s}{\sigma_n^2} \sum_{k=0}^{\eta N-1} \sum_{l=0}^{N-1} \left(\frac{2\pi l}{T}\right)$$
$$\times \sum_{p=-\infty}^{+\infty} \left[g^2\left(kT_s - \tau - pT\right) + g^2\left(kT_s - \tau - pT - \frac{T}{2}\right)\right] \quad \text{(F.12)}$$

$$\left[\mathbf{F}\right]_{(2,3)} = \left[\mathbf{F}\right]_{(3,2)} = \frac{2\pi T \gamma^2 a_2 T_s}{\sigma_n^2} \sum_{k=0}^{\eta N-1} k$$
$$\times \sum_{p=-\infty}^{+\infty} \left[g^2\left(kT_s - \tau - pT\right) + g^2\left(kT_s - \tau - pT - \frac{T}{2}\right)\right] \quad \text{(F.13)}$$

$$[\mathbf{F}]_{(2,2)} = \frac{\gamma^2 a_2 T}{\sigma_n^2} \sum_{k=0}^{\eta N-1} (2\pi k T_s)^2 \times \sum_{p=-\infty}^{+\infty} \left[g^2(kT_s - \tau - pT) + g^2\left(kT_s - \tau - pT - \frac{T}{2}\right) \right] \tag{F.14}$$

$$[\mathbf{F}]_{(3,3)} = \frac{\gamma^2 a_2 T}{\sigma_n^2} \sum_{k=0}^{\eta N-1} \sum_{p=-\infty}^{+\infty} \left[g^2(kT_s - \tau - pT) + g^2(kT_s - \tau - pT - T/2) \right] \tag{F.15}$$

Note that under the assumption ASS2 (see section 4.3)

$$\sum_{p=-\infty}^{+\infty} \left[g^2(kT_s - \tau - pT) + g^2(kT_s - \tau - pT - T/2) \right] = \frac{2}{T} \tag{F.16}$$

and

$$\sum_{p=-\infty}^{+\infty} \left[\dot{g}^2(kT_s - \tau - pT) + \dot{g}^2(kT_s - \tau - pT - T/2) \right] = \frac{2}{T} \bar{G}_2(0) \tag{F.17}$$

where $\bar{G}_2(f)$ is the Fourier transform of $\dot{g}^2(t)$. Then, by considering an SRRC Nyquist prototype filter it follows that $\bar{G}_2(0) = \frac{4\pi^2 \xi}{T^2}$ where $\xi = \left[\frac{1}{12} + \alpha^2 \left(\frac{1}{4} - \frac{2}{\pi^2} \right) \right]$. Therefore, we have

$$[\mathbf{F}]_{(1,1)} = 2\mathrm{SNRN}\eta \left(\frac{2\pi}{T} \right)^2 \left(\frac{(N-1)(2N-1)}{6} + \xi \right) \tag{F.18}$$

$$\left[\mathbf{F}\right]_{(1,2)} = \left[\mathbf{F}\right]_{(2,1)} = -2\pi^2 \mathrm{SNR}\,\eta N\left(N\eta - 1\right)\left(N-1\right) \tag{F.19}$$

$$\left[\mathbf{F}\right]_{(1,3)} = \left[\mathbf{F}\right]_{(3,1)} = -\frac{2\pi N\eta}{T}\mathrm{SNR}\left(N-1\right) \tag{F.20}$$

$$\left[\mathbf{F}\right]_{(2,3)} = \left[\mathbf{F}\right]_{(3,2)} = 2\pi N\eta T_s \mathrm{SNR}\left(N\eta - 1\right) \tag{F.21}$$

$$\left[\mathbf{F}\right]_{(2,2)} = \left(2\pi T_s\right)^2 \mathrm{SNR}\,\frac{\eta N\left(N\eta-1\right)\left(2N\eta-1\right)}{3} \tag{F.22}$$

$$\left[\mathbf{F}\right]_{(3,3)} = 2\mathrm{SNR}\,\eta N \tag{F.23}$$

The MCRB for normalized symbol timing, for normalized CFO and for phase is obtained by evaluating the corresponding diagonal element of inverse of MFIM and is given by

$$MCRB\left(\frac{\tau}{T}\right) = \frac{1}{8\pi^2 \mathrm{SNR}\,\eta N\left[\dfrac{N^2-1}{12} + \xi\right]} \underset{N\gg 1}{\approx} \frac{3}{2\pi^2 \mathrm{SNR}\,\eta N^3} \tag{F.24}$$

$$MCRB\left(\Delta fT\right) = \frac{3N}{2\mathrm{SNR}\,\pi^2\eta\left(N^2\eta^2-1\right)} \underset{N\gg 1}{\approx} \frac{3}{2\pi^2 \mathrm{SNR}\,\eta^3 N} \tag{F.25}$$

$$MCRB(\phi) = \frac{1}{2\mathrm{SNR}\eta N\left[1-\frac{3(\eta N-1)}{2(2\eta N-1)}\right]} + \frac{(N-1)^2}{8\mathrm{SNR}\eta N\left[\frac{N^2-1}{12}+\xi\right]} \underset{N\gg 1}{\cong} \frac{7}{2\mathrm{SNR}\eta N} \tag{F.26}$$

Finally it is interesting to note that the MCRB for the symbol timing does not change if the CFO does not belong to the parameters to be estimated. In fact the MFIM for the symbol timing and the carrier phase offset is given by the following minor of (F.8)

$$\mathbf{F}(\tau,\phi) = \begin{bmatrix} \mathbf{F}_{(1,1)} & \mathbf{F}_{(1,3)} \\ \mathbf{F}_{(3,1)} & \mathbf{F}_{(3,3)} \end{bmatrix} \tag{F.27}$$

and by considering (F.18), (F.20) and (F.23) the same result as that in (F.24) is obtained. Moreover, the MCRB for the CFO is the same as (F.25) also if the symbol timing is not included in the parameters to be estimated. In fact, the MFIM for the CFO and the carrier phase is given by

$$\mathbf{F}(\Delta f,\phi) = \begin{bmatrix} \mathbf{F}_{(2,2)} & \mathbf{F}_{(2,3)} \\ \mathbf{F}_{(3,2)} & \mathbf{F}_{(3,3)} \end{bmatrix} \tag{F.28}$$

and by considering (F.22), (F.21) and (F.23) the same result as that in (F.25) is obtained.

Appendix G

Expression of the UMLLS Cost Function in the Absence of Virtual Subcarriers

In this Appendix, we demonstrate that the UMLLS estimator in (4.53) cannot be used in the absence of virtual subcarriers. To such end, we consider an observations window of infinite length and substitute (4.45) and (4.46) into (4.52)

$$\Lambda\left(\tilde{\varepsilon}\right)=\sum_{p=-\infty}^{\infty}\sum_{l=0}^{N-1}\left[\left|\sum_{m=0}^{N-1}\sum_{k=-\infty}^{\infty}r_{k+p}\left(m\right)\right.\right.$$
$$\left.\times e^{-j\frac{2\pi}{N}\tilde{\varepsilon}\left(m+kN+pN\right)}g_k\left(m\right)e^{-j\frac{2\pi}{N}ml}\right|^2$$
$$+\left|\sum_{m=0}^{N-1}\sum_{k=-\infty}^{\infty}r_{k+p}\left(m\right)e^{-j\frac{2\pi}{N}\tilde{\varepsilon}\left(m+kN+pN\right)}\right. \tag{G.1}$$
$$\left.\left.\times g_k\left(m\right)e^{-j\frac{2\pi}{N}ml}\right|^2\right]$$

After simple algebraic manipulations we obtain

$$\Lambda(\tilde{\varepsilon}) = \sum_{h_1,h_2=-\infty}^{\infty} r(h_1) r^*(h_2) e^{-j\frac{2\pi}{N}\tilde{\varepsilon}(h_1-h_2)} \times \sum_{l=0}^{N-1} e^{-j\frac{2\pi}{N}l(h_1-h_2)} \left[\sum_{p=-\infty}^{\infty} g(h_1 - pN) \times g(h_2 - pN) + \sum_{p=-\infty}^{\infty} g(h_1 - pN - N/2) \times g(h_1 - pN - N/2) \right] \quad \text{(G.2)}$$

Exploiting the relationship

$$\sum_{l=0}^{N-1} e^{-j\frac{2\pi}{N}l(h_1-h_2)} = N\delta(h_1 - h_2 - qN) \quad \forall q \in \mathbb{Z} \quad \text{(G.3)}$$

it follows that

$$\Lambda(\tilde{\varepsilon}) = N \sum_{h=-\infty}^{\infty} r(h) r^*(h - qN) e^{-j\frac{2\pi}{N}\tilde{\varepsilon}qN} \times \sum_{p=-\infty}^{\infty} g(h - pN/2) g(h - pN/2 - qN) \quad \text{(G.4)}$$

Accounting for the orthogonality condition on the pulse-shaping filter (4.29), we obtain

$$\Lambda(\tilde{\varepsilon}) = 2 \sum_{h=-\infty}^{\infty} |r(h)|^2 \quad \text{(G.5)}$$

It must be observed that in the case of an observations window of finite length the likelihood function in (4.52) is weakly dependent on the unknown parameter $\tilde{\varepsilon}$, see Figure 45.

Appendix H

Derivation of the Variance of the Noise Terms $e_1(m)$ and $e_2(m)$

In this Appendix, we show that under assumptions AS1 and AS2 (see section 4.2) the "noise" term $e_1(m)$ ($e_2(m)$) in (4.58) (in (4.62)) has a variance $\mathcal{O}\left((N-m)^{-1}\right)$ $\left(\mathcal{O}\left(m^{-1}\right)\right)$. We observe that the random variable

$$\hat{R}(\lambda)=\frac{1}{N-\lambda}\sum_{k=0}^{N-\lambda-1} r^*(k)r(k+\lambda) \tag{H.1}$$

is characterized by the statistical expectation

$$E\left[\hat{R}(\lambda)\right]=\frac{1}{N-\lambda}\sum_{k=0}^{N-\lambda-1} R(k;\lambda) \tag{H.2}$$

and the variance

$$\begin{aligned}\operatorname{var}\left[\hat{R}(\lambda)\right]=&-\frac{1}{(N-\lambda)^2}\left|\sum_{k=0}^{N-\lambda-1} R(k;\lambda)\right|^2\\ &+\frac{1}{(N-\lambda)^2}\sum_{k=0}^{N-\lambda-1} E\left[r^*(k)r(k+\lambda)\right.\\ &\left.\times r^*(l)r(l+\lambda)\right]\end{aligned} \tag{H.3}$$

By assuming that the number of subcarriers is sufficiently large, the OFDM/OQAM signal is modelled as a zero-mean complex Gaussian random signal. Thus, by using the Isserlis identity

$$E\left[a^*bcd^*\right]=E\left[a^*b\right]E\left[cd^*\right] \\ +E\left[a^*c\right]E\left[bd^*\right]+E\left[a^*d^*\right]E\left[bc\right] \tag{H.4}$$

where a, b, c and d are zero-mean complex-valued jointly Gaussian random variables, the statistical expectation of the second term in the RHS of (H.3) can be written as

$$E\left[r^*(k)r\left(k+\lambda\right)r^*(l)r\left(l+\lambda\right)\right] \\ =R\left(k;\lambda\right)R^*\left(l;\lambda\right)+R\left(k;l-k\right)R^*\left(k+\lambda;l-k\right) \\ +C\left(l;k+\lambda-l\right)C^*\left(k;l-k+\lambda\right) \tag{H.5}$$

where $C\left(\rho;\beta\right)$ and $R\left(\rho;\beta\right)$ are the conjugate and the unconjugate correlation functions of the received OFDM/OQAM signal $r(k)$ (4.35) at time ρ and lag β, whose expressions, under assumptions AS1 and AS2, are given by

$$C\left(\rho;\beta\right)=\frac{\sigma_s^2\pi}{2\alpha N_u N}e^{j\left[\frac{2\pi}{N}\varepsilon\left(2\rho+\beta\right)+2\phi\right]} \\ \frac{\cos\left[2\pi/N\left(\rho-\beta/2\right)\right]\cos\left(\pi\alpha\beta/N\right)}{\left[\left(\pi/2\alpha\right)^2-\left(\pi\beta/N\right)^2\right]} \\ \times\sum_{l\in\mathcal{A}}e^{jl\pi}e^{j\frac{2\pi}{N}l\left(2\rho+\beta\right)} \tag{H.6}$$

and

$$R\left(\rho;\beta\right)=\frac{\sigma_s^2\pi}{N_u}e^{j\frac{2\pi}{N}\varepsilon\beta}\sum_{l\in\mathcal{A}}e^{j\frac{2\pi}{N}l\beta}z\left(\beta\right)+\sigma_n^2\delta\left(\beta\right) \tag{H.7}$$

where $z(l)$ is defined in (4.59). Plugging result (H.5) back into (H.3), it follows that

$$\begin{aligned}\mathrm{var}\left[\hat{R}(\lambda)\right] &= \frac{1}{(N-\lambda)^2} \\ &\times \sum_{k,l=0}^{N-\lambda-1} R(k;l-k)R^*(k+\lambda;l-k) + \frac{1}{(N-\lambda)^2} \\ &\times \sum_{k,l=0}^{N-\lambda-1} C(l;k+\lambda-l)C^*(k;l-k+\lambda)\end{aligned} \tag{H.8}$$

Under assumptions AS1 and AS2 and accounting for (H.7) we obtain

$$\begin{aligned}\mathrm{var}\left[\hat{R}(\lambda)\right] &= \frac{1}{(N-\lambda)^2} \sum_{k,l=0}^{N-\lambda-1} \left|R(l-k)\right|^2 \\ &+ \frac{1}{(N-\lambda)^2} \sum_{k,l=0}^{N-\lambda-1} C(l;k+\lambda-l)C^*(k;l-k+\lambda) \\ &\le \frac{1}{(N-\lambda)^2} \sum_{k,l=0}^{N-\lambda-1} \left|R(l-k)\right|^2 \\ &+ \frac{1}{(N-\lambda)^2} \sum_{k,l=0}^{N-\lambda-1} \left|C(l;k+\lambda-l)C^*(k;l-k+\lambda)\right|\end{aligned} \tag{H.9}$$

Accounting for (H.6) and using the inequalities

$$\left|\sum_{l\in\mathcal{A}} e^{jl\pi} e^{j\frac{2\pi}{N}l(2\rho+\beta)}\right|^2 \le N_u^2 \tag{H.10}$$

$$\cos\left[\frac{2\pi}{N}\left(\rho-\frac{\beta}{2}\right)\right]\cos\left(\frac{\pi\alpha\beta}{N}\right) \le 1 \tag{H.11}$$

and

$$\left|z(l)\right| \le 1 \tag{H.12}$$

we obtain

$$\begin{aligned}
&\mathrm{var}\left[\hat{R}(\lambda)\right] \le \frac{1}{(N-\lambda)^2}\sum_{k,l=0}^{N-\lambda-1}\Big[\left|R(l-k)\right|^2 \\
&+\gamma(\lambda-(l-k))\gamma(\lambda+l-k)\Big] \\
&=\frac{1}{(N-\lambda)}\sum_{q=-(N-\lambda-1)}^{N-\lambda-1}\Big[\left|R(q)\right|^2 \qquad \text{(H.13)} \\
&+\gamma(\lambda-q)\gamma(\lambda+q)\Big]\left(1-\frac{|q|}{N-\lambda}\right) \\
&<\frac{1}{(N-\lambda)}\sum_{q=-N+1}^{N-1}\Big[\left|R(q)\right|^2+\gamma(\lambda-q)\gamma(\lambda+q)\Big]
\end{aligned}$$

with

$$\gamma(p)=\frac{\sigma_s^2\pi}{2\alpha N}\frac{1}{\left[(\pi/2\alpha)^2-(\pi p/N)^2\right]} \qquad \text{(H.14)}$$

Substituting (H.7) and (H.14) in (H.13), after some algebraic manipulations, it follows that

$$\begin{aligned}
&\mathrm{var}\left[\hat{R}(\lambda)\right] < \frac{\left(\sigma_n^2+\sigma_s^2\right)^2}{(N-\lambda)}+\frac{\sigma_s^2\pi^2}{(N-\lambda)N^2 4\alpha^2} \\
&\times\sum_{q=-N+1}^{N-1}\frac{1}{(\pi/2\alpha)^2-(\pi(q+\lambda)/N)^2} \qquad \text{(H.15)} \\
&\times\frac{1}{(\pi/2\alpha)^2-(\pi(\lambda-q)/N)^2}
\end{aligned}$$

From (H.15) we can note that the random variable $\hat{R}(\lambda)$ has a variance $\mathcal{O}\left((N-\lambda)^{-1}\right)$. Clearly, this implies that the "noise" term $e_1(m)$ ($e_2(m)$) in (4.58) (in (4.62)) has a variance $\mathcal{O}\left((N-m)^{-1}\right)$ $\left(\mathcal{O}\left(m^{-1}\right)\right)$.

References

[1]. P.P. Vaidyanathan, Multirate Systems and Filter Banks, Prentice Hall, Englewood Cliffs, NJ, 1993.

[2]. G. Cherubini, E. Eleftheriou, S. Ölçer and J. M. Cioffi, "Filter bank modulation technique for very high-speed digital subscriber lines," *IEEE Commun. Mag.*, vol. 38, pp. 98-104, May 2000.

[3]. N. Benvenuto, S. Tomasin and L. Tomba, "Equalization methods in OFDM and FMT systems for broadband wireless communications," *IEEE Trans. Commun.*, vol. 50, no. 5, p. 1016-1028, June 2002.

[4]. T. Ihalainen, T. Hidalgo Stitz, M. Rinne and M. Renfors, "Channel equalization in filter bank based multicarrier modulation for wireless communications," *EURASIP J. Applied Signal Processing*, vol 2007.

[5]. D. Lacroix, N. Goudard and M. Alard, "OFDM with guard interval versus OFDM/offsetQAM for high data rate UMTS downlink transmission," in *Proc. VTC'01* Fall, Atlantic City, NJ, USA, October 2001.

[6]. P. K. Remvik and N. Holte, "Carrier frequency offset robustness for OFDM systems with different pulse shaping

filters," in *Proc. GLOBECOM 1997*, vol. 1, pp. 11-15, November 1997.

[7]. T. Fusco, A. Petrella and M. Tanda, "Sensitivity of multi-user filter-bank multicarrier systems to synchronization errors," in *Proc. ISCCSP 2008*, Malta, March 2008.

[8]. V. Lottici, M. Luise, C. Saccomando and F. Spalla, "Blind carrier frequency tracking for filterbank multicarrier wireless communications," *IEEE Trans. Commun.*, vol. 53, no. 9, pp.1762-1772, September 2005.

[9]. V. Lottici, M. Luise, C. Saccomando and F. Spalla, "Non data-aided timing recovery for filter bank multicarrier wireless communications," *IEEE Trans. Commun.*, vol. 54, no. 11, pp. 4365-4375, November 2006.

[10]. A. Assalini and A. M. Tonello, "Time-frequency synchronization in filtered multitone modulation based systems," presented at the IEEE WPMC'03, Yokosuka, Kanagawa, Japan, October 19-22, 2003.

[11]. H. Bölcskei, "Blind estimation of symbol timing and carrier frequency offset in wireless OFDM systems," *IEEE Trans. Commun.*, vol. 49, no. 6, pp. 988-999, June 2001.

[12]. P. Ciblat, E. Serpedin, "A fine blind frequency offset estimator for OFDM/OQAM systems," *IEEE Trans.*

Signal Processing, vol. 52, pp. 291-296, January 2004.

[13]. G. Lin, L. Lundheim and N. Holte, "New methods for blind fine estimation of carrier frequency offset in OFDM/OQAM systems," in *Proc. of SPAWC 2006*, Cannes, France, 2-5 July, 2005.

[14]. A. Tonello and M. Rossi, "Synchronization and channel estimation for filtered multitone modulation," in *Proc. WPMC 2004*, Abano Terme, pp-590-594, September 2004.

[15]. T.H. Stitz, T. Ihalainen and M. Renfors, "Practical issues in frequency domain synchronization for filter bank based multicarrier transmission," in *Proc. ISCCSP 2008*, Malta, Mar. 2008.

[16]. T. Fusco, A. Petrella and M. Tanda, "Data-aided symbol timing and CFO synchronization for filter bank multicarrier systems," *IEEE Trans. on Wireless Commun.*, vol. 8, no. 4, April 2009.

[17]. T. Fusco, A. Petrella and M. Tanda, "Joint symbol timing and CFO estimation in multiuser OFDM/OQAM systems," in *Proc. of SPAWC 2009*, Perugia, June 2009.

[18]. T. Fusco, A. Petrella and M. Tanda, "Blind CFO estimation for noncritically sampled FMT systems," *IEEE Trans. on Signal Proc.*, vol. 56, no. 6, June 2008.

[19]. T. Fusco, A. Petrella and M. Tanda, "Non data-aided carrier frequency offset estimation for pulse shaping OFDM/OQAM systems," *Signal Processing*, vol. 88, pp. 1958-1970, August 2008.

[20]. T. Fusco, A. Petrella and M. Tanda, "Blind symbol timing estimation for OFDM/OQAM systems," accepted for publication on *IEEE Trans. on Sign. Proc.*

[21]. T. Fusco, A. Petrella and M. Tanda, "Blind carrier frequency offset estimation for non-critically sampled FMT systems in multipath channels," in *Proc. of SPAWC 2007*, Helsinki, Finland, June 2007.

[22]. I. Berenguer, Filtered Multitone (FMT) Modulation for Broadband Fixed Wireless System, PhD Thesis, Laboratory for Communications Engeenering, Department of Engeenering, University of Cambridge.

[23]. N. Benvenuto, G. Cherubini, Algorithms for Communications Systems and their Applications, Wiley, 2003.

[24]. M. Bellanger, "Specification and design of a prototype filter for filter bank based multicarrier transmission," *Proc. of 2001 IEEE International Conference on Acoustics, Speech and Signal Processing*, *ICASSP'01*, Salt Lake City, May 2001.

[25]. H. Bölcksei, P. Duhamel and R. Hleiss, "Orthogonalization of OFDM/OQAM pulse shaping filters using the discrete Zak transform," *Signal Processing*, vol. 83, pp. 1379-1391, July 2003.

[26]. Document: IEEE 802.22-06/017r0, September 2006.

[27]. H. Minn, V.K. Bhargava, and K. B. Letaief, "A robust timing and frequency synchronization for OFDM systems", *IEEE Trans. Wireless Commun.*, vol. 2, pp. 822-839, July 2003.

[28]. P. Sihoan, C. Siclet and N. Lacaille, "Analysis and design of OFDM/OQAM systems based on filterbank theory," in *IEEE Trans, Signal Processing*, vol. 50, no.5, pp. 1170-1174, May 2002.

[29]. A. V. Dandawaté and G. B. Giannakis, "Asymptotic theory of mixed time averages and *k*th - order cyclic-moment and cumulant statistics, " *IEEE Trans. Inf. Theory*, vol. 41, no. 1, pp. 216-232, January 1995.

[30]. S. M. Kay, Fundamentals of Statistical Signal Processing: Estimation Theory, Englewood Cliffs, NJ: Prentice-Hall, 1993.

[31]. F. Gini, R. Reggianini and U. Mengali, "The modified Cramér-Rao bound in vector parameter estimation," *IEEE Trans. Commun.*, vol. 46, no. 1, pp. 52-60, January 1998.

[32]. T. Fusco, M. Tanda, "Blind frequency offset estimation for OFDM/OQAM systems," *IEEE Trans. Signal Proc.*, vol. 55, pp. 1828-1838, May 2007.

[33]. P. Stoica, T. Söerström, and F. N. Ti, "Asymptotic propoerties of the high-order Yule-Walker estimates of sinusoidal frequencies," *IEEE Trans. Acoustic Speech Signal Processing*, vol. 37, pp. 1721-1734, November 1989.

[34]. P. H. Moose, "A technique for orthogonal frequency division multiplexing frequency offset correction," *IEEE Trans. Commun.*, vol. 42, pp. 2908-2914, October 1994.